Università degli Studi di Ferrara

DOTTORATO DI RICERCA IN
FISICA

CICLO XXVI

COORDINATORE Prof. Vincenzo Guidi

Radioisotopes production via accelerator for nuclear medicine applications
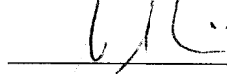
Settore Scientifico Disciplinare FIS/07

Dottorando	**Tutore**
Dott.ssa Pupillo Gaia	Prof. Gambaccini Mauro

Anni 2011/2013

Contents

Introduction

The use of radioactive tracers, i.e. chemical species labelled with a radionuclide, have experienced a great and fast development in nuclear medicine, biology and many other fields when nuclear reactors started to produce a large number of radioisotopes. Moreover, in the last century continuous efforts have been spent in the development of accelerators, in particular cyclotrons [1, 2], devoted to the production of isotopes for medical applications. This attempt led today to the knowledge of various technologies for radioisotope production, based both on reactors and accelerators [3].

In this contest has grown the LARAMED (LAboratory of RAdioisotopes for MEDicine) project, started in 2013 and funded by the Italian government and INFN (Istituto Nazionale di Fisica Nucleare). LARAMED is based on the high performance cyclotron that will be installed in 2014 at Legnaro National Laboratories (LNL, Padova, Italy), in the framework of SPES (Selective Production of Exotic Species) project. SPES represents the future of research at LNL, focusing on both basic research in nuclear physics and astrophysics and on interdisciplinary applications, ranging from the production of radionuclides of medical interest (LARAMED) to the generation of neutrons for material studies, nuclear technologies and medicine [4].

This future state-of-the-art facility is based on the performance of the incoming cyclotron, a dual-beam operational accelerator that promotes a useful co-operation of experts in different fields, from nuclear physics to radiochemistry, medical physics and nuclear medicine. In fact, while the first 40 MeV proton-beam will be used in nuclear physics research on Radioactive Ion Beams[1] (RIBs), the second proton-beam, with a tunable energy ranging from 30 to 70 MeV, will provide the basis for applied physics research and in particular for LARAMED project.

Among the set of radioisotopes that will be produced at LARAMED, particular attention has been paid to the most used nuclide in diagnostic applications, Technetium-99 metastable (^{99m}Tc, half-life 6.0067 h, γ-ray of 140.511 keV, 89% intensity), and its parent nuclide, Molybdenum-99 (^{99}Mo, half-life 65.976 h). In order to investigate the possible

---

[1] A second-generation ISOL (Isotope Selector On line) facility, dedicated to the forefront research in nuclear physics, is planned to be developed, by using the 40 MeV proton-beam from the cyclotron and injecting it to the PIAVE-ALPI linac accelerator complex [4].

future supply of these vital isotopes in Veneto region, basing on the incoming cyclotron at LNL, APOTEMA (Accelerator-driven Production Of TEchnetium/Molybdenum for medical Applications) project has started in 2012, funded by INFN and developed in collaboration between LNL, Ferrara and Padova sections[2].

Moreover, in the framework of LARAMED an international collaboration between INFN and GIP ARRONAX [5] (Accelerator for Research in Radiochemistry and Oncology at Nantes Atlantique, Nantes, France) has started, in order to develop innovative techniques aimed to the optimization of radioisotope production, sharing basic and fundamental knowledges on physical, radiochemical and medical topics.

The aim of my Ph.D. work has been the evaluation of the accelerator-based production of some important radioisotopes in nuclear medicine: the aforementioned ^{99m}Tc and ^{99}Mo, and the emerging isotope for RAdio-Immuno Therapy (RAIT), Copper-67 (^{67}Cu, half-life 61.83 h, β^-- and γ-emitter).

As outlined in Chapter 1, ^{99m}Tc is the most important radioisotope in SPECT (Single Photon Emission Computed Tomography), allowing worldwide about 30 million examinations per year [6], with approximately half of them in the United States [7]. ^{67}Cu is instead a promising nuclide for RAIT, thanks to its peculiar physical-chemical characteristics; its relatively long half-life permits to follow the slow bio-distribution of antibodies, the most used bio-active vectors for ^{67}Cu, while its *beta*-radiation have a therapeutic effects on the targeted cells. Moreover, the γ-rays emitted in the decay of ^{67}Cu permits to follow its track by using SPECT-cameras, making ^{67}Cu a promising nuclide for *Theragnostic*, a technique that include both therapy and imaging. However, the main limiting factor for a more consistent evaluation of ^{67}Cu in clinical trials is its availability [8].

On the contrary, accessibility is one of the key factors of ^{99m}Tc widespread use: thanks to the ^{99}Mo/^{99m}Tc generator system technology, based on the decay of the parent nuclide ^{99}Mo, ^{99m}Tc is efficiently provided worldwide in nuclear medicine departments. Indeed the production chain of ^{99m}Tc relies on ^{99}Mo sources, currently produced in nuclear reactors *via* neutron-induced fission of Highly Enriched Uranium targets, a material subjected to strict international regulations against the use of nuclear weapons. About 70% of ^{99}Mo production is covered by two facilities: the research reactor NRU at Chalk River (Ontario, Canada) and the HFR reactor at Petten (The Netherlands) [9]. In 2009/2010 both facilities have experienced long scheduled/unscheduled shut-downs, causing a worldwide ^{99m}Tc shortening [9, 10, 11]. These circumstances and the recent

---

[2]Pavia and Milano sections joined APOTEMA respectively in 2013 and in 2014.

incident at Fukushima[3] (Tokio, Japan), pushed the scientific community to find alternative supply sources of these vital nuclides [6, 13, 14]. One possibility is to replace the actual reactor-based production with accelerator-based routes, as recently investigated by many researchers [10, 15, 16, 17, 18] and analysed in this work, in the contest of APOTEMA.

It is well-known that a fundamental ingredient in the optimisation of cyclotron productions is the cross section of nuclear reactions involved [3, 19]. As pointed out in Chapter 2, nowadays in the scientific community methods and tools applied in the measurement of nuclear cross sections are well-established [20]. In fact, the knowledge of the cross section allows the yield maximization of the product, minimizing that of radioactive impurities. The non-isotopic impurities produced in-target can be removed by chemical separations. On the contrary, isotopic impurities can be suppressed or minimized only using enriched isotopes as target material and/or by carefully selecting the effective particle energy range in target. Recently, the attention paid to isomeric impurities has grown, since they can not be controlled through an accurate adjustment of the energy window and their cross sections depend on the type of the primary reactions involved [3].

In this work two accelerator-based routes have been considered for the production of ^{99}Mo and ^{99m}Tc isotopes: the p-induced reactions on enriched ^{100}Mo targets (Chapter 3) and the α-induced reaction on Zirconium (Chapter 4).

Chapter 3 reports a feasibility study performed in the contest of APOTEMA, aimed to assess the best irradiation condition for future production of ^{99}Mo and ^{99m}Tc at LNL. This study has been performed considering the already measured p-induced reactions on ^{100}Mo and the characteristics of the incoming cyclotron at LNL. In Chapter 3 a preliminary evaluation about the possible impact of long-lived Tc-impurities in accelerator-produced ^{99m}Tc-labelled radiopharmaceuticals is also given, as well as a quick mention to the development of a β-spectrometer, that will be used to measure the activity of pure β-emitter nuclides, as the Technetium-99 ground state (^{99g}Tc, half life $2.111 \cdot 10^5$ y).

In Chapter 4 results about the new measurement of the ^{96}Zr$(\alpha,$n$)^{99}$Mo cross section, performed at ARRONAX facility, are presented. This reaction was measured only in 1995 by Chowdhury et al. [21], but it has recently gained a strategic role as alternative solution to produce highly pure and high Specific Activity (SA) ^{99}Mo. In fact, due to different chemical species, the resulting ^{99}Mo can be separated from target and used in

---

[3]The Fukushima nuclear accident happened on 11 March 2011 at the I Nuclear Power Plant. The catastrophic failure occurred when the plant was hit by the tsunami caused by the Tohoku earthquake; substantial amounts of radioactive materials were released, becoming the largest nuclear incident since the 1986 Chernobyl disaster and the second (with Chernobyl) to measure Level 7 on the International Nuclear Event Scale [12], releasing an estimated 10-30% of the earlier incident's radiation.

the preparation of high SA ^{99}Mo/^{99m}Tc generator systems. Results of the new evaluation of the ^{96}Zr(α,n)^{99}Mo cross section have been compared with values of Chowdhury et al. (1995) [21]. Moreover, the production yield of ^{99}Mo has been estimated and a comparison of the quality of final products in case of α- and p-induced reactions is also given, taking into account the SA and the co-production of contaminant nuclides.

Regarding the production of ^{67}Cu, Chapter 5 reports the new measurement of the ^{68}Zn(p,2p)^{67}Cu cross section, the most efficient reaction for particle accelerators [11]. This cross section has been repeatedly measured in the last 60 years and a recommended cross section was recently evaluated, by selecting some experimental results and performing an interpolation curve [22]. Chapter 5 reports the results obtained in the new evaluation performed at ARRONAX, and a comparison with recommended and theoretical cross sections[4] of the ^{68}Zn(p,2p)^{67}Cu reaction. Also in case of ^{67}Cu, production yields have been calculated for enriched ^{68}Zn targets, considering the new evaluation of the p-induced reaction, the recommended and the theoretical cross sections. Moreover, ^{67}Cu production yields have been estimated for p-beams on different targets, i.e. enriched ^{70}Zn and natural Zinc (^{nat}Zn) materials, considering the theoretical and recommended cross sections available [22, 23]. At the end a comparison of these different production routes of ^{67}Cu is also given.

Appendixes show results obtained for the ^{68}Zn(p,xn)^{66}Ga,^{67}Ga cross sections (Appendix A) and a brief discussion about ^{27}Al(p,x)^{22}Na,^{24}Na reference cross sections (Appendix B).

---

[4]Theoretical cross sections considered in this work always refer to TENDL library database [23].

Chapter 1

Radionuclide production for nuclear medicine applications

Soon after the discovery of radioactivity in 1896, scientists started to think about a possible application of this phenomenon in medicine. Today over 10 thousands hospitals use radioisotopes in medicine, mostly for diagnostic applications. Annually 35 million *in vivo* procedures are performed, distributed 20 million in the USA, 9 in Europe, 3 in Japan and 3 in the rest of the world. It is impressive that in 2009 it was estimated that one out of two persons in developed countries should benefit from *in vivo* nuclear medicine during their life and that this probability was rising [24]. As discussed in Section 1.1 and in Section 1.2, radioactivity indeed can contribute to both diagnosis and therapy, respectively for its high detection sensitivity and through the biological effects of radiation [3].

As reported in [20], the general properties that a radioactive tracer should ideally have are the following:

- *Specificity*, i.e. the radionuclide should have a unique detection property;

- *Chemical equivalence and stability*, i.e. the introduction of the radionuclide in a compound should not alter the chemical properties of that compound and the radionuclide should not change its chemical state during the foreseen period;

- *Safety*, i.e. the radionuclide should cause only a low chemical and radiation dose; the chemical toxicity is guaranteed by the very low concentrations ($< 10^{-9}$ g), while the radiation dose has to be carefully assessed. For this reason, pure β^--emitters have to be avoided in therapeutic applications, since their radioactivity distribution can not be measured from outside the body [3].

Hereafter the development of several radio-labelling techniques and their influence in nuclear medicine is briefly outlined, with particular attention to imaging applications. The use of highly-selective bio-active molecules incorporating a radionuclide determined nowadays the growth of *Molecular imaging*, a method for investigating *in vivo* biological processes at the molecular level. With respect to radio-imaging, that only refers to functional images as main focus of early radio-pharmacy, molecular imaging aims at the visualization and localization of distinct molecular events in biological systems, with very high sensitivity and specificity [25]. For pursuing this attempt, molecular and nuclear imaging make use of single radio-labelled molecules, that act as molecular probes by transferring informations to the outside through their interaction with a target substrate.

At the early approaches to the design of radio-pharmaceuticals there is the *Tracer principle* (first formulated in 1957), that simply states that the path and concentration in particular areas of a definite quantity of radio-labelled substance, introduced into a biological or mechanical system, can be followed by measuring its radioactivity. When the scientific community understood that the observed bio-distribution did not merely represent the simple tracing of the radioactivity in the organism, but it was rather connected to the bio-molecular interaction responsible for the localization mechanism, a full molecular interpretation of functional images was achieved [26].

The most common approach in developing a true molecular probe was to label a selected chemical species that is known in advance to possess particular biological properties, such as a protein, a bio-active peptide or a synthetic drug [26]. This method is known as the *Bi-functional approach*, since the resulting imaging agent can be thought to be composed of essentially two parts: one with the radionuclide and the other with the bio-active group. Since it is considered that some positron-emitter nuclides (such as ^{18}F and ^{11}C) have a negligible perturbation effect when introduced into a molecule, these isotopes have been usually preferred. This fact easily explains the relevant role of β^+-emitters in molecular imaging, even if many bio-active molecules have been successfully labelled with ^{99m}Tc, a metallic radio-nuclides that is thought to occupy a larger molecular volume (as a convenient chelating system is usually required) [25, 26].

The later step in the development of radio-labelled structure has been the *Multifunctional approach*, in which a molecular agent (such as a protein), sufficiently large for hosting a number of different functional groups carrying out various biological functions, is used for forming a multifunctional ligand [26].

The future scenario of nuclear medicine involves the use of radio-pharmaceuticals that permit, at the same time, therapeutic and diagnostic applications, i.e. *theragnostic* nuclide. This can be reached by using for example multifunctional ligand labelled with particular radionuclides, such as ^{67}Cu, whose radiation is suitable for both diagnosis and therapy, or even by using pair of isotopes such as ^{64}Cu/^{67}Cu or ^{44}Sc/^{47}Sc (Table 1.1).

TABLE 1.1: Nuclear data of some radionuclides used in nuclear medicine.

	Half-life $\tau_{1/2}$	Radiation Emitted	Energy [keV]	Intensity [%]
C-11	20.334 m *24*	β^+	385.70 *44*	99.7669 *25*
N-13	9.965 m *4*	β^+	491.82 *12*	99.8036 *20*
O-15	122.24 s *16*	β^+	735.28 *23*	99.9003 *10*
Sc-44	3.97 h *4*	β^+	632.0 *9*	94.27 *5*
		γ	1157.020 *15*	99.9 *4*
Sc-47	3.3492 d *6*	β^-	142.6 *7*	68.4 *6*
			203.9 *8*	31.6 *6*
		γ	159.381 *15*	68.3 *4*
Cu-64	12.701 h *2*	β^+	278.21 *9*	17.60 *22*
		γ	1345.77 *6*	0.475 *11*
Cu-67	61.83 h *12*	β^-	121 *3*	57 *6*
			154 *3*	22.0 *22*
			189 *3*	20.0 *20*
		γ	93.311 *5*	16.10 *20*
			184.577 *10*	48.7 *3*
Ga-68	67.71 m *9*	β^+	352.59 *52*	1.190 *10*
			836.02 *56*	87.72 *9*
		γ	1077.34 *5*	3.22
Rb-82	1.2575 m *2*	β^+	1167.6 *33*	13.13 *14*
			1534.6 *34*	81.76 *17*
		γ	776.52 *1*	15.08
	6.472 h *6*	β^+	353 *11*	19.7 *16*
		γ	554.35 *10*	62.4 *9*
			619.11 *10*	37.98 *9*
			698.37 *10*	26.3 *7*
			776.52 *10*	84.39
			827.83 *10*	21.0 *6*
			1044.08 *10*	32.07 *8*
			1317.43 *10*	23.7 *6*
			1474.88 *10*	15.5 *3*
Y-90	3.19 h *6*	γ	202.53 *3*	97.3 *4*
			479.51 *5*	90.74 *5*
	64.00 h *21*	β^-	933.7 *12*	99.9885 *14*
Tc-99m	6.0067 h *5*	γ	140.511 *1*	89 *4*
In-111	2.8047 d *4*	γ	171.28 *3*	90.7 *9*
			245.35 *4*	94.1 *10*
I-124	4.1760 d *3*	γ	602.73 *8*	62.9 *7*
			722.78 *8*	10.36 *12*
			1690.96 *8*	11.15 *17*
I-131	8.0252 d *6*	β^-	96.62 *26*	7.23 *10*
			191.58 *30*	89.6 *8*
		γ	284.305 *5*	6.12 *6*
			364.489 *5*	81.5 *8*
			636.989 *4*	7.16 *10*
Re-188	18.59 m *4*	γ	105.96 *10*	10.8 *5*
	17.0040 h *22*	β^-	728.88 *18*	26.3 *5*
			795.41 *18*	70.0 *5*
At-211	7.214 h *7*	α	5869.5 *22*	41.80
		γ	687.0 *1*	0.261 *12*

1.1 The diagnostic applications of nuclides in medicine: SPECT and PET

Single-Photon Emission Computed Tomography (SPECT) and Positron Emission Tomography (PET) are the basis of nuclear medicine imaging tools, allowing precise investigations that are essential not only for early diagnosis but also for prognosis and monitoring of progress, regression or stagnation of a disease upon application of a particular therapy [25].

SPECT has been the cornerstone of nuclear medicine and today it is widely used for detecting molecular changes in cardiovascular, neurological and oncological diseases [27]. The principle of SPECT is well known from 1980s: a bioactive molecule or a pharmaceutical, labelled with a γ-emitter nuclide, characterized by suitable half-life and radiation properties, is injected in patients and SPECT-cameras (large scintillation crystals connected to Photo-Multiplier Tubes, PMTs) are used for detecting the out-coming γ-rays. The ideal characteristics of radiation depend on the specific application: however, the energy should be high enough to come out from patients' body but low enough to be detected in medium-size crystals; the intensity should be as high as possible and preferably only the useful radiation should be emitted, in order to reduce the dose delivered to patients.

In order to reconstruct the spatial distribution of the radio-pharmaceutical, i.e. its bio-distribution, SPECT-cameras are provided with collimators, that select a defined direction absorbing almost all the radiation coming from other directions. In this way, acquiring many views of patients from different angles, it is possible to reconstruct the 3D distribution of the radio-pharmaceutical used.
In some cases multi-headed cameras are used to increase the speed of acquisition. Software then allows integration of all individual projection views into a composite data set which can be re-displayed as tomographic slices. Obviously, patient or organ motion, as well as variations in attenuation from different viewpoints, can have a profound effect on the quality of tomographic views.
At this regard, the biggest change in the last decade has been the fusion of CT (Computed Tomography) with SPECT, determining a fast improve in attenuation corrections and image quality [27]. However, also advances in collimator design, software and reconstruction algorithms, as well as the replacement of sodium iodine (NaI) crystals with cadmium zinc telluride (CZT) detectors, have contributed to preserve SPECT as a fundamental technology in nuclear medicine [27].

Nowadays a wide spectrum of radio-tracers is available for use in cardiovascular, neurology and oncology applications. However, ^{99m}Tc is still the most commonly used SPECT
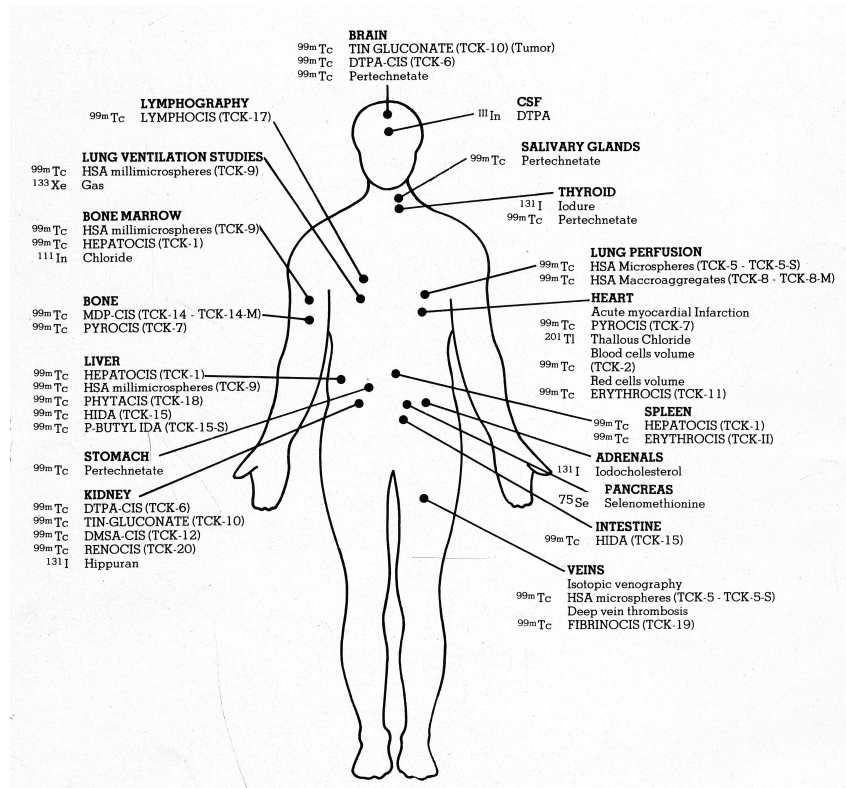
FIGURE 1.1: Scheme of ^{99m}Tc-radiopharmaceuticals and their target-organs [28].

radionuclide [11], allowing around 30 million diagnostic procedures worldwide each year [6], with approximately half of them in the United States [7]. It ideally emits a 140.511 keV photon (I = 89%), causing the least radiation dose to patients. It is almost always available in nuclear medicine departments *via* ^{99}Mo/^{99m}Tc generator systems, as described in Section 1.1.1. The versatile complex formation chemistry of ^{99m}Tc facilitated the establishment of various labelling methods to different compounds, allowing the diagnosis of almost all the major body organs like brain, liver, bone, lungs, kidney, heart *etc*, as shown in Figure 1.1.

Moreover, thanks to the well-known chemistry of ^{99m}Tc, also other Tc-isotopes have been studied: ^{94m}Tc (half-life 52.0 m) and ^{93}Tc (half-life 2.75 h) for their use in PET, ^{95m}Tc (half-life 61 d) and ^{95g}Tc (half-life 20.0 h) for SPECT applications, ^{96}Tc (half-life 4.28 d) for use in therapy (in particular in the prevention of coronary restenosis) [13].

In PET applications the radio-pharmaceutical is labelled with a β^+-emitter, that annihilates with an electron in few millimeters from the emission point, generating two *quasi*-opposite 511 keV γ-rays. The same principle of SPECT-cameras is used for PET-ones; but in this case PMTs are without collimators, since the detection in coincidence of both γ-rays simply define their Line Of Response (LOR).

In PET applications the most used nuclide is Fluorine-18 (^{18}F, half-life = 109.77 m),

mainly produced in small size cyclotrons. In the mid-1970s the use of ^{18}F-deoxyglucose (FDG) and PET-cameras yielded excellent quality images of the brain, the heart and tumours [1]. However, beside ^{18}F many other radionuclides are used in PET, such as ^{11}C (half-life = 20.334 m), ^{13}N (half-life = 9.965 m) and ^{68}Ga (half-life = 67.71 m), as well as many non-standard positron emitters, as reported in [29, 30]. Even if the main interest of radio-pharmaceutical chemists has progressively shifted towards the investigation of an increasing number of PET tracers, these do not add a significant improvement to diagnostic outcomes when compared to ^{99m}Tc agents [26].

As for the case of SPECT/CT combined imaging methods, with the advent of PET/CT or PET/MRI (Magnetic Resonance Imaging), much more precise insights have become available, allowing to merge anatomical and functional informations. Although clinical PET/CT applications have completely replaced PET in oncology, clinical applications of PET/MRI are currently not clearly defined, due to a lack of clinical data [31].

Since modern SPECT and PET imaging devices have reached a very high sensitivity, extremely small amounts of radio-pharmaceuticals can be detected in a living organism. As a drawback, the resolution of these cameras is in the range of mm, which limits the spatial localization of radio-pharmaceuticals. However, PET allows better quantification than SPECT, that has some limitation in resolution linked to the strong attenuation of the 140 keV γ-line and to the collimator size. On the other hand, MRI and CT can provide excellent spatial resolution; however, at the moment MRI still has a very limited sensitivity, although substantial efforts are under development [25].
Similarly a research towards the physically possible limits occurs for scintillation cameras, whose resolutions are constantly improving. Only in case of PET the spatial resolution is physically limited, due to the annihilation of the β^+-radiation that occurs in about few mm around the emission point.

Even if PET/CT has completely replaced PET for oncology applications, SPECT continues to be the workhorse in many hospitals and nuclear medicine centers [27].
Moreover, the cost of SPECT instruments also make it more attractive in developing countries where the cost of a scan is still prohibitive for many patients.

At the end it has to be noted that worldwide approximately 70% of nuclear medicine procedures are still based on ^{99m}Tc-radiopharmaceuticals and almost all of nuclear imaging in cardiology is carried out by using ^{99m}Tc perfusion tracers [26]. For these reasons the current and future supply of ^{99m}Tc (and thus ^{99}Mo) is one of the key points of this work, as hereafter discussed.
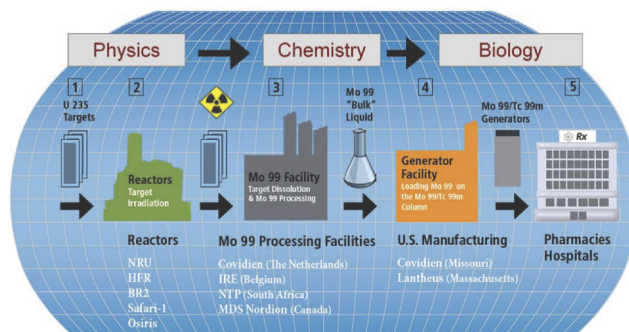
FIGURE 1.2: Sketch of the actual ^{99m}Tc production chain, based on the production of ^{99}Mo in reactors and the delivery in hospitals of ^{99}Mo/^{99m}Tc generator systems [32].

1.1.1 Present and future of ^{99}Mo, ^{99m}Tc supply

As already mentioned in Chapter 1, ^{99m}Tc is the most commonly used SPECT radionuclide and it is almost always available in nuclear medicine departments *via* ^{99}Mo/^{99m}Tc generator systems [11]. Figure 1.2 outlines the actual ^{99m}Tc production chain, based on the production of ^{99}Mo *via* the ^{235}U(n,f)^{99}Mo fission route on HEU targets (typically containing more than 80% of ^{235}U). The second stage is the radiochemical extraction and purification of ^{99}Mo, and the third stage is the production of ^{99}Mo/^{99m}Tc generator systems, then delivered in hospitals.

^{99}Mo/^{99m}Tc generator systems are composed by an Al_2O_3-column loaded by adsorption with ^{99}Mo as ammonium molybdenate, in which the daughter activity is periodically removed by elution with saline solution (since the $[^{99m}TcO_4]^-$ is less tightly bound to the column than $[^{99}MoO_4]^{2-}$). Conveniently for daily use, the maximum ^{99m}Tc activity is reached in generator systems about four half-lives after the previous elution, i.e. each 24 hours, as shown in Figure 1.3 [33]. In this way the fast decay of ^{99m}Tc (half-life $\tau_{1/2}$ = 6.0067 h) is not a problem during production and delivery times, since it is produced by decay of the longer lived parent nuclide ^{99}Mo (half-life $\tau_{1/2}$ = 65.976 h).

It is important to remind that due to the particular decay scheme of ^{99}Mo (Figure 1.4), about 87.6% of times decays to ^{99m}Tc, while the remaining 12.4% decays directly to the ground state β-emitter ^{99g}Tc (half-life $\tau_{1/2}$ = 2.111·10^5 y). This branching ratio means that the ^{99m}Tc post equilibrium activity is actually lower than the ^{99}Mo one. In fact, the post equilibrium activity is reached in *transient equilibrium* generators after about 16 daughter half-lives: in general at this time the daughter activity slightly exceeds the parent activity. In case of ^{99}Mo/^{99m}Tc generator systems, the post equilibrium activity is reached after about 72 hours post elution and ^{99m}Tc activity never reaches the ^{99}Mo one.
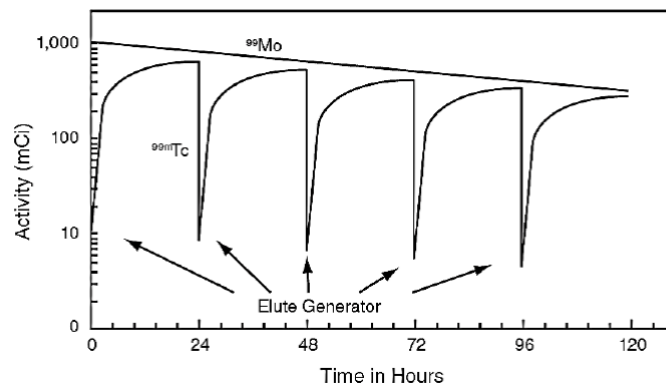
FIGURE 1.3: In-generator activity vs time of ^{99}Mo (normalized at 1000 mCi) and ^{99m}Tc in case of elution every 24 hours [33].
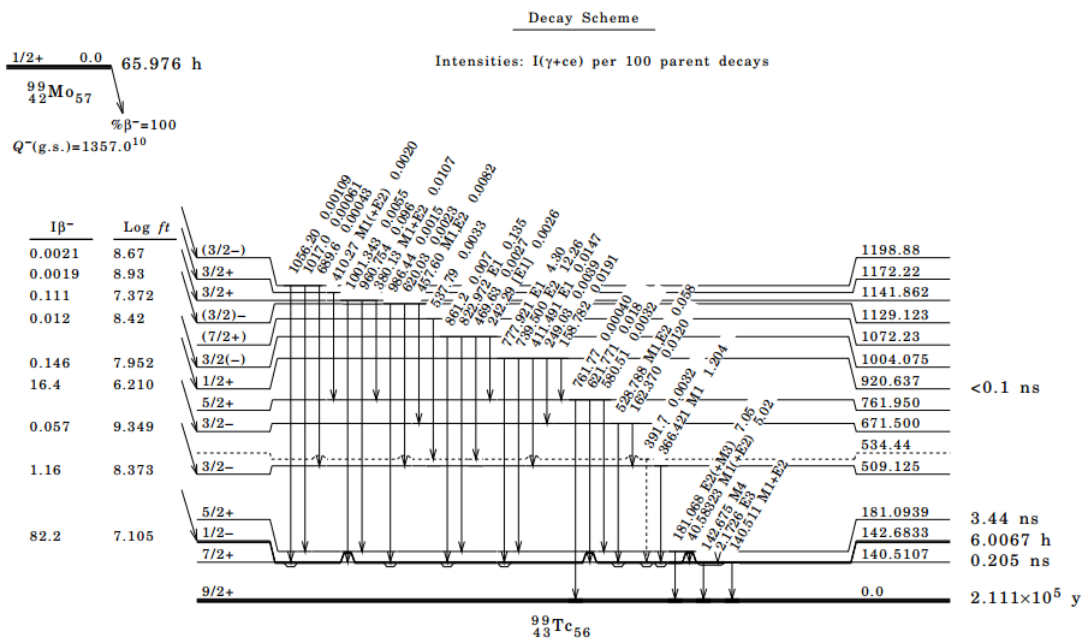

FIGURE 1.4: Decay scheme of ^{99}Mo [34].

Currently in hospital ^{99m}Tc is extracted from generators as a sterile, colourless and isotonic solution of sodium pertechnetate Na^{99m}TcO$_4$, which is the base of every subsequent ^{99m}Tc-labelled radiopharmaceutical.

As previously mentioned, ^{99}Mo sources are currently produced in nuclear reactors. Uniquely to meet the world demand of ^{99}Mo, five reactors and four precessing facilities are currently needed (Figure 1.5).

All major producers today generate this vital nuclide *via* the ^{235}U(n,f)^{99}Mo fission route on HEU targets, maximizing the ^{99}Mo production rate and minimizing the quantity of minor actinides generated. However, an international effort is in progress to reduce and eventually eliminate the use of HEU to LEU targets, since they contain weapons-grade
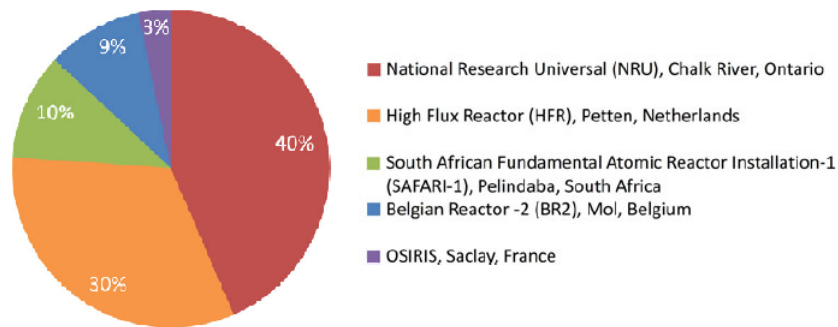
FIGURE 1.5: Worldwide reactors used by large-scale producers of ^{99}Mo and percent production [35].

TABLE 1.2: Alternative surveyed technologies for the production of ^{99}Mo [6].

Short-term technologies before 2017	- Current LEU targets in research reactors - LEU solution reactors - ^{98}Mo activation in research reactors - ^{100}Mo(p,x)^{99}Mo,^{99m}Tc in cyclotrons
Mid-term technologies 2017 - 2015	- Photofission of ^{238}U - ^{100}Mo(γ,n)^{99}Mo
Long-term technologies 2015 - 2035	- LEU fission with spallation neutrons - ^{100}Mo(n,2n)^{99}Mo

uranium [36]. Moreover, in recent years (2007-2010) repeated scheduled/unscheduled shut-downs of the main production facilities of North America and Europe caused temporary shortages of ^{99}Mo/^{99m}Tc radionuclides on the international market. It is the case of the National Research Universal (NRU) reactor at Chalk River in Canada, the principal producer of ^{99}Mo with about 40% of the global production (mainly for Canada and the USA market), and the High Reactor Flux (HRF) in Petten (The Netherlands), the main European supplier with about 25% of worldwide ^{99}Mo production. The first reactor was expected to be definitely shut down in 2010, the second one has a scheduled closure in 2016.

Repeated shortages of these vital nuclides and the control actions against the proliferation of nuclear weapons have prompted new ideas about alternative arrangements, both based on accelerators and the use of non-strategic materials in reactors. The useful report of the Nuclear Energy Agency (NEA) summarizes all assessment results of alternative technologies for ^{99}Mo production [6], divided into three categories (short-term, mid-term and long-term solutions), as indicated in Table 1.2.

In the following sections the short-term technologies will be discussed in detail, i.e. the reactor- and cyclotron-based production routes, while the mid- and long-term technologies will be not examine in depth, since they are currently not mature and lack informations about production yields and costs. In this work particular attention has been given to the use of accelerators, since after the Fukushima incident in Japan in

TABLE 1.3: Specific Activity (SA) of commercial ^{99}Mo/^{99m}Tc generator systems.

Activity	SA
0.2 Ci	10 Ci/g
7.4 GBq	370 GBq/g
2 Ci	100 Ci/g
74 GBq	3.7 TBq/g
20 Ci	1000 Ci/g
740 GBq	37 TBq/g

March 2011 the importance of founding new production-routes not based on reactors has been increased in today's radioisotope production scenario [13].

It is important to note that a common issue of almost all alternative technologies aimed to future production of this vital nuclide is the final ^{99}Mo Specific Activity (SA), i.e. the ratio of total ^{99}Mo activity and target mass [Bq/g], that is usually lower than that of standard technetium generator systems (Table 1.3). In order to reach the same ^{99}Mo activity, an heavier mass has to be loaded into the column, that has to be bigger than the ordinary ones, since the capacity of alumina to adsorb Mo is limited to about 20 mgMo/g of alumina [37], determining larger dimensions of the final generator system. Moreover, the risk of ^{99}Mo breakthrough in such eluate is high and the eluate volumes are large [11]. This determines the impossibility to use the standard generator technology (i.e. made with alumina column) or the need to apply a later concentration procedure for the ^{99m}Tc solution, as proposed in [37].

Instead of ordinary ^{99}Mo/^{99m}Tc generator technology, in order to produce technetium for local use, a large centralised generator or ^{99m}Tc separating facility, named *extraction generator*, has been proposed [38]. Several countries (India, Kazakhstan, Uzbekistan and some others) use ^{99m}Tc extraction generator facilities for regional ^{99}Mo production or utilize the innovative *gel generator* technology [39, 40, 41].

These portable generators operate even with ^{99}Mo of low- and medium-specific activity, since the MoZr mixture is used as column matrix itself. Significant research and development is being done to improve this powerful technology [42, 43, 44]. Recently a novel possibility to provide portable technetium generators with low specific activity ^{99}Mo was proposed [45]. This technology, based on nanocrystalline γ-Al$_2$O$_3$ as column matrix, has a very high maximum sorption capacity (about 10 times higher than that of ordinary generator, i.e. 200±5 mg Mo/g) and provides good ^{99m}Tc elution yield (yield > 80%), with adequate radioactive concentration of high purity technetium, suitable for radiopharmaceuticals formulation.

Among the accelerator-based routes, the α-induced reaction on zirconium targets is the only one that permits to reach high SA and for this reason it has been studied in this work, as briefly presented hereafter and in detail in Chapter 4.
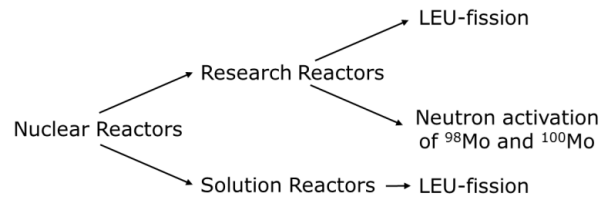
FIGURE 1.6: Possible reactor-based ^{99}Mo production technologies.

1.1.2   Reactor-based production methods

The possible reactor-based ^{99}Mo production technologies that could replace the current HEU route are indicated as short term solutions (namely available before 2017) and are outlined in Figure 1.6.

The principle option, already adopted by some of the ^{99}Mo producers, is the fission of Low Enriched Uranium (LEU) targets in research reactors. This method involves only proliferation-safe reactor-grade uranium, with an enrichment in ^{235}U lower than 20%. The main technological issue of LEU route is the need of fabrication of dense targets, i.e. targets with high specific ^{235}U content, compatible with the well established ^{99}Mo separation process [6]. In 2008 were proposed LEU metallic targets, that could achieve ^{99}Mo yields comparable or even higher than in the current HEU targets made with U-Al alloys, thanks to the higher metallic uranium density (about 19 g/cm^3), than the uranium amount in HEU U-Al targets (about 16.6 g/cm^3) [46].
Another point is the volume of nuclear wastes generated during the processing of the irradiated targets, that is considerably higher than in the case of HEU targets. However, the LEU-based route presents also some advantages over the HEU-based one, i.e. the proliferation resistance, the easier availability of the target material and the easier compliance for targeting transportation and processing.

An alternative to standard solid targets is the use of solution nuclear reactors for the ^{99}Mo production [1]. In particular, it is currently under development an Aqueous Homogeneous Reactor (AHR) for this purpose that it is expected to be operational by 2014 (The Babcock and Wilcox Company, Charlotte, North Carolina). This option could potentially have many favourable characteristics (yield, production rate and costs), but has yet to reach full technological maturity and acceptance by regulators and users.

Beside the uranium-fission route, as indicated in Figure 1.6, there is the neutron activation of Mo-targets in research reactors *via* the ^{98}Mo(n,γ)^{99}Mo reaction (also possible with ^{nat}Mo targets) [36]. Although neutron activation in a nuclear power reactor could be feasible, currently this is not attractive for commercial users or power plant operators, as it competes with their primary purpose of generating power and it would required a

detailed safety case and potentially long approval process.

The main benefits of the activation process are the feasibility in almost any reactor with sufficient neutron flux (since the Mo-containing targets are not fissile), the lower amount of wastes generated during the irradiation and processing and the considerably lower activation of the irradiated target in comparison with the HEU case. In fact, irradiated targets in the fission route are highly radioactive and their transport to the processing facility requires careful management; with the activation route the targets transport is in principle easier, since they are less radioactive (but the volumes are considerably larger and often suitable large certified containers are not available).

On the other hand, the main issues for the activation route are the resulting medium-specific activity of ^{99}Mo, that complicates the generator technology (as discuss previously), and the possible use of highly enriched ^{98}Mo targets, that is a high cost, difficult available material and raise the problem of an efficient recovery of the target material. In fact, according to [47], up to the 90% of the target material can be recycled.

1.1.3   Accelerator-based production methods

In planning the production of a radionuclide for specific applications, particular attention has to be paid to nuclear reaction data, as they allow the optimization of irradiation parameters such as suitable target-projectile combination, projectile energy and target thickness [3, 13]. Also the knowledge of decay and chemical data is very important, since the first quantify the *in vivo* and *in vitro* effects of radiation, and the second are mandatory in the separation of produced nuclide from the stable and bulk matrix, assuring the purity of the final product [13].

In this section the cross sections of the short-term accelerator-based production routes will be presented, i.e. the ^{100}Mo(p,x)^{99}Mo,^{99m}Tc and ^{96}Zr$(\alpha,$n$)^{99}$Mo reactions, discussed in detail respectively in Chapter 3 and 4. However, even if not studied in this work, different accelerator-based production routes are currently investigated by the scientific community worldwide. In recent papers the photo-fission processes of ^{235}U, ^{238}U and ^{100}Mo targets are analysed [48, 49], as the neutron-induced reaction on ^{98}Mo and ^{100}Mo targets [50, 51], the deuteron-induced reactions on ^{98}Mo [52] and ^{232}Th targets (recently measured at ARRONAX and soon published), and the proton-induced fission of ^{232}Th [53].

1.1.3.1   The p-induced reactions ^{100}Mo(p,x)^{99}Mo,^{99m}Tc

The first evaluation of the ^{100}Mo(p,x)^{99}Mo,^{99m}Tc reactions was performed in 1971 [54]. In the last 40 years different experimental campaigns repeated such measurements [17,
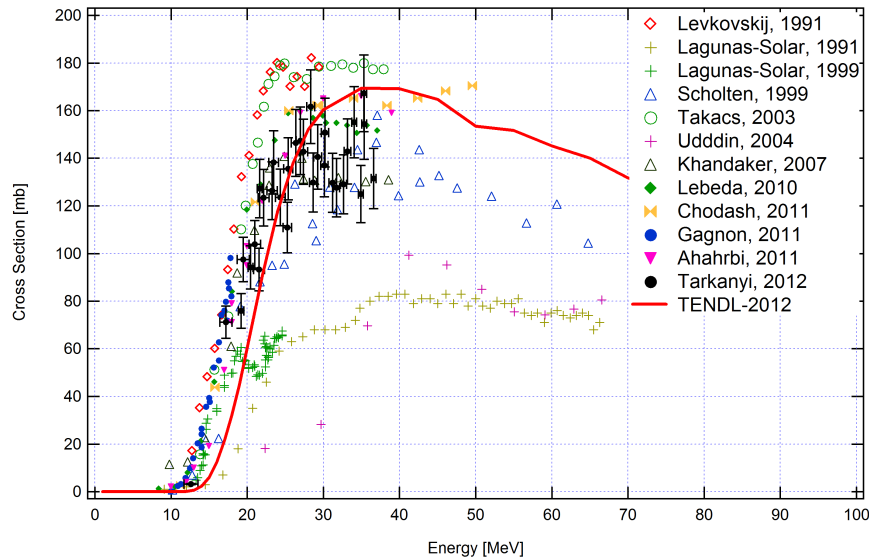
FIGURE 1.7: Collection of the cumulative cross sections of the ^{100}Mo(p,x)^{99}Mo reaction theoretically and experimentally evaluated.

55, 56, 57, 58, 59, 60, 61, 62, 63, 64, 65, 66, 67], obtaining an unexpected spread in results, due to the different Tc isotopes and isomeric states generated and the use of non standard experimental procedures. This is the reason why in 2012 all these measurements have been investigated in detail by Tarkanyi et al. [68], also presenting a new evaluation of all the p-induced reactions on natural molybdenum targets. However, due to the use of ^{nat}Mo as target the authors obtained several other Tc-isotopes, and thus further experimental investigations on ^{100}Mo(p,x)^{99}Mo,^{99m}Tc reactions are still demanded [9], by using enriched ^{100}Mo targets commercially available and applying adequate techniques for γ-ray identification.

The ^{99}Mo nuclide can be produced by the main (p,pn) reaction on ^{100}Mo targets (E_{THR} = 8375.45 keV [69]), and also from the decay of ^{99m}Nb ($\tau_{1/2}$ = 15.0 s) and ^{99g}Nb ($\tau_{1/2}$ = 2.5 m), for proton energies E_P > 10 MeV. Figure 1.7 shows the theoretical excitation functions available from TENDL library [23] and the most recent evaluations of the cumulative ^{100}Mo(p,x)^{99}Mo reaction. Experimental evaluations are consistent up to $E_P \approx 25$ MeV, while at higher energy values a spread can be noted among the results obtained by different authors (including error bars extension, the maximum spread value is about 100 mb). This large disagreement can be referred to systematic errors in the contributing parameters (beam intensity, detector efficiency, etc) [68]. In fact, no corrections have to be applied at the 739.5 keV γ-line of ^{99}Mo.

Regarding the ^{100}Mo(p,2n)^{99m}Tc cross section, Figure 1.8 collects the theoretical and experimental evaluations, showing that in the energy range 5-70 MeV there is a single peak, centred around 15 MeV and twenty years ago estimated to be about 300 mb [55]. The theoretical excitation function [23] seems to underestimate the peak value. In fact
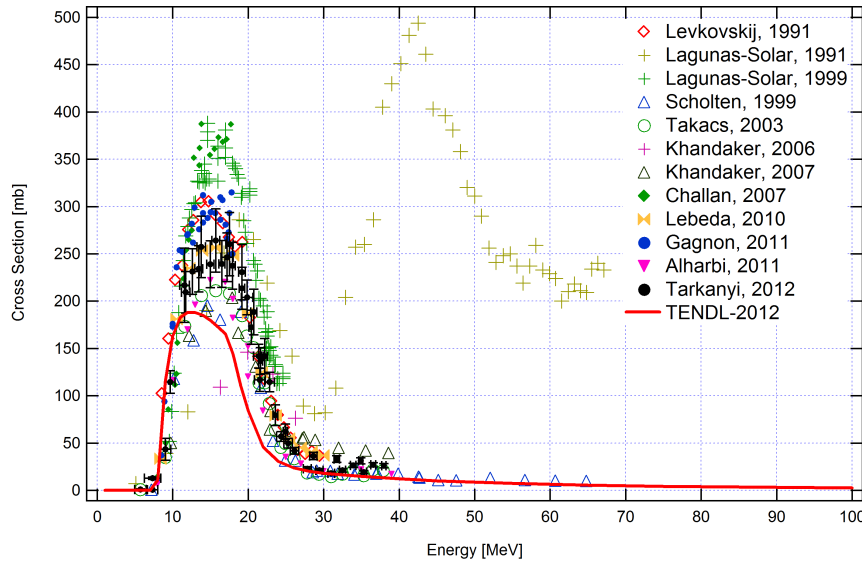
FIGURE 1.8: Collection of the cross sections of the ^{100}Mo(p,2n)^{99m}Tc reaction theoretically and experimentally evaluated.

later measurements have reduced such a value to about 200 mb [57, 58, 61], while more recent evaluations point out higher peak values about 250 mb [64, 68] and up to 300 mb [17].

Analysing the different works, many reasons may be advanced to explain such an unusual spread: different experimental set-ups, target material purity, contaminant levels, isotopic compositions, *ad-hoc* procedures followed during sample irradiations and detection methods. Moreover different correction methods are applied in calculating the ^{99m}Tc activity, as deduced by the 140.511 keV photon peak emission through γ-spectrometry measurements. Indeed the total counts (C_{TOT}) at the 140.511 keV γ-line are due to different contributions: the ^{99m}Tc direct produced in-target (Tc_{DIR}), the ^{99m}Tc produced by ^{99}Mo decay (Tc_{DEC}) and the small contribution of direct ^{99}Mo decay (Mo_{DIR}). The small contribution of ^{99}Mo to the 140.511 keV line is not similarly reported in different databases: for example, in [69] such contribution is not present, while in [34] the 140.511 keV line it is reported with a relative intensity $I_{140}^{R} = 5.1\%$ (considering $I_{739}^{R} = 100$ %), thus with an absolute intensity $I_{140} \approx 0.625\%$, since $I_{739} = 12.26$ %.

In order to estimate the number of counts (and consequently the activity) of ^{99m}Tc direct produced in-target, the following correction has to be applied:

$$Tc_{DIR} = C_{TOT} - (Tc_{DEC} + Mo_{DIR}) \tag{1.1}$$

Particular care must be taken in the activity evaluation of the co-produced ^{99}Mo nuclide and a specific protocol has to be followed aimed to a final reasonable relative uncertainty ($< 20\%$) of the direct produced ^{99m}Tc.
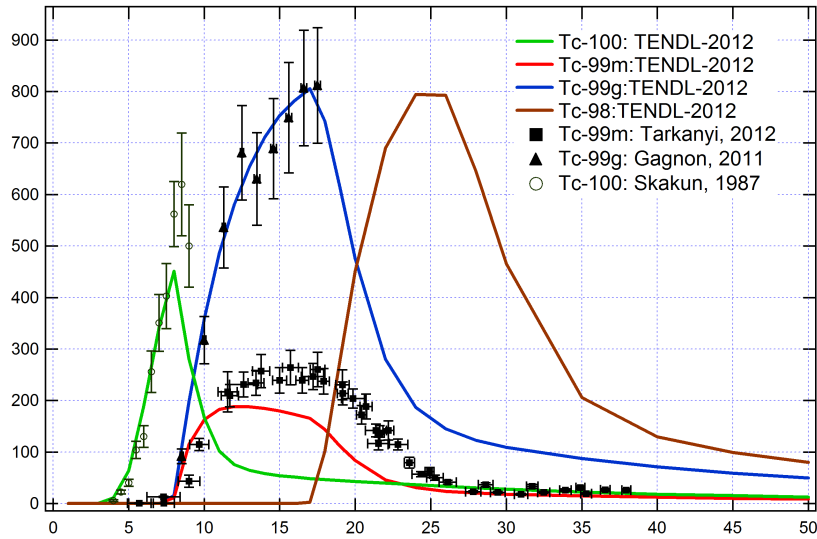
FIGURE 1.9: Collection of the cross sections up to the (p,6n) level theoretically and experimentally evaluated for all Tc-isotopes produced during the proton irradiation of a 100% ^{100}Mo target.

In case of a direct ^{99m}Tc production, the production of Tc-contaminants has to be carefully considered, since they would remain in the final Tc product (more details can be found in Chapter 3). For this reason, Figure 1.9 reports the cross sections up to the (p,6n) level theoretically [23] and experimentally [17, 58, 70] evaluated for all Tc-isotopes produced during the proton irradiation of a 100% ^{100}Mo target.

Considering $E_P < 25$ MeV, only the long lived contaminants ^{99g}Tc ($\tau_{1/2} = 2.111 \cdot 10^5$ y), ^{98}Tc ($\tau_{1/2} = 4.2 \cdot 10^6$ y) and ^{97g}Tc ($\tau_{1/2} = 4.21 \cdot 10^6$ y) are co-produced in ^{100}Mo target (Table 1.4). Among them, ^{99g}Tc is the most important one, as it is directly produced in target and also by decay of ^{99m}Tc and ^{99}Mo. Further studies and experimental campaigns are necessary in to validate the ^{100}Mo(p,2n)^{99g}Tc cross section in the entire energy range, since the estimation made by [17], in agreement with the theoretical one, ends at $E_P = 18$ MeV.

1.1.3.2   The α-induced reaction ^{96}Zr(α,n)^{99}Mo

The first evaluation of the ^{96}Zr(α,n)^{99}Mo cross section was performed in 1995 [21], by using ^{nat}Zr targets (its natural composition is reported in Table 1.5) and re-scaling the results for an ideal 100% enriched ^{96}Zr target. In case of the ^{96}Zr(α,n)^{99}Mo route, no Tc-contaminants are co-produced in target, and the resulting ^{99}Mo is characterized by a very high specific activity, since it is the only radioactive Mo-isotope produced. In fact, the only radioactive Mo-isotopes that could be produced *via* the ^{96}Zr(α,7n) reaction are

TABLE 1.4: Technetium isotopes expected to be produced by the ^{100}Mo(p,x) reactions.

Reaction	E_{THR} [MeV]	Product	Decay	$t_{1/2}$	Daughter
p,6n	41.72	^{95m}Tc	EC	61 d	^{95}Mo (96.1%) (stable)
			IT		^{95g}Tc (3.9%)
		^{95g}Tc	EC	20 h	^{95}Mo (stable)
p,5n	33.77	^{96m}Tc	EC	51.5 m	^{96}Mo (2.0%)(stable)
			IT		^{96g}Tc (98.0%)
		^{96g}Tc	EC	04.28 d	^{96}Mo (stable)
p,4n	24.21	^{97g}Tc	EC	$4.2 \cdot 10^6$y	^{97}Mo (stable)
		^{97m}Tc	IT	91 d	^{97g}Tc (96.1%)
			EC		^{97}Mo (3.9%) (stable)
p,3n	16.85	^{98}Tc	β^-	$4.2 \cdot 10^6$y	^{98}Ru (stable)
p,2n	7.794	^{99m}Tc	IT	6.01 h	^{99g}Tc (99.9963%)
			β^-		^{99}Ru (0.0037%) (stable)
		^{99g}Tc	β^-	$2.1 \cdot 10^5$y	^{99}Ru (stable)
p,n	0.962	^{100}Tc	β^-	15.46 s	^{100}Ru (99.9982%)(stable)
			EC		^{100}Mo (0.0018%) (stable)

TABLE 1.5: Natural composition of Zirconium [69].

Zr-90	Zr-91	Zr-92	Zr-94	Zr-96
51.45%	11.22%	17.15%	17.38%	2.80%

^{93m}Mo and ^{93g}Mo (half-life 6.85 h and $4.0 \cdot 10^3$ y respectively), with a threshold energy of 54.9 MeV [69].

Figure 1.10 reports the ^{96}Zr(α,n)^{99}Mo cross section experimentally [21] and theoretically [23] evaluated, while in Chapter 5 the new measurement performed in this work is presented and discussed.

Figure 1.10 shows that the experimental and theoretical evaluations of the ^{96}Zr(α,n)^{99}Mo reaction both report a single peak around 13-15 MeV, with a maximum value of 110-130 mb. These cross sections have an energy shift of about 1.5 MeV, but an excellent agreement in the trend.

Figure 1.10 also reports the theoretical cross sections (taken from TENDL library [23]) for the production of ^{99m}Nb and ^{99g}Nb isotopes, when irradiating ^{96}Zr targets with α-beams (right axis). Considering these theoretical cross sections, since no experimental evaluations have been found in EXFOR database [71], it is evident that up to 20 MeV the production of ^{99}Mo by decay of ^{99m,g}Nb isotopes is negligible, since the (α,p)$^{99m+g}$Nb reaction is less than 5% of the (α,n)^{99}Mo one. On the contrary, the contribution from ^{99m,g}Nb isotopes decay is important for energies higher than 26 MeV, as the cross section associated to the overall production of ^{99m}Nb and ^{99g}Nb is about 30% of the (α,n) reaction.

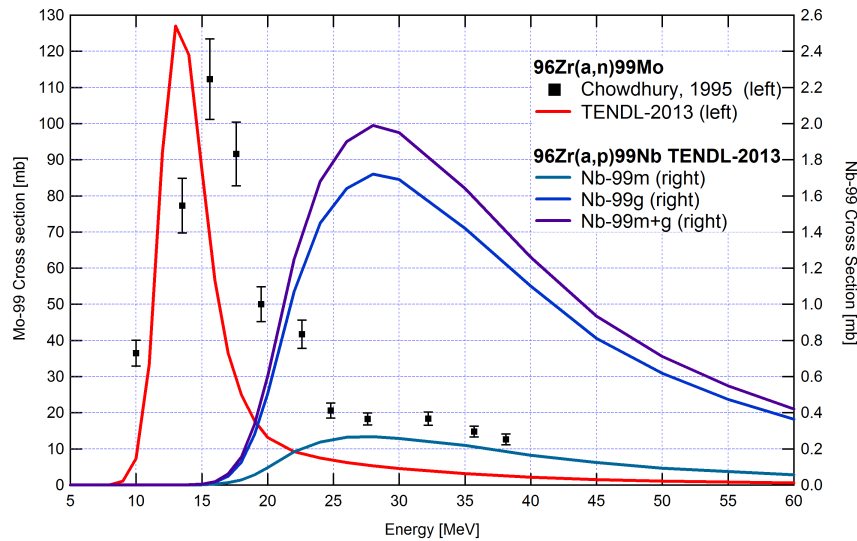In the evaluation performed by Chowdhury et al. no corrections have been applied for

FIGURE 1.10: Collection of the theoretical and experimental evaluations of $(\alpha,\text{n})^{99}$Mo and $(\alpha,\text{p})^{99m,g}$Nb reactions on ^{96}Zr targets (respectively on the left and right axis) [21, 23].

the $(\alpha,\text{p})^{99m,g}$Nb reactions, that have been considered negligible in the entire energy range [21]. The same assumption has been taken into account for the cross section measurement performed in this work and presented in Chapter 4.

1.2 Radiotherapy

Radiation therapy is mostly performed by using external beams of electrons, x-rays and γ-rays from radioactive sources (as ^{60}Co), high-energy γ-rays from accelerators or hadrons as neutron, protons (enough quantities of short-lived positron emitters formed during proton therapy allow PET studies for dose localization [72]) and heavy ions. In particular, the use of electrons and photons constitutes conventional therapeutic practice and thus the data needed are well documented [73].

In addition to external therapy, some radioisotopes are used internally, introducing the therapeutic nuclide in a given part of the body either mechanically, *Brachytherapy*, or biochemically, *Endoradiotherapy.*

In brachytherapy both liquid (conglomerates or colloids) and solid sources (as seeds) can be used, respectively introduced by injection or surgery. On the contrary, endoradiotherapy is a systemic and non-invasive treatment modality that nevertheless presents some disadvantages, such as determining the exact range of radiation, the *in vivo* stability of radio-pharmaceuticals, the possibility of immuno-chemical agents, etc. [73]. However, in this work the attention is focused on endoradiotherapy applications, that allow treatment at a cellular level, killing the cancer cells without harming patient.

Depending on the size, type and position of the tumour, the radioisotope used in endoradiotherapy has to be optimized, by choosing appropriate half-life (according to the bio-distribution of the vector) and emitted radiation. For example, β^--radiation with E < 1 MeV dissipate over 1 to 10 mm, thus allowing the treatment of macro-clusters cells; on the contrary, α-radiation with E < 6 MeV dissipate its energy over 0.1 mm, being appropriated for isolated cells or micro-clusters.

As already mentioned, theragnostics is a forefront treatment strategy that combines therapeutics with diagnostics. By using a single nuclide, such as ^{67}Cu, that emits radiation both suitable for therapy (such as α or β^- particles) and diagnostics (as γ radiation), or by using pairs of isotopes, such as ^{44}Sc/^{47}Sc, ^{64}Cu/^{67}Cu, ^{124}I/^{131}I, etc., it is possible to make dosimetry prior therapy and monitor patient response.

In conclusion there is a need of radionuclides with different decay radiation, half-life and chemical properties; Table 1.1 reports some isotopes used in targeted therapy and their radiation characteristics, but many emerging nuclides are currently studied worldwide.

1.2.1 The emerging role of ^{67}Cu in RAIT

A crucial branch of endotherapy is RAdio-Immuno Therapy (RAIT), that uses monoclonal antibodies as highly selective bio-active molecules for systemic nuclide therapy. Thanks to continuous efforts to improve their efficacy, a clinical impact of RAIT is already apparent in the treatment of haematological malignancies, especially for non-Hodgkin's lymphoma [74].

Currently ^{131}I (half-life 8.0252 d) and ^{90}Y (half-life 64.053 h) are most widely used β^--emitters in RAIT clinical trials. However, the physical properties of ^{67}Cu, reported in Table 1.6, are very well suited for its application in RAIT. In fact, the β^--radiation emitted during ^{67}Cu decay (characterized by a mean energy of 141 keV and a total intensity of 100% [69]) has a mean range of about 0.2 mm, resulting to be very appropriate for the treatment of small tumours, especially up to 5 mm in diameter [74].

Moreover, the low intensity γ-rays emitted in the energy range 91-184 keV, makes ^{67}Cu more suitable for pre-therapy diagnostic imaging than ^{131}I, that instead presents high intensity γ-radiation, increasing the whole dose to patients and the radiation burden of the hospital staff [74].

In addition, the half-life of ^{67}Cu (61.83 h) is long enough to permit the accumulation of antibodies in the tumour site, due to their relatively slow pharmaco-kinetics. In fact, residence time of antigen-antibody complex is quite variable, especially on solid tumours, ranging from 12 hours up to 3 days; however, in general 1-2 days are required to attain maximum concentration in tumours [75].

TABLE 1.6: Physical properties of ^{67}Cu (half-life 61.83 h) [69].

β^--radiation	Energy [keV]	Intensity [%]
	51.0	1.10
	121	57
	154	22.0
	189	20.0
γ-radiation	Energy [keV]	Intensity [%]
	91.266	7.00
	93.311	16.10
	184.577	48.7

At the end it is important to note that ^{67}Cu has a stable daughter (^{67}Zn) and presents favourable coordination chemistry for attachment of various chelate-monoclonal conjugates [75].

For these reasons in 1993 a pilot study with ^{67}Cu, produced at Brookhaven National Laboratory (BNL, New York, USA), was performed in a human lymphoma therapy trial [76, 77], while in 2002 a detailed review about the use of ^{67}Cu in RAIT has been performed by Novak-Hofer and Schubiger [74].

1.2.2 Production of ^{67}Cu: the ^{68}Zn(p,2p)^{67}Cu reaction

Similarly to the case of ^{99m}Tc, also the production of the emerging nuclide ^{67}Cu started in nuclear reactors: as reported in a work by Rowshanfarzad [8], the first paper about the use of the ^{67}Zn(n,p)^{67}Cu reaction was published in 1969 by O'Brien et al. [78]. However, also the production of ^{67}Cu is shifting over cyclotrons, since the quality (co-production of many active and inactive impurities) and quantity of the final product obtained in nuclear reactors do not meet the specification required for its used in RAIT [11].

In a recent paper by Qaim (2013) the need of 70 MeV proton beams for the production of ^{67}Cu is underlined [79]. As reported, a large scale production of ^{67}Cu is not feasible *via* the new routes ^{64}Ni(α,p), ^{70}Zn(d,αn) and ^{70}Zn(p,α), even if highly enriched target material are used [80, 81, 82, 83, 84].

On the contrary, the ^{68}Zn(p,2p) reaction is the most efficient way for producing high quality ^{67}Cu. Since 1955 this route has been investigated by many researcher, as a possible way to produce no-carrier added (i.e. a preparation of a radioactive isotope which is essentially free from stable isotopes of the element in question) ^{67}Cu [55, 75, 85, 86, 87, 88, 89].

In 2005 Bonardi et al. performed an evaluation of the ^{67}Cu production by using natural zinc targets irradiated by proton-beams [90]: this route is however not favourable, due to both lower ^{67}Cu specific activities and higher amounts of Cu-contaminants co-produced.
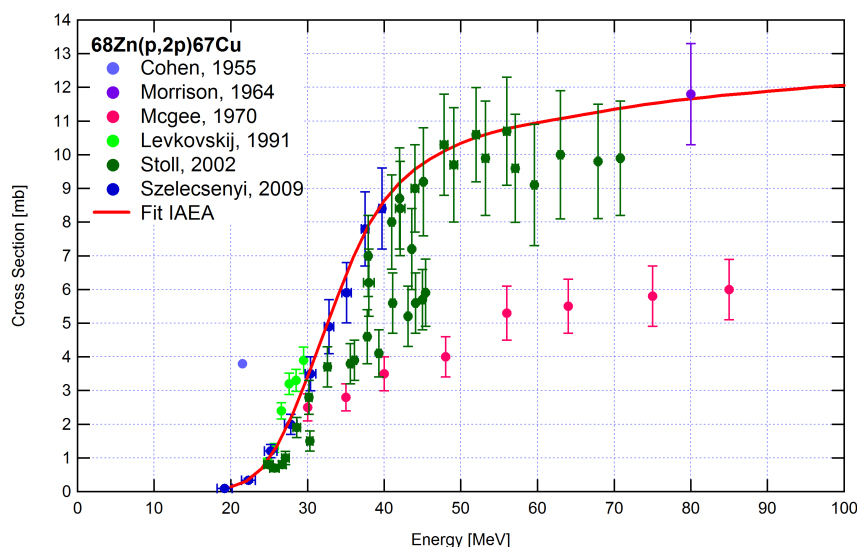
FIGURE 1.11: Collection of the experimental evaluations of the $^{68}Zn(p,2p)^{67}Cu$ cross section in the energy range 0-100 MeV.

In 2007 a comparison between ^{67}Cu production in cyclotrons (*via* the $^{68}Zn(p,2p)$ reaction) and in electron accelerators (*via* the $^{68}Zn(\gamma,p)$ reaction) has been performed by Ayzatskiy et al. [91]. The photo-nuclear reaction induced by high-energy bremsstrahlung photons is the only method that seems to be competitive with the proton-induced one. However, results refer to natural zinc targets and are thus affected by impurities (such as ^{62}Zn, ^{65}Zn and ^{69m}Zn). Moreover, authors stated that the disadvantage of the photo-nuclear route is the necessity of treat a large-mass target of low specific activity (about 10 mCi/g, i.e. 370 MBq/g) [91].

For these reasons, many studies have been carried out about the separation procedure for ^{67}Cu from proton irradiated zinc [75, 92, 93], collected in 1995 in a review by Schwarzbach et al. [94].

In 2008 an interesting paper about the production of ^{67}Cu *via* the $^{68}Zn(p,2p)^{67}Cu$ reaction considering also target recovery was published by Katabuchi et al. [95]. In 2012 another engaging paper about all aspects of ^{67}Cu production has been published by Medvedev et al., proving how this kind of research still continues to have a key role at BNL [96].

The first evaluation of the $^{68}Zn(p,2p)^{67}Cu$ cross section has been performed in 1955 by Cohen et al. [85] and over the last 58 years has been repeatedly measured in different experimental campaigns, as shown in Figure 1.11 (in the energy range 0-100 MeV) and in Figure 1.12 (up to 450 MeV). Recently the IAEA Institution has pushed the scientific community to analyse all these cross section measurements, in order to get a recommended curve, also shown in Figure 1.11 and in Figure 1.12 [22, 97].
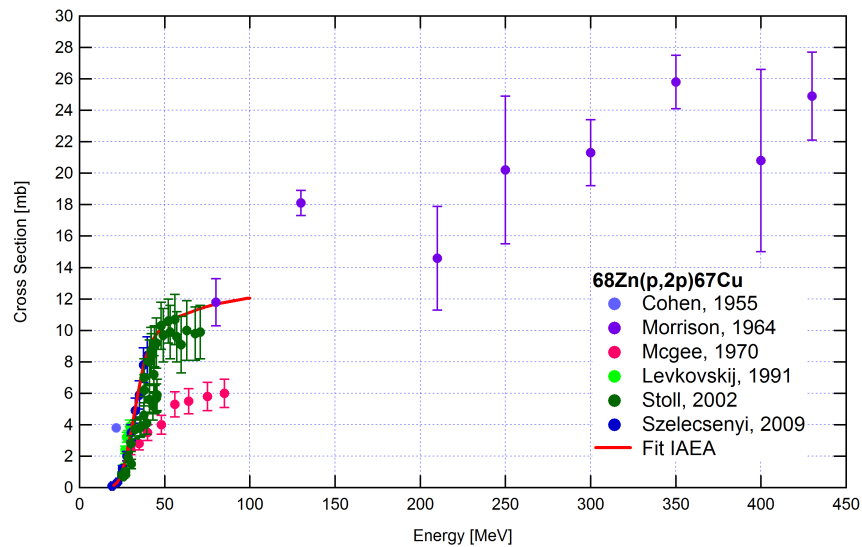
FIGURE 1.12: Collection of the experimental evaluations of the ^{68}Zn(p,2p)^{67}Cu cross section up to 450 MeV.

As can be noted from Figure 1.11 and Figure 1.12, the trend of the ^{68}Zn(p,2p)^{67}Cu cross section is quite constant and without peaks, always maintaining small values (less than 30 mb up to 450 MeV), ranging around 10 mb at 50 MeV.

It is important to note that some measurements have not been considered in the interpolation curve promoted by IAEA [22, 97], that ends at 100 MeV. In fact, the first measurement of Cohen et al. [85] has been neglected, since ≪*the error of ^{67}Cu is much higher than the 25% estimated for other cross sections.*≫. Also data of McGee et al. [87] were neglected because ≪*data needed adjustment in order to account for up-to-date IAEA monitor data. After adjustment the resulting data still do not reproduce the expected shape of the excitation function therefore they were deselected.*≫. Since the evaluation has been performed up to 100 MeV, the point at 200 MeV measured by Mirzadeh et al. [75] has been neglected. In the work of Bonardi et al. [90] only the values below 100 MeV were considered (and rescaled to 100% enriched ^{68}Zn targets, since they used natural zinc targets) and similarly from the results of Morrison et al. [86] only the value at 80 MeV was considered. The values obtained by Stoll et al. [88] were considered in the interpolation, but ≪*data in the energy range 35-45 MeV were deleted due to systematic errors in that energy range (information from authors).*≫. In a private communication one of the authors did not confirm such comment, affirming that no clear explanation has been found for the discrepancy between the series of values around 5 mb and 10 mb, as discussed in detail in Chapter 5. The low energy points measured by Levkovskij [55], once ≪*normalized by a factor of 0.8 as it was pointed out in [98]*≫, were considered in the recommended cross section. At the end, also the results obtained by Szelecsenyi et al. [89] were considered for the entire energy range (19-40 MeV).
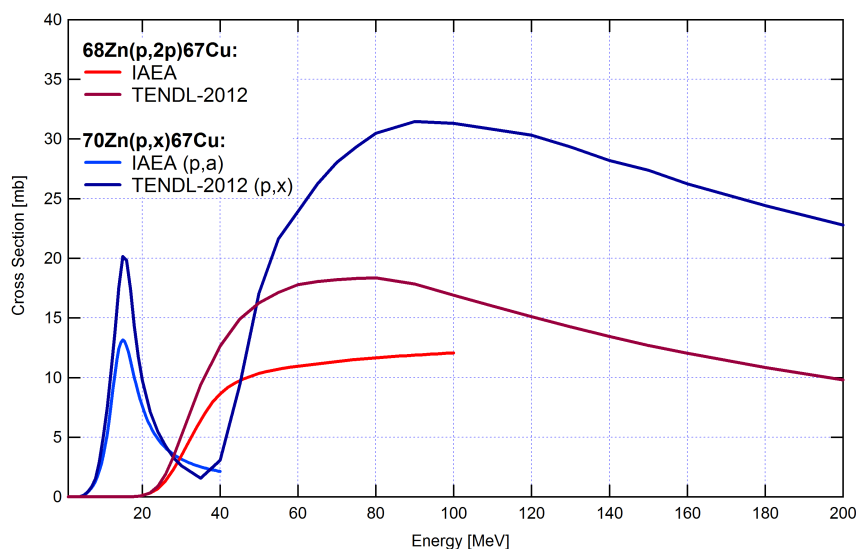
FIGURE 1.13: Theoretical evaluations of the p-induced cross section on ^{68}Zn and ^{70}Zn targets for ^{67}Cu production, in the energy range 0-200 MeV.

Since no points over 100 MeV have been considered in the recommended cross section, its trend seems to slightly underestimate the ^{68}Zn(p,2p)^{67}Cu reaction at high energy, in particular considering the results of Bonardi et al. [90] up to 150 MeV. In fact, even if the values obtained by Morrison et al. [86] end at 450 MeV, they are characterized by big oscillations and large error bars (Figure 1.12). Particular attention has to be also paid to the results of Bonardi et al., especially at high energy, since they are affected by the (p,x) reaction channels opened on ^{70}Zn. Figure 1.13 shows the recommended and theoretical cross sections for the production of ^{67}Cu on ^{68}Zn and ^{68}Zn targets, respectively from IAEA website [22] and TENDL library [23]. As already mentioned, the recommended cross section on ^{68}Zn targets ends at 100 MeV and the one on ^{70}Zn ends at 40 MeV, while all theoretical cross sections on TENDL library end at 200 MeV. Figure 1.14 shows the theoretical contribute at the ^{67}Cu production when ^{nat}Zn targets are used, respectively due to the ^{68}Zn(p,2p) and ^{70}Zn(p,x) reactions.

It is important to note that up to 70 MeV the contribution due to the ^{70}Zn(p,x) reaction may be considered negligible, since it is lower than 5%, while at higher energies such contribution increases up to 8%. However this estimation has been done by using theoretical cross sections that often overestimate the recommended ones, as reported in Figure 1.13. In particular the ^{68}Zn(p,2p) reaction, in the energy range 50-100 MeV, is overestimated of about 55%. However for the ^{70}Zn(p,x) reaction no measurements have been performed above 35 MeV (Figure 1.15), thus it is not possible to experimentally evaluate its contribute at the ^{67}Cu production when ^{nat}Zn targets are used. In conclusion, in the energy range 30-70 MeV natural zinc targets may be used in order to
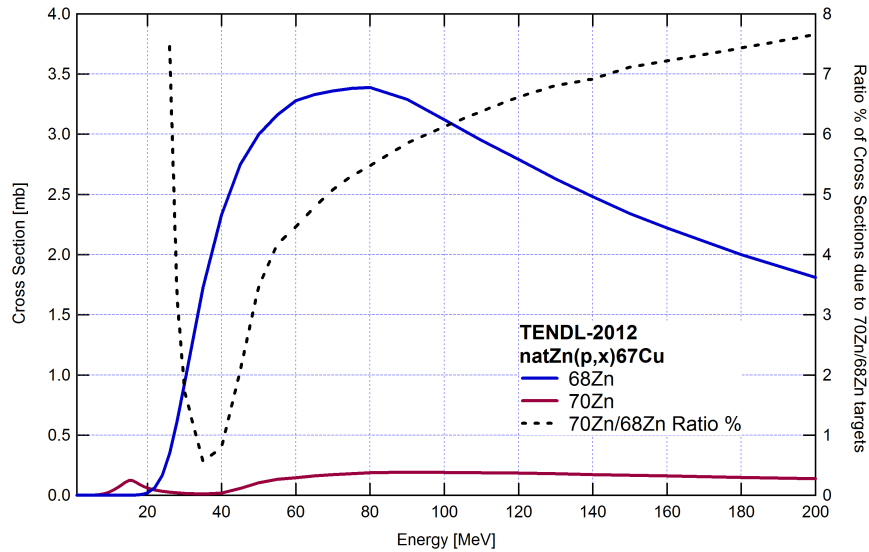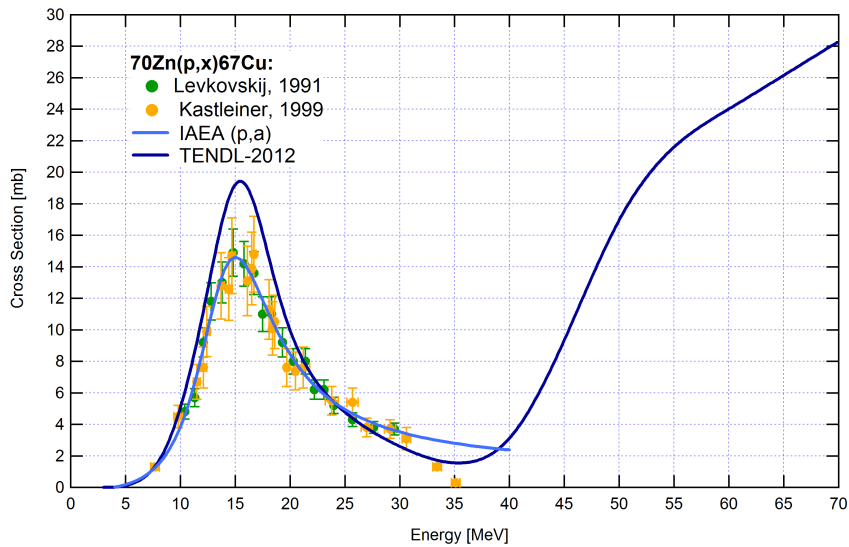
FIGURE 1.14: Theoretical evaluations of the p-induced cross section on ^{68}Zn and ^{70}Zn targets for ^{67}Cu production, in the energy range 0-200 MeV.

FIGURE 1.15: Collection of the theoretical and experimental evaluations of the cross section ^{70}Zn(p,x)^{67}Cu in the energy range 0-70 MeV.

estimate the ^{68}Zn(p,2p)^{67}Cu reaction (since the ^{70}Zn(p,x) contribute may be considered negligible), while at higher energy it is possible to overestimate the final results.

In order not to have such contamination, in this work enriched ^{68}Zn targets have been used for the measurement of the ^{68}Zn(p,2p)^{67}Cu cross section, as outlined in Chapter 5.

TABLE 1.7: Characteristics of the available beams at ARRONAX.

Beam	Accelerated particles	Energy range [MeV]	Intensity [μA]	Dual beam
Proton	H-	30-70	<375	Yes
	HH+	17	<50	No
Deuteron	D-	15-35	<50	Yes
Alpha	He++	68	<70	No

1.3 High performance cyclotrons

An interesting review of cyclotrons used in the production of radionuclides for medical applications has been written by Schmor et al. in 2010 [2]. In particular, a list of manufacturers, cyclotron models and their specifications is given (including ACSI, ABT, Best, CIAE, NIIEFA, EUROMEV, GE, IBA, KIRAMS, Siemens and Sumitomo cyclotrons). In Italy, about 50 facilities are actually installed while in 2007 about 156 cyclotrons were estimated to be used for medical purposes in Europe. In the following sections the characteristics of the cyclotron installed at ARRONAX facility (Nantes, France) and the incoming cyclotron at LNL (Padova, Italy) are outlined in detail.

1.3.1 ARRONAX

ARRONAX facility is based on a multi-particle, high energy and high intensity IBA cyclotron (Cyclone 70), installed at Nantes (France) in 2007 and fully operational since January 2011. This facility is funded by the Regional Council of Pays de la Loire, the University of Nantes, the French government (with the Centre National de la Recherche Scientifique, CNRS, and the Institut National de la Sante et de la Recherche Medicale, INSERM) and the European Union.

Table 1.7 reports the characteristics of the available beams at ARRONAX, while Figure 1.3.1 shows the scheme of the facility (the laboratories around the vaults are not reported): 4 vaults (A1, A2, P2, P3) are devoted to isotope production and are connected to hot cells through a pneumatic system; vault P1 is dedicated to the development of a neutron activator system (in collaboration with AAA company, recently validated at 350 μA proton on target); vault AX is devoted to physics, radiolysis and radiobiology experiments [5].

ARRONAX priority list covers both isotopes for therapy (^{211}At, ^{67}Cu, ^{47}Sc) and imaging (^{82}Sr, ^{68}Ge, ^{64}Cu, ^{44}Sc).

In particular, ^{82}Sr is produced routinely as radiochemical product aimed to the preparation of ^{82}Sr/^{82}Rb generator systems, irradiating RbCl targets for a week (24/24) at 2*100μA. The optimized energy range required by the ^{nat}Rb(p,x)^{82}Sr reaction (E =
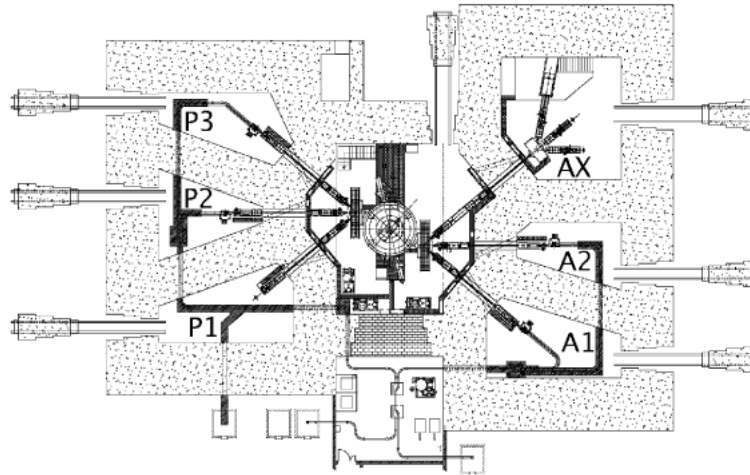
FIGURE 1.16: Scheme of the facility ARRONAX without the laboratories around the vaults [5].

68.7-40 MeV), permits the tandem production of ^{68}Ge for the realization of ^{68}Ge/^{68}Ga. In fact, the required energy for ^{68}Ge production *via* the ^{69}Ge(p,2n) reaction is E<40 MeV (exit energy from RbCl targets) and irradiation times are comparable, since ^{82}Sr and ^{68}Ge have both long half-lives with respect to the irradiation duration, respectively 25.34 and 270.95 d [69].

At ARRONAX also ^{64}Cu is routinely produced 2 times at month, *via* the ^{64}Ni(d,2n)^{64}Cu reaction (E = 16-13 MeV, I = 50 μA, tilted targets). The d-based route provides a similar yield in comparison with the ^{64}Ni(p,n)^{64}Cu reaction (E = 12-9 MeV), i.e. respectively 206 and 228 MBq/μAh, requiring a thinner target, i.e. 23.3 μm instead of 31.1 μm, and thus a lower initial cost of target material. Resulting Cu-isotopes co-produced by using deuteron- or proton-beams on ^{64}Ni targets are different, due to various open channels; by using NNDC and TALYS database, it has been estimated that 3.8 atoms of ^{64}Cu for 1 atom of cold copper are produced at EOB, when considering the (d,2n) reaction with E=16 MeV, t_{IRR}=1h, I=1μA [23, 69]. Considering this the production of ^{64}Cu has started at ARRONAX, obtaining a highly pure final product, characterized by a radio-isotopic purity higher than 99.96% (determined by using γ-spectrometry), a specific activity >10 MBq/nmol (assessed by using an ICP-OES) and a total activity of 3.5 GBq (all values refer to EOB+24h and 3 irradiation runs).

At last the production of the α-emitter ^{211}At is also under development at ARRONAX, exploiting the ^{209}Bi(α,2n)^{211}At reaction in the energy range E = 20-28.3 MeV. In this case an energy degrader has to be used in front of the target, in order to reduce the initial α-beam energy from 68 to 28.3 MeV. In this case it is extremely important to irradiate Bi-targets in the energy range E = 20-28.3 MeV, in order to minimize the

FIGURE 1.17: Photograph of the beam line at ARRONAX: A. Target support - B. End of the beam line.

production of ^{210}At (half-life 8.1 h), that decays into the extremely dangerous and toxic ^{210}Po (half-life 138.376 d)[1]. Currently at ARRONAX few hundreds of MBq at EOB are produced, useful for preclinical studies on ^{211}At-targeted therapy.

Regarding the research on radiolysis, physics and soon radiobiology, the AX vault is present at ARRONAX (Figure 1.3.1), equipped with 3 beam lines, 2 horizontal (Figure 1.17) and 1 vertical. Radiolysis experiments carried out by Fattahi et al. regard H_2 radiolytic yield vs LET (Linear Energy Transfer) under low intensity alpha beam ($\sim$ 70 nA). Physics research includes the measurements of production cross sections by using protons, deuterons and alpha beams (as outlined in detail in Chapter 4 and Chapter 5 and in the work of C. Duchemin et al.), as well as the study of Proton Induced X-ray Emission (PIXE), carried out by Ragheb et al. [99].

Figure 1.17 shows the horizontal beam line and the target support used during experiments aimed to the measurements of cross sections. The target support (A) and the end of the beam line (B) are indicated on Figure 1.17; their distance is about 6 cm and this layer of air is always taken into account in the calculation of incoming beam-energy on target, as well as the 75 μm kapton foil at the end of the beam line.

1.3.2 Future cyclotron at LNL

As previously mentioned, in 2013 has started in Italy the LARAMED (LAboratory of RAdioisotopes for MEDicine) project, funded by Italian government and INFN. LARAMED is based on the incoming cyclotron (BEST 70p model) that will be installed in autumn 2014 at LNL (Figure 1.18 and Figure 1.19), in the context of the SPES (Selective Production of Exotic Species) project. In fact, SPES is the hope of the laboratory, as its Latin name implies. In analogy with the four-leaved clover, symbol of SPES, four phases are foreseen:

- α, the acquisition, installation and commissioning of a high performance cyclotron with high output current and high energy (Table 1.8), together with the related infrastructure for the accelerator and experimental stations;

- β, the acceleration of neutron-rich unstable nuclei and collision with suitable targets for the production of new, extremely neutron-rich nuclei, which are similar to

---

[1]It has been estimated that a median lethal dose of ^{210}Po is 15 MBq (0.41 mCi) or 0.089 μg.

those generated in advanced stellar stages and are not present on Earth due to their short lifetime; the investigation of such systems is a new frontier of physics, for extending our knowledge of nuclei structure at extreme conditions and for providing basic information in the study of stellar evolution (SPES-β has been approved and partially funded by the Italian Government within the PREMIUM-PROJECTS 2011);

- γ, the production of radionuclides of medical interest in the context of LARAMED project (approved by MIUR within the PREMIUM-PROJECTS 2012, as result of a collaboration between INFN, CNR, Italian universities and a private partner);

- δ, the development of an intense neutron source; applications of neutron sources range from nuclear astrophysics (in particular for testing electronic damage in space), to characterization of nuclear waste or experimental tumour treatments (as Boron Neuron Capture Therapy, BNCT).

The cyclotron will be provided with two exit ports (Table 1.8), a configuration well suited for the double mission of the laboratory: basic research and technological applications. The cyclotron will accelerate protons, providing a maximum total current at the exit port of 500 μA, approximately distributed in 200 μA at the first and 300 μA at the second exit [4]. However, an upgrade is scheduled to increase the maximum current at each port up to 500 μA, i.e. providing a total current of 1 mA (Table 1.8).
As already mentioned, the first exit will provide a proton-beam with a maximum energy of 40 MeV, that will be exploited in the forefront research on Radioactive Ion Beams (RIBs), as described in SPES-β phase. In fact, a second-generation ISOL (Isotope Selector On line) facility dedicated to nuclear physics research is planned to be developed, by using the 40 MeV proton-beam from the cyclotron and injecting it to the PIAVE-ALPI linac accelerator complex, already working at LNL [4].
The second proton-beam provided by the incoming cyclotron is characterized by a tunable energy ranging from 30 to 70 MeV and will be dedicated to applied physics research, in particular being the fundamentals of LARAMED project (SPES-γ phase). The aim of LARAMED is the production of emerging radionuclides, such as Cu-64 (12.701 h), Cu-67 (61.83 h, whose production is discussed in detail in Chapter 5) and others, innovative generator systems, as Sr-82/Rb-82 and Ga-68/Ge-68, as well as the production of conventional radionuclides with new accelerator-based approaches. In fact, in this context the 3-years APOTEMA (Accelerator-based Production Of TEchnetium/Molybdenum for medical Applications) project has started in 2012, funded by INFN and focused on the production of ^{99}Mo and ^{99m}Tc with accelerators. As already mentioned, at this regard a detailed discussion is given in Chapter 3 and Chapter 4, respectively focused on

TABLE 1.8: Characteristics of the incoming cyclotron at LNL.

Proton beam	Accelerated particles	Energy range [MeV]	Intensity [μA]	Up-graded Int. [μA]	Dual beam
Exit 1	H-	40	$\sim$200	$\sim$500	Yes
Exit 2	H-	35-70	$\sim$300	$\sim$500	Yes

FIGURE 1.18: Photograph of excavations for the building construction at LNL.
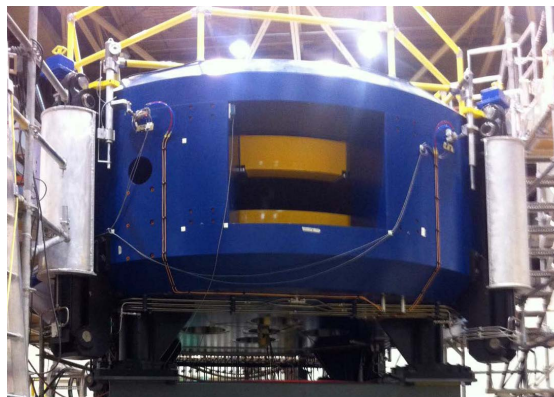
FIGURE 1.19: Photograph of incoming cyclotron (BEST 70p model).

the production of these vital nuclides *via* the ^{100}Mo(p,x)^{99}Mo,^{99m}Tc and ^{96}Zr(α,n)^{99}Mo reactions.

Chapter 2

Fundamental physics of the cross section measurement

2.1 Nuclear reaction cross section and additional significant definitions

A nuclear reaction is a process in which a nucleus reacts with another nucleus or an elementary particle. In some cases one or more other nuclei are formed and the reaction is called nuclear transmutation; in others the nucleus remains unchanged (elastic scattering) or it is excited to a higher energy state (inelastic scattering). In this work a nuclear reaction will be always referred to a nuclear transmutation, even if for brevity it will be implied.

The probability of a nuclear reaction to occur it is generally described in terms of its cross section (σ), that has units of area and has been traditionally been measured in *barn*: 1 b = 10^{-28} m^2. This unit comes from the fact that the probability for a neutron to interact with a target is proportional to the area of the nucleus, which compared to the size of the incident particle appears to be as large as a *barn* [100].

The cross section of a nuclear interaction also depends on the energy of the incident particle and may be calculated if the form of the basic interaction between the particles is known [101]. For example, the probability of a nuclear reaction to occur is very small if the energy of the incident particle is smaller than the one needed to overcome the Coulomb barrier (in this case the nuclear reaction will occur only by tunnelling effects); moreover, it is known that there is a linear relationship between the energy required to induce a nuclear reaction and the Z value of the target material [100]. However, the accurate knowledge of the cross section is difficult to obtained using theoretical calculations and experiments are needed to get precise results (uncertainties around 10-15%)

about this fundamental element in the optimization of accelerator-based radionuclide production.

In order to experimentally evaluate the cross section of a nuclear reaction, it is necessary to irradiate a thin target foil with a well known particle beam. A thin target is defined as a target in which the energy loss is negligible in respect to the beam energy, i.e. $\Delta E/E \sim 0.01$ - 0.05 [102]. The cross section $\sigma(E)$ is a function of the average energy E of the incoming (E^{IN}) and out coming (E^{OUT}) particle energies in the target, i.e. $E = \frac{(E^{IN}+E^{OUT})}{2}$, whose principal ingredient in its calculation is the activity of the nuclide of interest produced at the End Of Instantaneous Bombardment (Act_{EOIB}), as shown in Equation 2.1:

$$\sigma(E) = \frac{Act_{EOIB}A}{\Phi N_A \rho p x (1 - e^{-\lambda t_{IRR}})} \tag{2.1}$$

Where A is the mass number of the target foil [g/mol], Φ is the incident beam flux [1/s], N_A is the Avogadro constant [1/mol], ρ, p and x are the density [g/cm^3], the purity [≤ 1] and thickness [cm] of the target foil, λ is the decay constant [1/s] of the nuclide of interest and t_{IRR} is the irradiation time [s]. It has to be noted that in this work for the target density it has always been considered the values present in the software *Stopping power and Range of Ions in Matter* (SRIM[1]), while a mean value of the target thickness is always inferred by measuring its weight (using a calibrated balance) and its dimensions (using a digital caliper).

The activity at EOIB Act_{EOIB} can be evaluated from the activity Act measured by detectors, applying the corrections regarding the decay during the irradiation time t_{IRR}, the measuring time t_R (Real time indicated by the detector) and the time elapsed from the EOB to the beginning of the measurement t (Equation 2.2):

$$Act_{EOIB} = Act \cdot e^{\lambda t} \left(\frac{\lambda t_{IRR}}{1 - e^{-\lambda t_{IRR}}} \right) \left(\frac{\lambda t_R}{1 - e^{-\lambda t_R}} \right) \tag{2.2}$$

As already mentioned, the activity of a nuclide can be measured by using detectors. In this work the γ-radiation emitted during the decay of the nuclide of interest is always revealed by using HPGe detectors, as discussed in Section 2.3. In order to have adequate corrections for the pile-up effect during the counting time t_R and a good estimation of the Live time t_L, in this work the Dead Time (DT) is always maintained below the value of 10%. Equation 2.3 shows the relation between the net photopeak area at the energy E (number of counts C) measured by the detector and the corresponding nuclide activity:

---

[1]The software SRIM is available at www.srim.org .

$$Act = \frac{C}{\varepsilon(E)I(E)t_L} \qquad (2.3)$$

Where $\varepsilon(E)$ is the detector efficiency and $I(E)$ is the abundance of the γ-emission at the energy E. When the nuclides of interest present two or more γ-lines with no interference, a weighted mean value of the corresponding activities has been calculated, by using Equation 2.4 [101]:

$$Act^* = \frac{\sum Act_i/\sigma_i^2}{\sum 1/\sigma_i^2} \qquad \sigma(Act^*) = \sqrt{\frac{1}{\sum 1/\sigma_i^2}} \qquad (2.4)$$

Where $\sigma(Act^*)$ is the resulting uncertainty related to Act^* and σ_i is the uncertainty associated to each value Act_i. In this way the systematic errors associated to γ-radiation detection are reduced and the resulting uncertainty $\sigma(Act^*)$ is lower than the single-ones uncertainties σ_i.

Summarizing, by using detectors it is possible to evaluate the nuclide activity at time t (Equation 2.3) and thus the activity at EOIB (Equation 2.2). By knowing the target details (ρ and x) and particle flux (Φ) it is possible to finally estimate the cross section of the nuclear reaction (Equation 2.1). Since the incident beam flux Φ is a fluctuating parameter whose measure is difficult to obtain precisely, in this work the cross sections of the nuclide of interest are calculated by taking as reference a monitor reaction $\sigma'(E')$ (i.e. a well-known nuclear reaction that produces a nuclide whose activity is taken as reference) and applying Equation 2.5:

$$\sigma(E) = \sigma'(E')\frac{Act_{EOIB}A\rho'p'x'(1 - e^{-\lambda't_{IRR}})}{Act'_{EOIB}A'\rho px(1 - e^{-\lambda t_{IRR}})} \qquad (2.5)$$

Where Act'_{EOIB} and λ' are the activity at EOIB [Bq] and the decay constant [1/s] of the reference nuclide, ρ', p' and x' are the density [g/cm^3], the purity [≤ 1] and the thickness [cm] of the monitor foil used.

Once calculated the activity at EOIB of the nuclide of interest or its nuclear cross section, it is possible to estimate the thin target yield at the energy E, $y_{EOIB}(E)$ [$\frac{Bq}{CMeV}$], by using the following Equation:

$$y_{EOIB}(E) = \frac{\lambda Act_{EOIB}}{Q[dE/dx|_E\Delta x]} = \frac{\lambda(\rho px)(N_A/A)\sigma(E)}{Q\Delta E} \qquad (2.6)$$

Where Q is the total integrated charge [C], $dE/dx|_E$ is the target stopping power at energy E [MeV cm^2/g], Δx is the target mass thickness [g/cm^2] and ΔE is the thin

target energy loss at the energy E [MeV]. Equation 2.6 refers to mono-isotopic or highly enriched target made of a pure element, but in case of non-pure target elements a more general equation must be taken into account [102].

The activity produced in a thick target after a generic irradiation t_{IRR}, i.e. the Thick Target Yield $Y_{EOIB}(E, \Delta E)$ [Bq/C], can be calculated by integrating vs energy the thin target yield y_{EOIB}, as shown in Equation 2.7:

$$Y_{EOIB}(E, \Delta E) = \int_{Eout}^{Ein} y_{EOIB}(E)dE = \frac{\lambda(N_A/A)}{Q} \int_{E-\Delta E}^{E} \frac{\sigma(E)}{dE/dx}dE \qquad (2.7)$$

Multiplying Equation 2.7 for beam intensity I [μA] and irradiation time t_{IRR}, it is possible to calculate the final activity Act_F [MBq] that is theoretically produced with an incident beam of energy E and intensity I on a thick target of energy loss ΔE:

$$Act_F(E, \Delta E, t_{IRR}, I) = Y_{EOB}(E, \Delta E) \cdot I \cdot t_{IRR} \qquad (2.8)$$

Once known the final in-target activity produced, it is possible to evaluate:

- $A_s(t)_{Y-i}$ [Bq/g], the Specific Activity or activity concentration in time t, i.e. the activity of the radioisotope Y-i divided by the mass target M:

$$A_s(t)_{Y-i} = \frac{A(t)_{Y-i}}{M} \qquad (2.9)$$

- $RNP(t)_{Y-i}$ [adu], the Radio Nuclidic Purity (RNP) in time t, i.e. the fractional activity of radioisotope Y-i compared with the total activity of all its isotopes Y-x co-produced in-target:

$$RNP(t)_{Y-i} = \frac{A(t)_{Y-i}}{\sum A(t)_{Y-x}} \qquad (2.10)$$

- $IP(t)_{Y-i}$ [adu], the Isotopic Purity (IP) in time t, i.e. the fractional number of Y-i atoms compared with the total number of isotopes atoms Y-x co-produced in-target:

$$IP(t)_{Y-i} = \frac{N(t)_{Y-i}}{\sum N(t)_{Y-x}} \qquad (2.11)$$

2.2 Stopping power and energy straggling: definition and estimation

When charge particles travel through matter some interactions occur with target atoms or molecules, causing a decreasing of the initial particles energy. The stopping power dE/dx [MeV/cm] describes the expectation value of the rate of energy loss per unit path length x by a particle of charge z. It depends on the atomic and mass number of the medium, Z and A, and on the specific type and kinetic energy of the incoming particle. The stopping power is composed by two contributions, the electronic and the nuclear stopping power. Considering that a charged particle is surrounded by its Coulomb electric force field, it interacts with one or more electrons of practically every atom it passes; most of these interactions individually transfer only small fractions of the incident particle's kinetic energy, such as in a friction-like process. This gradual kinetic energy loss is described by the Continuous Slowing Down Approximation (CSDA) [103] and explains why the electronic stopping power is much larger than the nuclear one, that can usually be neglected. Many models may be used to describe the energy loss of a charge particle in matter, but the main one is the modern form of the Bethe-Block's formula:

$$-\frac{dE}{dx} = K\frac{z^2 Z\rho}{\beta^2 A}[ln(\frac{2m_e\gamma^2\beta^2}{I}) - \beta^2 - \frac{\delta}{2} - \frac{\eta}{Z}] \tag{2.12}$$

where K is a constant $(0.3071 \ \frac{MeVcm^2}{g})$, β is the normalized velocity v and γ the relativistic factor of the incoming particle[2], m_e is the electron mass, I is the ionization potential of the medium[3], δ and η are correction factors, respectively at high and low energies. The factor δ takes into account the correction at high energy for the polarization of electrons by the electric field of the moving ion, that could shield distant electrons. The factor η is applied at low energy when the collisions are no longer adiabatic and it depends on the orbital velocities of the electrons.

The hypothesis behind the Bethe-Block's formula is the complete ionization in the medium of the incoming particle. In case of light charge particles (such as protons) this is true, but for heavy charged particles also a partial ionization may occur. Moreover, various low-energy effects are not taken into account in the given Equation 2.12. For these reasons the software SRIM is used in the analysis of experimental data, in order to estimate the stopping power. The software presents many corrections missing in the Bethe-Block's formula and can be easily inserted in the code developed in C used for the yield estimation (Chapter 4 and Chapter 5).

---

[2] $\beta = v/c$, with c light's velocity, and $\gamma = (1 - \beta^2)^{-1/2}$.

[3] In Thomas-Fermi model the ionization potential is $I \approx 10 \cdot Z$ [104].

FIGURE 2.1: Photograph of the HPGe detectors used: on the right, *Research* detector (g0 and g1 geometries); on the left, *Arrofixe* detector (Level 0 and Level 5 geometries).

2.3 γ-spectrometry with HPGe detectors

The evaluation of samples activity, and thus all physical quantities related to it (such as cross section and yield), has been done by using γ-spectrometry; at this regard a wide literature can be analysed and this work we referred to [101, 105]. At ARRONAX facility two HPGe detectors, named *Research* and *Arrofixe*, were used (Figure 2.1). The first was used for the acquisition of the spectra of liquid samples aimed to the measurement of the ^{68}Zn(p,2p)^{67}Cu cross section, the second for the acquisition of the spectra of thin foils for the ^{96}Zr(α,n)^{99}Mo reaction evaluation.

In order to correctly interpreter the γ-ray spectrum in terms of energy and amount of activity, it is necessary to calibrate the detector. First, it is necessary to find out the conversion between channels and energy (*Energy calibration*) and then the relation between number of counts and activity (*Efficiency calibration*). As the *Energy calibration* does not depend on the geometry chosen, i.e. it is the same for all distances detector-source since it converts channel into energy values, the *Efficiency calibration* depends on the geometry chosen, i.e. it has to be calculated for each distance detector-source used, since it converts number of counts into activity values.

It has to be underlined the importance of the nuclear data used for calibration process and γ-spectrometry analysis: in this work it has always been chosen the NuDat database [69].

2.3.1   Calibration curves and sources

As previously mentioned, the *Research* detector has been used to quantify activities of liquid samples and thus for its calibration a vial containing 5 mL of standard liquid

TABLE 2.1: Standard liquid sources used for the calibration of *Research* detector, used for acquiring the spectra for the ^{68}Zn(p,2p)^{67}Cu reaction.

Radionuclide	γ-ray Energy [keV]	Reference Activity [Bq]	Uncertainty Ref. Act. [%]
Am-241	59.540	668.36	5
Cd-109	88.030	5978	5
Co-57	122.060	326.732	4
Co-57	136.470		
Ce-139	165.860	355.936	4
Sn-113	255.134	991.76	4
Cr-51	320.080	4729.48	4
Sn-113	391.700	991.76	4
Sr-85	514.000	1044.68	4
Cs-137	661.660	1301.44	4
Y-88	898.050	2065.84	4
Co-60	1173.230	1877.68	4
Co-60	1332.540		
Y-88	1836.050	2065.84	4

TABLE 2.2: Point-like sources used for the calibration of *Arrofixe* detector, used for acquiring the spectra for the ^{96}Zr(α,n)^{99}Mo reaction. The intensity of the 25 keV line of Cd-109 is considered as the summed of the intensities of the lines at 24.912, 24.943 and 25.455 keV [69].

Radionuclide	γ-ray Energy [keV]	Reference Activity [Bq]	Uncertainty Ref. Act. [%]
Cd-109	22.16	1400	3.5
Cd-109	25*		
Am-241	59.54	36000	3.5
Cd-109	88.03	1400	3.5
Eu-152	121.8	3437	2
Eu-152	244.8		
Eu-152	344.4		
Eu-152	779.3		
Eu-152	867.8		
Eu-152	964.5		
Eu-152	1112.6		
Eu-152	1408.7		

sources has been used (Table 2.1), while for *Arrofixe* detector point-like sources have been taken for the calibration processes (all calibrated sources have been supplied by Cerca Lea, France), shown in Table 2.2.

Equation 2.13 shows the function used for the energy calibration, for both detectors:

$$Energy(Ch) = k_1 + k_2 \cdot Ch + k_3 \cdot (Ch)^2 \qquad (2.13)$$
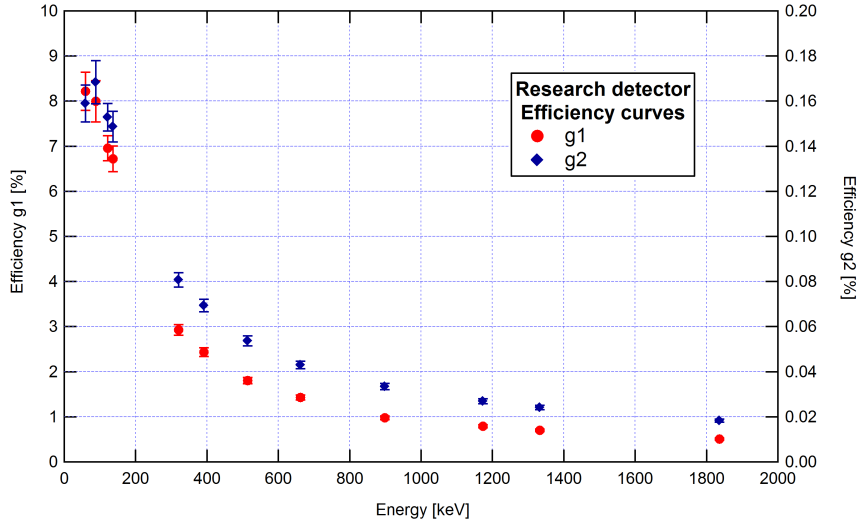
FIGURE 2.2: Efficiency curves for g0 (left) and g1 (right) geometries on *Research* detector.

where k_{1-3} are parameters that have to be determined for each detector. Equation 2.14 refers to the efficiency calibration (conversion from number of counts to activity), a VI order function, i.e. the highest order function possible to use with Fitzpeak software [106] during the efficiency calibration process:

$$\epsilon(E) = c_1 + c_2 \cdot ln(E) + c_3 \cdot (ln(E))^2 + c_4 \cdot (ln(E))^3 + c_5 \cdot (ln(E))^4 + c_6 \cdot (ln(E))^5 \quad (2.14)$$

where c_{1-6} are parameters that have to determine for each configuration (detector and geometry considered). In particular, in case of *Research* detector two geometries have been used: in the first, named *g0*, the vial was directly placed on the HPGe-detector, while in the second, named *g1*, the vial was placed at about 21 cm from the detector (a thin plastic support, about 3 mm thick, was placed between the detector and the vial). Also for *Arrofixe* detector two geometries have been used: in the first, named *Level0*, the vial was placed on a plastic support (about 3 mm thick) in the closest position to the HPGe-detector (about 5.2 cm far from it), while in the second, named *Level5*, the plastic support was about 15.2 cm from the detector (Figure 2.1).

Figure 2.2 and Figure 2.3 respectively report the efficiency curves for *Research* and *Arrofixe* detectors as a function of energy, while Figure 2.4 shows a typical efficiency curve obtained by using Fitzpeak software [106].
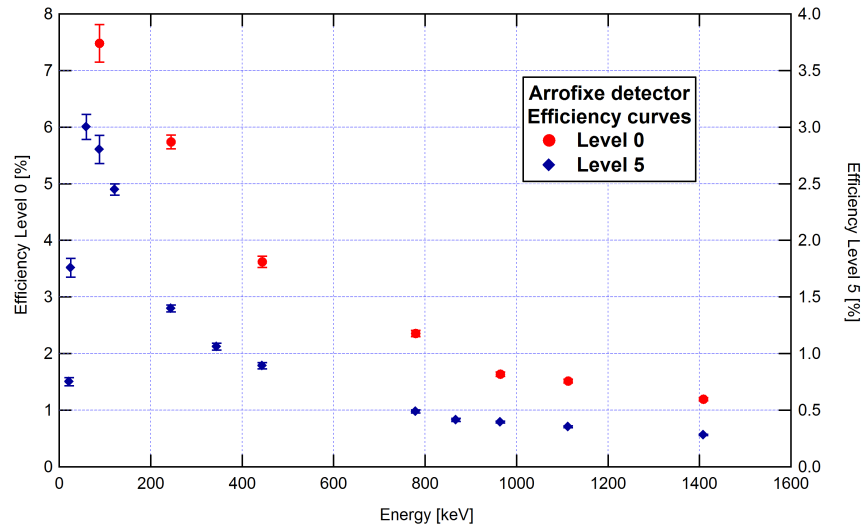
FIGURE 2.3: Efficiency curves for Level0 (left) and Level5 (right) geometries on *Arrofixe* detector.
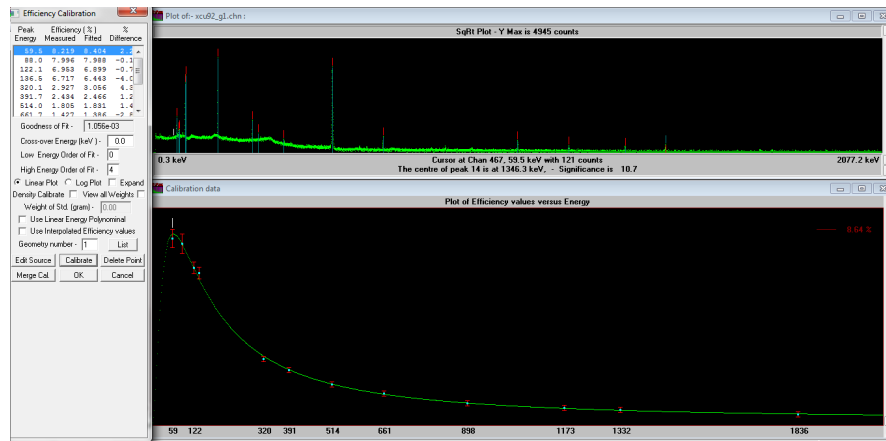
FIGURE 2.4: Typical efficiency curve calculated by Fitzpeak software [106] and related to the g0 geometry on *Research* detector.

2.4 Stacked foil target technique

The well known *Stacked foil target technique* was always used in the cross section measurements performed in this work, as described in detail in Chapter 4 and Chapter 5. This techniques allows to bombard many target foils in the same irradiation, thus obtaining in each run several values of the analysed cross section. One of the first paper containing the description of stacked targets was published in 1992 by Pillai et al. [107], but also a more recent paper describes this technique [108].

In this work stacked targets have been prepared by piling many foils and interposing target with monitor and catcher foils, depending on the specific nuclear reaction studied.

In order to keep all foils well aligned and pressed (avoiding any air layer or displacement between target and monitor foils), a target holder has been used and positioned in front of the beam, at a distance of about 6 cm, by using the target support shown in Figure 1.17.

As already mentioned, this air layer and the 75 μm kapton foil at the end of the beam line have been always taken into account in the calculation of the particle energy in each foil of the stacked targets.

Chapter 3

Feasibility study for ^{99}Mo and ^{99m}Tc production at LNL

In the framework of LARAMED project a feasibility study about the alternative, accelerator-driven production of ^{99}Mo and ^{99m}Tc has started at Legnaro National Laboratories (LNL). The INFN project APOTEMA (Accelerator-based Production Of TEchnetium/-Molybdenum for medical Applications), started in 2012, has been focused on this subject gathering different skills (from nuclear physics to nuclear medicine through radiochemistry), and involving the INFN divisions of LNL, Ferrara, Padova, Pavia (since 2013) and Milan (since 2014). Results of this interdisciplinary collaboration have been recently presented in two papers, both published in a special issue of Science and Technology of Nuclear Installations focused on ^{99}Mo and ^{99m}Tc nuclides [9, 109], and are here briefly discussed.

Considering the incoming high-beam-current, high-energy proton cyclotron at LNL (Section 1.3) and previous measurements of proton-induced reactions on highly enriched Mo-100 metallic targets (Section 1.1.3.1), a comprehensive map of radionuclides expected inside irradiated samples has been estimated. These results have been integrated with a detailed theoretical investigation extended up to (p,6n), (p,5n) and (p,2p4n) levels (Figure 1.9), by using the TENDL excitation functions [23]. It is important to note that in case of direct ^{99m}Tc production particular attention has to be paid to the co-production of Tc-isotopes. Since they can not be chemically separated from ^{99m}Tc, they will be also present in the final Tc-labelled pharmaceutical, causing a higher dose to patient. At this regard some theoretical studies have been already performed by Celler et al. and Hou et al. [10, 110], in order to assess the best irradiation conditions for direct ^{99m}Tc production and also compare the radiation dose to different organs due to cyclotron and

generator-produced ^{99m}Tc. In 2007 a study performed by Challan et al. assessed the thin target yields of ^{nat}Mo(p,x) irradiations from threshold up to 18 MeV, both experimentally and theoretically (EMPIRE II) [62]. However, only ^{99m}Tc and ^{96m}Tc, ^{96g}Tc have been considered, neglecting other Tc-isotopes and different nuclides co-produced. In this work some assumptions have been done in the estimation of in-target contaminants aliquot at the EOB: in particular all the radionuclides with half-life longer than 10^3 years have been considered stable. However some long-lived nuclides such as ^{97g}Tc, ^{98}Tc and ^{99g}Tc are co-produced and thus have an impact on the specific activity of the final produced. In particular the cross section for the production of the ground state ^{99g}Tc (half-life $\tau_{1/2} = 2.111 \cdot 10^5$ y) presents a peak in the same energy range of ^{99m}Tc (Figure 1.9), but about four times bigger than the one of ^{99m}Tc. The ^{100}Mo(p,2p)^{99g}Tc reaction has been evaluated only up to 18 MeV by Gagnon et al. [17], but the estimation of such reaction in the entire energy range is needed. However, good agreement can be noted up to 18 MeV with its theoretical cross section available in TENDL library (Figure 1.9). As other Tc-isotopes, also ^{99g}Tc is not chemically separable from Tc-mixture, and furthermore its amount is significant since it is directly produced in target and it also results from the decay of ^{99}Mo and ^{99m}Tc (Figure 1.4). For these reasons in our estimation of the final map of radionuclides expected inside irradiated samples ^{99g}Tc has not been neglected but specific attention has been paid to its production. In fact a detail analysis of the possible influence in radiochemical purity (RCP) and stability of radiopharmaceuticals labelled with Tc-pertechnetate (TcO$_4^-$) containing high amounts of ^{99g}Tc has been performed and it will be precisely discussed in this chapter.

3.1   Estimations of ^{99}Mo and ^{99m}Tc yields expected inside irradiated samples via the ^{100}Mo(p,x) reaction

As reported in [9], ^{99}Mo and ^{99m}Tc yields have been estimated considering a proton current of 500 μA and:

- two target thickness configurations: the first thickness was enough for decreasing the proton energy down to the threshold energy of the reaction, avoiding the Bragg peak of the proton beam (and thus the correlated heat deposition); the second option considered was chosen analysing the yield distribution versus beam penetration depth, and avoiding the drop-off region because of cross section lowering;

TABLE 3.1: Isotopes distribution [%] of enriched Mo-100 supplied by Isoflex company and compared with natural molybdenum.

Abundance [%]	Mo-100	Mo-98	Mo-97	Mo-96	Mo-95	Mo-94	Mo-94
ISOFLEX	99.05	0.54	0.07	0.11	0.10	0.05	0.08
^{nat}Mo	9.82	24.39	9.60	16.67	15.84	9.15	14.53

- different incoming proton energies: in case of ^{99}Mo the 40 and 70 MeV energies have been chosen, while for direct ^{99m}Tc production the 15, 20 and 25 MeV beam-energies have been studied;

- various irradiation times: for ^{99}Mo production t_{IRR} = 12 hours, 24 hours and 21 days (saturation) have been considered, while for ^{99m}Tc production short irradiation times have been taken into account (1, 2, 3 and 6 hours).

As target material has been considered a realistic enriched Mo-100, supplied by ISOFLEX company (ISOFLEX-USA,2012), whose isotopic composition is reported in Table 3.1.

In order to get the activities of all the nuclides in-target produced, many radioactive decay chains have been taken into account, one for each open reaction channel. Since the same radionuclide may be created through a number of production-decay routes, all of them have been summed up when estimating the final number of atoms and activity available inside the target. At the end of the irradiation the nuclide yields by nuclear reactions stop, while the decays still continue. This can be described by the same set of equations, setting to zero the production rate for each nuclide and considering only its decay. It has to be noted that only nuclear reactions on Mo-100 were taken into account in calculations (secondary reaction, i.e. reaction on produced nuclides, have not been considered in this work), as well as the number of target nuclei during the irradiation process, that has been considered constant.

In order to analytically estimate the local yield contribution of the i-th species dY_i, i.e. the yield referred to the infinitesimal thickness dt at depth t of the target material, a slab geometry model has been used, as reported in Figure 3.1.

Equation 3.1 has been applied for calculating the total production yield Y_i normalized for incident proton flux n_p, the number of protons per unit time, calculated by dividing the proton current I [μA] by the electric charge unit e [C], i.e. $n_p = \frac{I}{e}$:

$$\frac{Y_i}{n_p} = n_{Mo} \cdot \int_0^{T0} \sigma_i(E_0 - \int_0^t \frac{dE}{dx}dx)dt \qquad (3.1)$$

where n_{Mo} is the atomic density of target material [1/cm^3], σ_i is the ^{xx}Mo(p,x) cross section for the production of the i-th nuclide species [cm^2], as a function of the proton
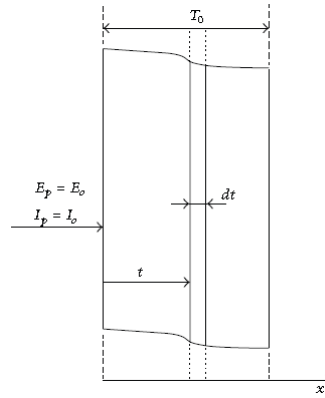
FIGURE 3.1: Scheme of the slab approximation geometry used in the calculation of yield distributions inside molybdenum sample thickness [9].

TABLE 3.2: Estimated ^{99}Mo production yields, in-target and specific activities for different irradiation conditions.

^{99}**Mo production**	E_P = 70 MeV	E_P = 70 MeV	E_P = 40 MeV	E_P = 40 MeV
Target	Thick (TT)	Optimized (OT)	Thick (TT)	Optimized (OT)
Thickness [mm]	6.74	5.93	2.47	1.82
Irradiation time: 12 h				
Integral yield [GBq/μA]	4.42	4.31	1.28	1.28
In-target activity [TBq]	2.21	2.16	0.64	0.64
Specific Activity [GBq/g]	4.43	5.05	5.90	7.59
Irradiation time: 24 h				
Integral yield [GBq/μA]	8.32	8.11	2.42	2.41
In-target activity [TBq]	4.16	4.06	1.21	1.21
Specific Activity [GBq/g]	8.34	9.51	11.1	14.28
Saturation: $\approx$ 21 d				
Integral yield [GBq/μA]	37.12	36.20	10.80	10.75
In-target activity [TBq]	18.56	18.10	5.40	5.38
Specific Activity [GBq/g]	37.42	42.64	49.76	64.05

energy E at each thickness t (estimated by an iterative calculation process once known the proton stopping power dE/dx and the incident proton energy E_0). The atomic density of target material n_{Mo} is given by $n_{Mo} = \rho f_x \frac{N_A}{A_{xx}}$, where ρ is Mo-density [g/cm^3], f_x the weight fraction of the Mo-xx considered, N_A the Avogadro constant [1/mol] and A_{xx} the mass number of the Mo-xx considered.

Table 3.2 and Figure 3.2 report the estimated production yields of ^{99}Mo for different irradiation conditions, based on 99.05% ^{100}Mo-enriched metallic molybdenum (thick and optimized target configurations), 500 μA proton current and 500 W/cm^2 mean areal power density on target [9].

As shown in Figure 1.7, the accelerator production of ^{99}Mo is interesting at energies E > 40 MeV. In fact from Table 3.2 and Figure 3.2 it can be noted that the total in-target production of ^{99}Mo is 3 times bigger in case of 70 MeV proton-beam than for 40 MeV-protons. However, the estimated specific activities for optimized targets are always higher for 40 MeV beams, as can be easily noted in Figure 3.2 (at saturation the specific
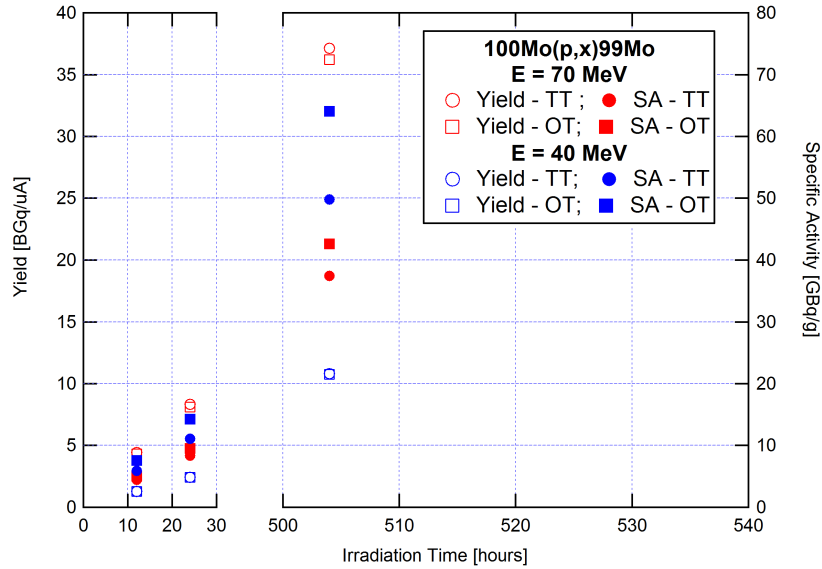
FIGURE 3.2: Estimated ^{99}Mo production yields and specific activities for different irradiation conditions.

activity for 70 MeV-beam is about 33% lower than the one for 40 MeV-beam). Although these in-target ^{99}Mo activity levels seem to be enough to cover a regional demand, it should be noted that the resulting specific activities are a factor of 10^2-10^4 lower than the ones commonly found in commercial generators (Table 1.3), i.e. about 0.37-37 TBq/g (equivalent to 10-1000 Ci/g). If the current industrial method for Mo/Tc generator manufacturing has to be maintained, the accelerator production of ^{99}Mo is therefore not a favourable option of practical interest, considering the high cost of the target material, the very large alumina column needed, and the resulting large elution volumes [111].

A promising alternative is the direct production of ^{99m}Tc *via* the ^{100}Mo(p,2n) reaction, by using accelerators (Figure 1.8). Table 3.3 and Figure 3.3 report the estimated production yields of ^{99m}Tc for different irradiation conditions, based on the hypothesis previously mentioned. As already mentioned, in case of direct ^{99m}Tc production particular attention has to be paid to the production of Tc-isotopes, listed in Table 1.4. For this reason Table 3.3 also reports the ^{99m}Tc IP and RNP at EOB, while Figure 3.4 shows the time evolution of these important parameters for each irradiation condition.

The biggest ^{99m}Tc yield is produced when using the highest proton energy for the longest irradiation time (25 MeV for 6 hours), while the highest specific activity is reached when using the lowest energy beam for the shortest irradiation time (15 MeV for 1 hour). The best irradiation condition is thus a compromise between these two limits, as it should provide enough quantities of ^{99m}Tc, minimizing the production of other Tc-nuclides.
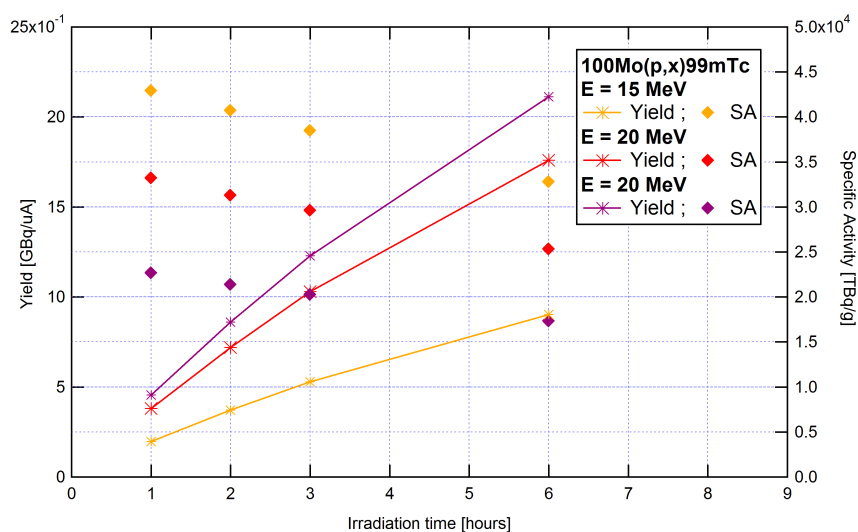
FIGURE 3.3: Estimated ^{99m}Tc production yields and specific activities for different irradiation conditions.
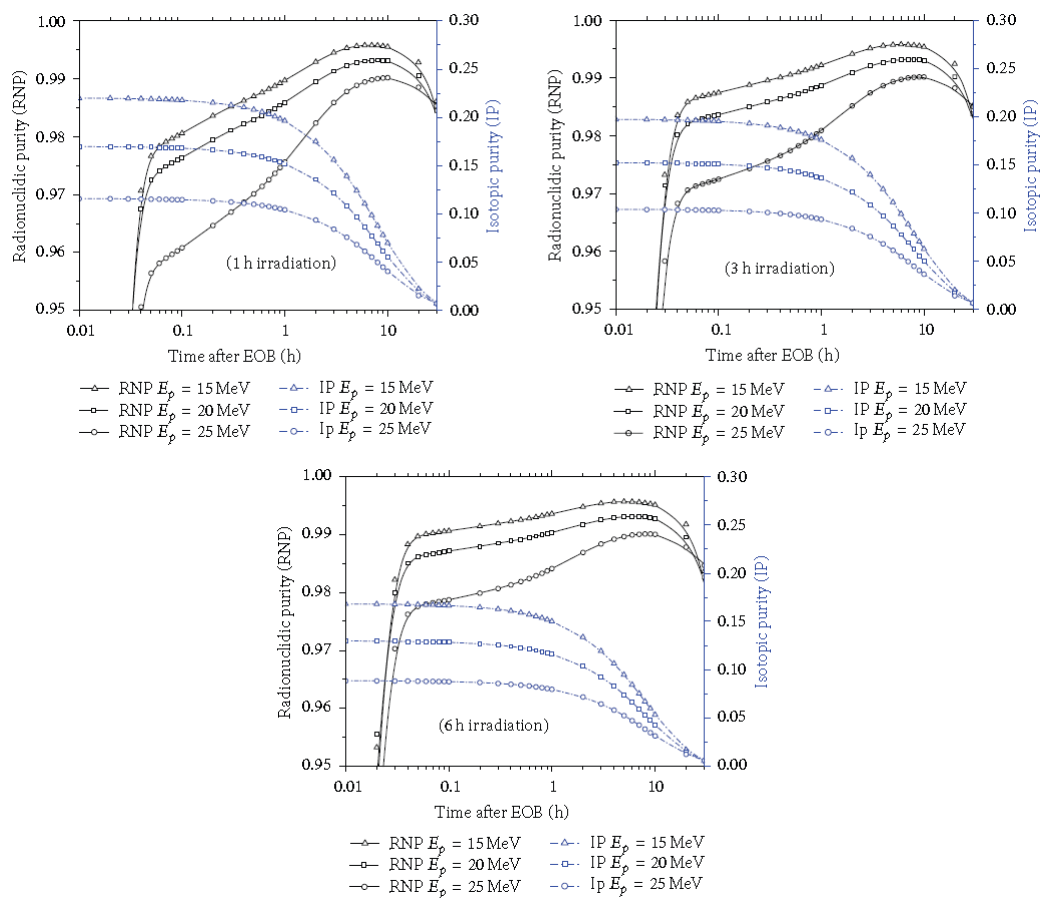
FIGURE 3.4: The evolution of ^{99m}Tc IP and RNP expected versus the decay time after EOB, for 1, 3 and 6 hours irradiation [9].

TABLE 3.3:   Estimated ^{99m}Tc production yields, in-target and specific activities for different irradiation conditions.

^{99m}Tc production				
$E_P = 15$ MeV	1h	2h	3h	6h
Integral yield [GBq/μA]	0.20	0.37	0.53	0.90
In-target activity [TBq]	0.10	0.19	0.26	0.45
Specific Activity [TBq/g]	$4.29 \cdot 10^4$	$4.07 \cdot 10^4$	$3.85 \cdot 10^4$	$3.28 \cdot 10^4$
IP	0.220	0.208	0.197	0.168
RNP	0.183	0.297	0.375	0.506
$E_P = 20$ MeV	1h	2h	3h	6h
Integral yield [GBq/μA]	0.38	0.72	1.03	1.76
In-target activity [TBq]	0.19	0.36	0.51	0.88
Specific Activity [TBq/g]	$3.32 \cdot 10^4$	$3.13 \cdot 10^4$	$2.96 \cdot 10^4$	$2.53 \cdot 10^4$
IP	0.170	0.161	0.152	0.130
RNP	0.210	0.333	0.415	0.547
$E_P = 25$ MeV	1h	2h	3h	6h
Integral yield [GBq/μA]	0.46	0.86	1.23	2.11
In-target activity [TBq]	0.23	0.43	0.61	1.06
Specific Activity [TBq/g]	$2.26 \cdot 10^4$	$2.14 \cdot 10^4$	$2.02 \cdot 10^4$	$1.73 \cdot 10^4$
IP	0.116	0.109	0.104	0.088
RNP	0.183	0.297	0.375	0.506

Table 3.3 shows that in case of direct ^{99m}Tc production the resulting specific activities are similar to the ones provided by standard Mo/Tc generators eluted each 24 hours, i.e. about $5.55 \cdot 10^4$ TBq/g (about $1.5 \cdot 10^6$ Ci/g). In fact considering the highest specific activity produced with accelerators (for 15 MeV beam and 1 hour irradiation) the discrepancy is about 20% only; in case of 25 MeV beam for 6 hours irradiation, the resulting SA is about 70% lower than standard generator's elutions.

As reported in [9], the biggest contribution to the total activity is due to the production of the short-lived ^{100}Tc, that however does not play a disturbing role in the final Tc contaminants, since in few minutes it transmutes into ^{100}Ru (stable). Due to the fast decay of ^{100}Tc, in few minutes after EOB the RNP sharp increases up to values higher than 95%, as shown in Figure 3.4. Considering the reference case of 20 MeV protons and 3 hours irradiation, the RNP increases to values as high as 99% in about 1 hour after EOB, due to the decays of other short-lived Tc isotopes. In fact, considering this reference case, the contribution to the overall activity (in order of decreasing activity) is due to ^{96m}Tc, ^{94g}Tc, ^{92}Tc, ^{94m}Tc, ^{93g}Tc, ^{95g}Tc, ^{93m}Tc and ^{96g}Tc [9]. RNP values above 99% for accelerator-produced Tc are quite important, considering that the reference parameter from the generator-produced Tc is about 99.99%. Such a limit is basically approached (i.e., 99.58%) if the irradiations at proton energies as low as 15 MeV are performed, whatever the irradiation time chosen. From the comparison with generator-produced ^{99m}Tc, it can be inferred that irradiations at 25 MeV have to be avoided, since the resulting ^{99m}Tc has RNP values never higher than 99% and IP ones always lower than 10% 1 h after EOB, as reported in Figure 3.4.

In fact, for 15 MeV protons the major contribution to all Tc-isotopes activity is due to ^{99m}Tc and ^{99g}Tc with about 10% due to the short-lived ^{100}Tc. At 20 MeV proton beam also other Tc-contaminants contribute to final activity (i.e. mainly ^{98}Tc, $^{97m+g}$Tc $^{96m+g}$Tc, and at lesser extent by $^{95m+g}$Tc produced by the reaction routes due to the other Mo target isotopes), while at 25 MeV such contribution is not negligible. In particular, the contribution from Tc-nuclides other than $^{99m+g}$Tc, compared with ^{99m}Tc, indeed increases to about 17% and 37%, respectively for 20 and 25 MeV proton beam.

In a recent work of Takacs presented at the II IAEA CRP meeting on ≪*Accelerator-based Alternatives to Mo-99 /Tc-99m production*≫ (held in October 2013 at Legnaro (PD) Italy), similar evaluations have been presented. It resulted that the best irradiation condition for direct ^{99m}Tc production are 17 MeV proton-beam and 3 hours of irradiation. For this irradiation condition the relative physical dose (i.e. the dose of the radiation emitted during the decay when totally absorbed) for all Tc-isotopes is about 1% of the one due to ^{99m}Tc, considering 2 hours cooling after EOB. In fact, from this work it results that the total Tc-contaminant activity is lower than 1% of ^{99m}Tc activity and that even after 100 irradiations the enriched Mo-100 target material is not consistently affected by other Mo-isotopes. After 100 steps it has been estimated a total Mo-100 recovery of about 99.94% (considering an initial abundance of 99.54% it is 99.48%), while only Mo-97 increases up to 8% of initial abundance (i.e. from 0.0016% it becomes about 0.0017%). However, the main issue in target recovery is the contamination by chemical agents that may compromise target composition.

From the work of Takacs it results that the main contribution to Tc-isotopes activity and physical dose is due to ^{94g}Tc ($t_{1/2}$ = 293 m = 4.88 hours), even if the long-lived ^{99g}Tc has the highest number of atoms at EOB. Considering 3 hour irradiation at 17 MeV beam and 2 hour cooling, the number of ^{99g}Tc atoms it resulted to be about 4.86 times the number of ^{99m}Tc atoms. However, the ^{99g}Tc activity, in comparison with the ^{99m}Tc one, is about $1.58 \cdot 10^{-8}$ times lower, while the ^{94g}Tc activity is 4 orders of magnitude higher, i.e. about $1.71 \cdot 10^{-4}$ times smaller than ^{99m}Tc. When comparing the physical doses, ^{94g}Tc is the main contribution of Tc-nuclides, providing about $3.11 \cdot 10^{-3}$ of ^{99m}Tc dose. Even if negligible for a dosimetry point of view, the possible impact of the long-lived nuclides ^{99g}Tc, ^{98}Tc, and ^{97g}Tc in the radiochemical quality of the accelerator-Tc labelled pharmaceuticals has to be considered [112]. In fact in a report by the European commission [113], a limiting purity of the end product, approximately composed by 25% of ^{99g}Tc and 75% of ^{99m}Tc (i.e. a ^{99m}Tc/$^{99m+g}$Tc ratio R = 0.25), is reported to interfere with the function of some labelled radiopharmaceuticals, thus reducing the effectiveness of Tc-based scans. Unfortunately, it is not clear in [113] how such an IP level should affect the diagnostic procedures, as neither the radiolabelling processes nor the resulting SPECT images quality are mentioned.

TABLE 3.4: Radiopharmaceuticals used in the study [109].

Name	Radiopharmaceuticals
Neurolite (Brystol-Myer Squibb)	^{99m}Tc-ECD (^{99m}Tc-Bicisato)
Cardiolite (Brystol-Myer Squibb)	^{99m}Tc-SESTAMIBI
Stamicis (IBA)	^{99m}Tc-SESTAMIBI
Technemibi (Mallinckrodt)	^{99m}Tc-SESTAMIBI
TechneScan (Mallinckrodt)	^{99m}Tc-MAG3
Pentacis (IBA)	^{99m}Tc-DTPA
Medronato II (GE Healthcare)	^{99m}Tc-MDP
Osteocis (IBA)	^{99m}Tc-HMDP
Nanocoll (GE Healthcare)	^{99m}Tc-nanocolloids
Renocis (IBA)	^{99m}Tc-DMSA

In order to assess the possible impact of such long-lived nuclides on the radiochemical quality of the accelerator-Tc labelled pharmaceuticals, a detailed study has been performed by using standard generators' eluate containing different amounts of ^{99g}Tc, miming the presence of all long-lived Tc-isotopes produced *via* the ^{100}Mo(p,x) reactions (i.e. ^{99g}Tc, ^{98}Tc, and ^{97g}Tc).

3.2 Preliminary evaluation of the effect of the long-lived Tc-isotopes on the final product

The aim of the work here presented and recently published in a special issue of Science and Technology of Nuclear Installations focused on ^{99}Mo and ^{99m}Tc nuclides, is the evaluation of possible impacts of different ^{99g}Tc/^{99m}Tc isomeric ratios on the preparation of different Tc-labelled pharmaceutical kits, miming the presence of all long-lived Tc-isotopes, such as ^{99g}Tc, ^{98}Tc, and ^{97g}Tc [109]. A set of measurements with ^{99m}Tc, eluted from a standard ^{99}Mo/^{99m}Tc generator, has been performed, and results on both Radio-Chemical Purity (RCP) and stability studies (following the standard quality control procedures) are reported for a set of widely used pharmaceuticals (Table 3.4).

All pharmaceuticals have been reconstituted with either the first $[^{99m}\text{TcO}_4]^-$ eluate obtained from commercial generators (coming from two different companies, a *dry-* and a *wet*-generator (respectively a DRYTEC generator, GE Healthcare, Milan, Italy and an Elumatic III generator, IBA-CIS Bio International, Gif-Sur-Yvette, France) or eluates after 24, 36, 48, and 72 hours from last elution. All generators, with ^{99}Mo calibrated activity of 10 GBq, have been eluted with 5 mL of saline solution, as indicated by each manufacturer. All Quality Control (QC) tests required by European Pharmacopoeia[1] and Italian Pharmacopoeia[2] have been applied. In particular, the elution yield, the

---

[1]European Pharmacopoeia, 7th Ed., Sodium pertechnetate (^{99m}Tc) injection (fission) (0124).

[2]Italian Pharmacopoeia, 12th Ed., Norme di Buona Preparazione dei Radiofarmaci per Medicina Nucleare, All. A, p.to A.2 ≪*Generatore di* $^{99}Mo/^{99m}Tc$ *(molibdeno/tecnezio)*≫.

visual inspection, the aluminum content, the RNP and RCP have been verified for each generator's elution, always getting results in agreement with requirements [109].

3.2.1 Determination of the long-lived ^{99g}Tc to ^{99m}Tc Ratio (R) in commercial generator's elution

As reported in Section 1.1.1, ^{99}Mo decays into ^{99g}Tc (BR = 12.4%) and ^{99m}Tc (87.6%), that in turn decays into ^{99g}Tc (Figure 1.4). Due to this particular branching decay of ^{99}Mo, even fresh elutions from a generator always contain both isotopes (^{99m}Tc and ^{99g}Tc), indistinguishable from the chemical point of view. The amount (expressed in μg) of total technetium present in the eluate is directly related to the amount of ^{99}Mo atoms present on the column (i.e., ^{99}Mo activity) and the time that elapsed since the previous elution. The total number of Tc atoms, namely the sum of ^{99g}Tc and ^{99m}Tc, has been calculated as follows:

$$N_{Tc(TOT)} = N^0_{Mo-99}(1 - e^{-\lambda_1 t}) \tag{3.2}$$

where N^0_{Mo-99} is the initial ^{99}Mo atoms number present on the column, λ_1 is the decay constant of ^{99}Mo (0.0105 hours^{-1}), and t is the time that elapsed since the last elution. The number of ^{99m}Tc atoms (N_{Tc-99m}) has been calculate by using the following Equation:

$$N_{Tc-99m} = BR\frac{\lambda_1}{\lambda_2 - \lambda_1}N^0_{Mo-99}(e^{-\lambda_1 t} - e^{-\lambda_2 t}) \tag{3.3}$$

where λ_2 is the decay constant of ^{99m}Tc (0.1149 hours^{-1}) and BR is the Branching Ratio, i.e. the probability of ^{99}Mo to turn into ^{99m}Tc ($BR = 0.876$). From equations above the number of ^{99g}Tc atoms can be easily calculated as follows:

$$N_{Tc-99g} = N_{Tc(TOT)} - N_{Tc-99m} \tag{3.4}$$

and thus the ^{99g}Tc to active ^{99m}Tc ratio can be easily estimated.

The determination of the ^{99g}Tc content in a fresh eluate requires an immediate measurement after the elution of the ^{99m}Tc activity and a later measurement of the total activity of ^{99g}Tc (after 3 months almost all the ^{99}Mo and ^{99m}Tc atoms decay into ^{99g}Tc). The evaluation of ^{99m}Tc activity in the sample has been performed by using a dose calibrator (PET-dose, Comecer, Castelbolognese, Italy), while the evaluation of ^{99g}Tc activity

TABLE 3.5: RCP of radiopharmaceuticals at t_0, prepared with generator DRYTEC eluates at time superior to 24 h from the last elution [109].

Commercial Name	DRYTEC RCP$_{36}$	DRYTEC RCP$_{48}$	DRYTEC RCP$_{72}$	RCP Requirements
Ratio R	4.34	6.50	11.84	
Neurolite	98.57±0.45	99.41±1.51	98.73±1.85	≥ 90%
Cardiolite	97.91±0.38	98.35±1.02	99.40±1.23	≥ 94%
Stamicis	97.88±0.28	97.90±0.15	98.16±0.11	≥ 94%
Technemibi	98.18±0.23	97.77±0.33	98.53±0.27	≥ 94%
TechneScan	98.89±0.64	99.1±0.44	99.31±0.14	≥ 95%
Pentacis	98.84±1.01	98.91±0.24	99.12±0.33	≥ 95%
Medronato II	99.01±0.24	98.44±0.16	99.63±0.64	≥ 95%
Osteocis	99.22±0.14	98.01±0.52	99.13±0.11	≥ 95%
Nanocoll	99.34±0.09	99.38±0.16	98.94±0.41	≥ 95%
Renocis	99.55±0.08	99.22±0.77	99.11±0.03	≥ 95%

has been performed using the TRI-CARB 2810TR liquid scintillation analyzer (Perkin Elmer Inc., Monza, Italy). The samples for ^{99g}Tc activity measurements were prepared taking an aliquot of 0.8 mL from an eluate decayed for 60 days (total volume of the eluate: 5 mL) and adding 5.4 mL of liquid scintillator (Ultima Gold LLT cocktail, Perkin Elmer Inc., Monza, Italy). Measurements of ^{99g}Tc activity have been performed by using the 0–295 keV energy window, since the end-point energy of β-radiation emitted in the decay of ^{99g}Tc is at 293.5 keV [69].

3.2.2 Radiochemical purity and stability study of several radiopharmaceuticals at different ratio R

Elutions were used to label different commercial kits (Table 3.4), following the methods described in the package included within kits. The RCP of radiopharmaceuticals has been evaluated after preparation for different ratio R (R = 4.34 - 11.84, corresponding to time intervals from previous elution of 36 - 72 hours), as reported in Table 3.5 and Table 3.6, respectively for DRYTEC and Elumatic III generator systems. For simplicity, data at the end of the stability period specified by the manufacturer are not reported, because they fell within the specifications required. Table 3.7 reports all RCP of radiopharmaceuticals at the end of the stability period indicated by the manufacturer (t_{EX}), using the first eluate of each generator. All tables reports the mean value and the standard deviation obtained by performing 3 tests for each case, as well as the RCP requirements imposted by Pharmacopoeia.

The values of radiochemical purity are always superior to the standards required by the manufacturer. Results show that the total amount of technetium ($^{99m+g}Tc$) present in the first eluate and in the eluates obtained at longer intervals, from 24 h up to 72 h, did not affect the RNP of final products.

TABLE 3.6: RCP of radiopharmaceuticals at t_0, prepared with generator Elumatic III
eluates at time superior to 24 h from the last elution [109].

Commercial Name	Elumatic III RCP_{36}	Elumatic III RCP_{48}	Elumatic III RCP_{72}	RCP Requirements
Ratio R	4.34	6.50	11.84	
Neurolite	98.77±0.89	99.21±0.71	98.68±0.95	≥ 90%
Cardiolite	97.88±0.78	98.83±0.92	99.13±0.63	≥ 94%
Stamicis	98.78±0.23	98.90±0.02	98.00±0.19	≥ 94%
Technemibi	98.45±0.09	98.17±0.23	98.11±0.06	≥ 94%
TechneScan	99.79±0.64	98.1±0.44	99.44±0.14	≥ 95%
Pentacis	99.14±0.12	98.88±0.15	98.12±1.03	≥ 95%
Medronato II	99.11±0.33	99.44±0.15	99.11±0.43	≥ 95%
Osteocis	99.01±0.24	98.44±0.16	99.63±0.64	≥ 95%
Nanocoll	98.99±0.03	99.18±0.49	98.11±0.11	≥ 95%
Renocis	99.35±0.22	98.67±0.17	99.03±0.29	≥ 95%

TABLE 3.7: RCP of radiopharmaceuticals at t_0 and t_{EX}, prepared with first eluate
obtained from commercial generator systems and RCP requirements [109].

Commercial Name	DRYTEC $RCP(t_0)$	DRYTEC $RCP(t_{EX})$	Elumatic III $RCP(t_0)$	Elumatic III $RCP(t_{EX})$	RCP Requirements
Neurolite	99.17±0.25	99.13±0.21	98.38±0.54	98.74±0.25	≥ 90%
Cardiolite	97.67±1.24	97.71±1.13	97.68±0.56	97.77±0.88	≥ 94%
Stamicis	98.65±0.40	98.57±0.57	98.42±1.02	99.03±0.48	≥ 94%
Technemibi	98.15±0.11	98.01±0.04	97.99±0.11	98.15±0.14	≥ 94%
TechneScan	98.79±0.02	98.11±0.15	98.11±0.62	98.43±0.29	≥ 95%
Pentacis	99.03±0.24	99.88±0.11	99.16±0.32	99.19±0.11	≥ 95%
Medronato II	98.10±0.13	98.02±0.15	99.13±0.04	98.77±0.08	≥ 95%
Osteocis	99.23±0.18	98.15±0.16	99.17±0.12	98.76±0.29	≥ 95%
Nanocoll	98.22±0.13	98.33±0.39	98.79±0.16	98.92±0.59	≥ 95%
Renocis	99.28±0.07	98.55±0.21	99.11±0.35	99.01±0.32	≥ 95%

TABLE 3.8: Evaluation of total technetium amount in ^{99m}Tc eluates coming from
a generator with ^{99}Mo calibrated activity of 10 GBq, at different times by previous
elution [109].

Time by the previous elution	Amount of total Tc calculated	$^{99g}Tc/^{99m}Tc$ ratio calculated	Amount of total Tc found	$^{99g}Tc/^{99m}Tc$ ratio found
72 h	0.30 μg	11.84		
48 h	0.22 μg	6.50	0.22±0.01	6.68±0.31
36 h	0.18 μg	4.34		
24 h	0.13 μg	2.54	0.12±0.01	3.23±0.15

Table 3.8 shows an estimation of the total amount of technetium present in an eluate
obtained from a ^{99m}Tc generator with ^{99}Mo calibrated activity of 10 GBq.

The ratios R of three ^{99m}Tc eluates at 24 hours and two ^{99m}Tc first eluates at 48
hours have been measured, and the results have been $R_{24} = 3.23\pm0.15$ and $R_{48} =$
6.68±0.31, respectively. While the experimental value of first eluates at 48 hours is in
good agreement with the theoretical value of 6.5, the experimental value of eluates at
24 hours shows a large difference with respect to the theoretical value of 2.55. This
discrepancy could be explained by taking into account the elution efficiency $\epsilon = 0.91$
of ^{99}Mo generators used in our work. Indeed, the recalculated ratio R at 24 hours is
included in the range (2.78–3.38) and depends on temporal sequence of previous elutions.
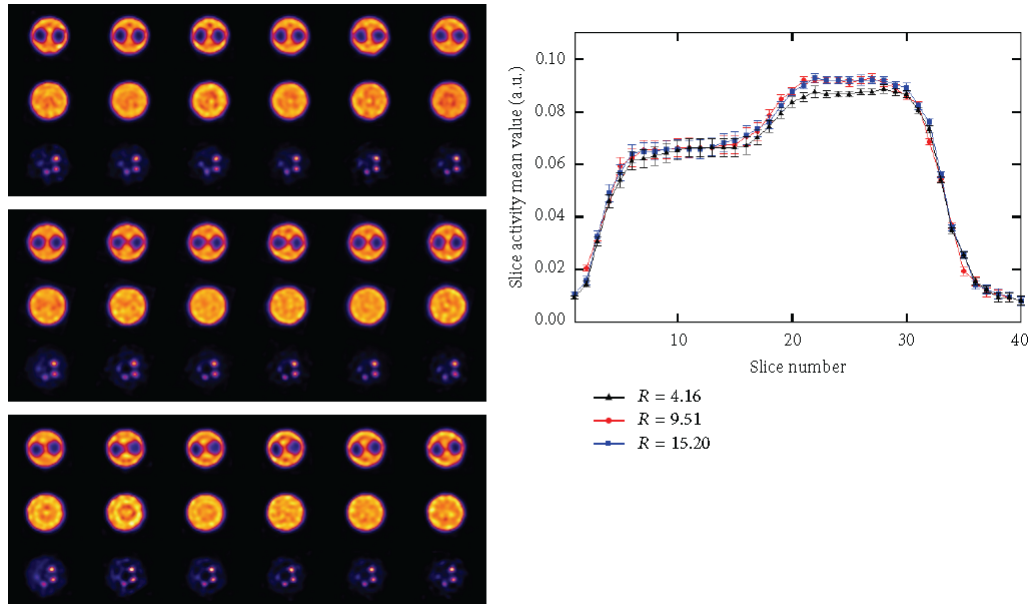
FIGURE 3.5: Reconstructed SPECT trans-axial slices of NEMA NU 4-2008 filled with ^{99m}Tc-pertechnetate solution. Top image refers to $R = 4.16$, middle image to $R = 9.51$, and bottom image to $R = 15.2$. On the right it is reported the average reconstructed activity along the phantom axis, for the three values of R [109].

A future goal will be to repeat the experiments with ^{99m}Tc eluates coming from generators with ^{99}Mo calibrated activity higher than 10 GBq, in order to check the possible impact of ^{99g}Tc in higher ^{99m}Tc activities solutions at different ^{99g}Tc/^{99m}Tc ratio. Another future goal will be to study the impact of accelerated-based ^{99g}Tc and other Tc-isotopes on the image quality and determine the allowed limit for ^{99g}Tc and other Tc-isotopes in the final accelerator-produced Tc.

3.2.3 Imaging study of commercial generator's elutions at different ratio R

In order to find a protocol to assess the image quality for accelerator-produced ^{99m}Tc (and other Tc-isotopes), a preliminary imaging study has been performed, by using three ^{99m}Tc eluates produced by commercial generator with different ^{99g}Tc/^{99m}Tc ratio R. In particular, eluates with R equals to 4.16, 9.51, and 15.2 were used for filling a NEMA phantom NU 4-2008 with 74 MBq of ^{99m}Tc-pertechnetate solution. Each tomographic acquisition has been acquired with the YAP-(S)PET small animal scanner prototype [114] and reconstructed by using an EM-ML algorithm, as shown in Figure 3.5. The same Figure also reports the average reconstructed activity along the phantom axis, for the three values of R.

As expected, the visual inspection on the images and the qualitative analysis performed do not show significant difference in image quality or radioactivity distribution up to R
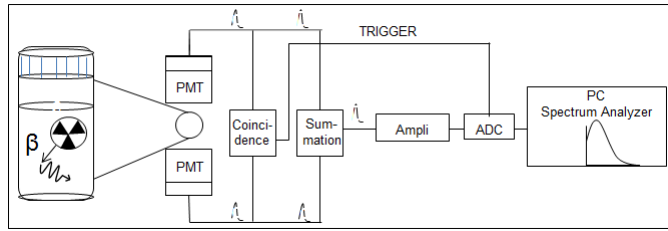
FIGURE 3.6: Scheme of the β-spectrometer under development.
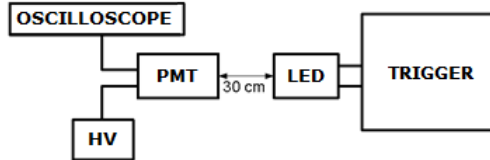
FIGURE 3.7: Scheme of the apparatus used for PMTs' gain alignment.

= 15.2. However, since the NEMA NU 4-2008 phantom had been filled with $^{99m+g}Tc$-pertechnetate solution, no variations in image quality could have been found. The aim of this study was to develop a protocol for testing imaging variations in case of accelerator-produced ^{99m}Tc, when other Tc-nuclides are produced and thus infer in SPECT images.

3.2.4 β-spectrometer development for ^{99g}Tc activity estimations

In order to have a precise measurement of the activity of the pure β-emitter ^{99g}Tc, a β-spectrometer, schematizes in Figure 3.6, is under development in the framework of APOTEMA. This work has been carried out in collaboration with Dr. Giovanni Di Domenico and Laura Fornasini, that focused her bachelor degree thesis on this topic (March 2013 at University of Ferrara).

The pure β-emitter ^{99g}Tc is mixed with a liquid scintillator in a plastic vial, that is placed between two HAMAMATSU R329-02 photomultiplier tubes (PMT). In order to improve the signal to noise ratio (SNR), only the signals in coincidence are considered and acquired. As shown in Figure 3.6, the signals in coincidence are summed together, in order to acquire with a multichannel analyzer (MCA) the total energy deposited in the liquid scintillator by the β-radiation.

In order to avoid distortion effects in the final spectra, for the same light source the PMTs have to produce equal signals. Thus some calibration tests have been performed on each PMT, in order to find out the dependence of the output signal on the applied high voltage (HV), when using a constant LED source, as shown in Figure 3.7. The LED source was previously tested, in order to work in a linear operational range. The distance LED-PMT was 30 cm.
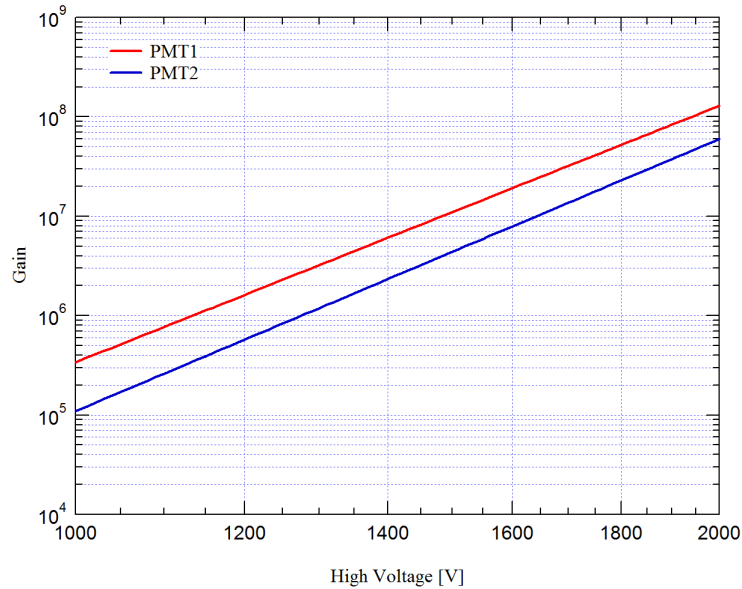
FIGURE 3.8: PMTs' gain dependence on the HV applied.

Keeping constant the LED source and varying the HV to each PMT, it was possible to evaluate the dependence of the signal on the HV, and thus to estimate the Gain (G) as a function of HV (Figure 3.8).

Figure 3.8 shows that in order to get the same output signal, to the PMT1 has to be applied a lower HV than to the one applied to PMT2.

Moreover, due to the need of coincidence trigger, the Transit Time Spread (TTS) has to be as low as possible for both PMTs. For this reason the HAMAMATSU R329-02 model has been chosen, since it provides TTS = 1.1 ns. By using a pulse trigger generator and a Time to Amplitude Converter (TAC) module, signals with known delay have been acquired with each PMT, in order to measure the effective TTS. Figure 3.9 reports the results obtained for both PMTs, as a function of the HV applied.

Figure 3.9 shows that the measured TTS are smaller than the reference value of 1.1 ns, since for both PMTs the TTS always smaller than 0.7 ns and quite constant varying the HV.

Also the dark current of each PMT was measured and within the value reported on the data sheet.

The future step will be to assembly the β-spectrometer and calibrate it with certified ^{99g}Tc activities, in order to estimate its efficiency and correct the measurements for quench effects.
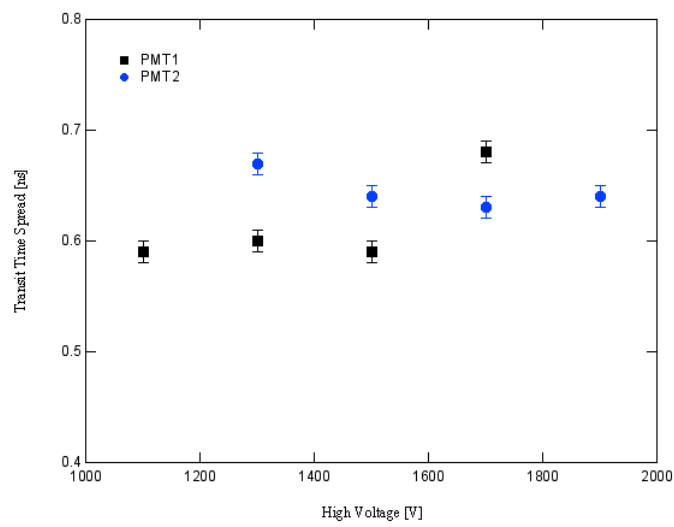
FIGURE 3.9: TTS dependence as a function of the HV applied to each PMT.

Chapter 4

New cross section measurement for ^{99}Mo production and yield estimation

4.1 Evaluation of the ^{96}Zr(α,n)^{99}Mo reaction

The ^{96}Zr(α,n)^{99}Mo reaction was evaluated only once in 1995 by Chowdhury et al. [21] and here it is presented a new measurement of this cross section, performed in 2013 at ARRONAX facility. Highly pure natural Zirconium foils has been used as target (purity 99.8%) but the cross section has been later rescaled to 100% ^{96}Zr, as (α,n) is the only open channel for the production of ^{99}Mo on ^{nat}Zr (Figure 4.1).

FIGURE 4.1: Scheme of ^{99}Mo production via (α,n) reaction on ^{96}Zr target [69].
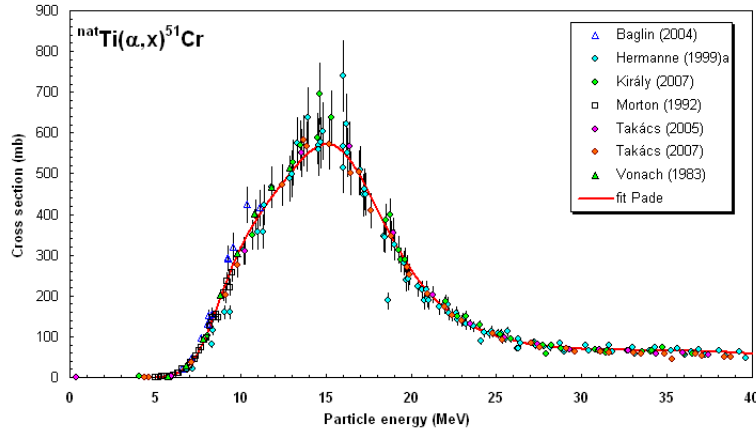
FIGURE 4.2: Recommended cross section of the ^{nat}Ti(α,x)^{51}Cr reaction [115, 116].

TABLE 4.1: Nuclear data used in the ^{96}Zr(α,n)^{99}Mo cross section calculation.

	Half-life $\tau_{1/2}$	γ-line Energy [keV]	γ-line Intensity [%]
Mo-99	65.976 h *24*	181.068	6.14 *12*
		366.421	1.204 *22*
		739.500	12.26 *22*
		777.921	4.30 *8*
Tc-99m	6.0067 h *5*	140.511	89 *4*
Cr-51	27.7025 d *24*	320.0824	9.910 *10*

TABLE 4.2: Isotopic distribution of natural Zirconium used as target [69].

Isotope Content	Zr-90 [%]	Zr-91 [%]	Zr-92 [%]	Zr-94 [%]	Zr-96 [%]
Natural ^{nat}Zr	51.45	11.22	17.15	17.38	2.80

Figure 4.2 shows the monitor reaction ^{nat}Ti(α,x)^{51}Cr taken as reference for the entire energy range (8-34 MeV), while 4.1 reports all nuclear data used for the ^{96}Zr(α,n)^{99}Mo cross section calculation [69].

4.1.1 Staked foil target preparation and irradiations

Stacked foil targets containing highly pure ^{nat}Zr foils (purity 99.8%) were irradiated with the 67 MeV α-beam and a current $I < 200$ nA. Considering that ^{96}Zr is 2.8% of natural Zr targets (Table 4.2), in order to produce an adequate ^{99}Mo activity the irradiation time was about 4 hours (Table 4.3).

Figure 4.3 outlines a typical stacked target structure. In front of the target some Al foils were used as beam energy degrader (1.00-1.26 mm thick) and then was added 2-4 times

TABLE 4.3: Resume of the irradiations performed at the facility ARRONAX.

Irradiation No.	Irradiation Date	Zr foils No.	Energy α-beam [MeV]	Irradiation time [s]	Mean value current [nA]
1	03/05/2013	2	67.4	17100	184.25
2	10/05/2013	3	67.2	19500	118.58
3	27/05/2013	3	67.4	12540	190.31
4	05/06/2013	4	67.2	15900	140.93

FIGURE 4.3: Scheme of a typical stacked target.
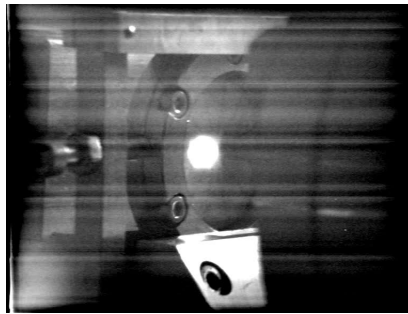
FIGURE 4.4: Picture of the α-beam at the end of the alignment process (4th irr.).

a pattern composed by a ^{nat}Ti foil (10 μm) as monitor, a ^{nat}Zr foil (10 μm) as target and an Al foil (10, 20, 100 μm) as catcher of recoils particles and energy degrader. All the high purity foils (purity >99%) were supplied by Goodfellow (England).

Before positioned the stacked target on the beam line (Figure **??**), the alpha-beam has been always well centred on the target by using an Alumina (Al$_2$0$_3$) foil and a camera for detecting the fluorescence emitted. Figure 4.4 reports a picture of the beam at the end of the alignment procedure, for the case of the 4th irradiation (E$_\alpha$ = 67.2 MeV , I $\sim$ 140 nA).

4.1.2 γ-spectrometry and cross section calculation

After a cooling time of at least 10 hours, the activities of irradiated samples have been measured without any chemical separation using γ-ray spectroscopy. The High Purity
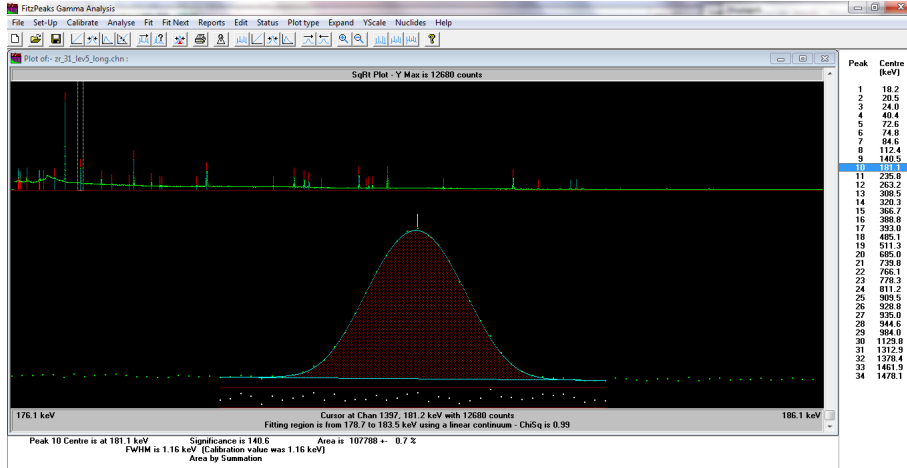
FIGURE 4.5: Typical spectra of an irradiated ^{nat}Zr foil (*Zr-31*, 3rd irr., 1st target foil, *Level 5*) and fit of the 181 keV peak.

Germanium (HPGe) detector named *Arrofixe*, previously calibrated with standard point-like sources (Section 2.3), has been always used.

The counting time was about 14-20 hours in case of ^{nat}Zr and Al foils, and about 12-15 hours for ^{nat}Ti foils. In order to have good estimation of the live time, during spectra acquisition the dead time was always kept below 6%, by using two distances sample-detector (respectively 5.2 cm and 15.2 cm, as described in Section 2.3). Figure 4.5 shows a typical spectra of an irradiated ^{nat}Zr foil.

In order to calculate the activities at EOIB, in the software FitzPeaks it is necessary to indicate for each sample some irradiation details (starting and stopping time), an efficiency calibration (Section 2.3) and an appropriated library, that was created by taking as reference nuclear data from [69]. In order to calculate the ^{51}Cr activity, the γ-line at 320 keV was used, while for ^{99}Mo a weighted mean value of the γ-lines at 739 keV and 181 keV has been considered. Other γ-lines of ^{99}Mo have been neglected: the one at 140.5 keV due to the interference of ^{99m}Tc γ-rays, the one at 366.4 keV because of low abundance and thus low statistics, the one at 778 keV present interference with the co-produced ^{96}Nb (half-life $\tau_{1/2} = 23.35$ h) (Table 4.1).

In order to calculate the ^{96}Zr(α,n)^{99}Mo cross section, the well-known activation formula has been applied (Equation 2.5), taking the ^{nat}Ti(α,x)^{51}Cr cross section as reference (Figure 4.2).

The amount of recoil atoms was measured for both target and monitor foils. In case of ^{99}Mo the quantity of recoils in the Al catcher foil was negligible, while the amount of ^{51}Cr recoil atoms in ^{nat}Zr foils were about 10% of the activity measured in ^{nat}Ti foils. Thus the total ^{51}Cr activity produced, Act'_{TOT}, considered in Equation 2.5, has been

calculated as the sum of the activities in the monitor, Act'_{Ti}, and in the following target foil, Act'_{Zr} (Equation 4.1):

$$Act_{TOT} = Act_{Ti} + Act_{Zr} \qquad \sigma(Act_{TOT}) = \sigma(Act_{Ti}) + \sigma(Act_{Zr}) \qquad (4.1)$$

Where $\sigma(Act_{TOT})$ is the resulting uncertainty, calculated from $\sigma(Act_{Ti})$ and $\sigma(Act_{Zr})$, the overall uncertainties related to the ^{51}Cr activities in the monitor and in the target foil (since the parameters are independent there is no need to add the covariance term in the error propagation).

Moreover, in order to get a better estimation of the reference cross section $\sigma'(E')$ (Equation 2.5), a weighted value of the possible reference cross sections has been calculated, considering as weighting function the probability to have a particle at a given energy in the beam. Therefore for the energy distribution of α-particles a Gaussian distribution has been considered, characterized by a mean value equal to the energy in the foil ($\mu = E'$) and a standard deviation equal to the beam energy uncertainty ($s = \delta(E')$). The energy uncertainty for each ^{nat}Zr and ^{nat}Ti foil has been evaluated by considering the estimated value of 300 keV (provided by IBA), as initial uncertainty of the α-beam energy and calculating the beam energy straggling in each foil of the stacked-target with the software SRIM. For example considering an initial beam energy of 67.4 MeV, the energy straggling in each foil of the stacked target has been calculated also for the initial beam energies of 67.1 MeV and 67.7 MeV, obtaining respectively the lower and higher energy uncertainty limit. The highest discrepancy between the weighted and nominal reference cross sections was less than 5%, but an higher discrepancy could have been found for larger energy uncertainty values or faster variations in the reference cross section.

The overall cross section uncertainty has been measured by taking the square root of the sum of the squares of the individual uncertainties: reference cross section (8% or 12%), detector efficiency and sample-detector geometry (5%), statistical errors (2-6%), target thickness (1%), decay data errors ($\approx 1\%$) [69]. The uncertainty related to the reference cross section is the biggest contribution to the final one, and it has been estimated by taking the uncertainty of the closest experimental value considered in the interpolation curve [115, 116].

Table 4.4 and Figure 4.6 report the evaluation of the $^{96}Zr(\alpha,n)^{99}Mo$ reaction performed in this work (rescaled to a 100% enriched ^{96}Zr target). Figure 4.6 also shows its spline interpolation curve and the previous measurement performed by Chowdhury et al. in 1995 [21].

TABLE 4.4: Results of the $^{96}Zr(\alpha,n)^{99}Mo$ cross section measurements. When missing, ^{99}Mo activity was lower than the detection limit.

	Energy ± Unc. [MeV]	Energy Unc. [%]	Cross Section ± Unc. [mb]	Cross Section Unc. [%]
Zr-11	26.15 ± 0.93	3.6	33.55 ± 4.35	13.0
Zr-12	18.26 ± 1.21	6.6	133.69 ± 14.62	10.9
Zr-21	23.12 ± 1.00	4.3	38.57 ± 4.34	11.3
Zr-22	18.75 ± 1.17	6.3	123.75 ± 13.54	10.9
Zr-23	14.95 ± 1.37	9.1	91.59 ± 10.04	11.0
Zr-31	20.49 ± 1.11	5.4	77.06 ± 8.45	11.0
Zr-32	17.14 ± 1.29	7.5	160.79 ± 17.59	10.9
Zr-33	13.11 ± 1.54	11.7	18.69 ± 2.10	11.3
Zr-41	32.86 ± 0.81	2.5	24.19 ± 2.93	12.1
Zr-42	26.55 ± 0.92	3.5	31.28 ± 3.75	12.0
Zr-43	18.99 ± 1.15	6.1	115.50 ± 12.65	11.0
Zr-44	7.81 ± 2.09	26.7	-	-
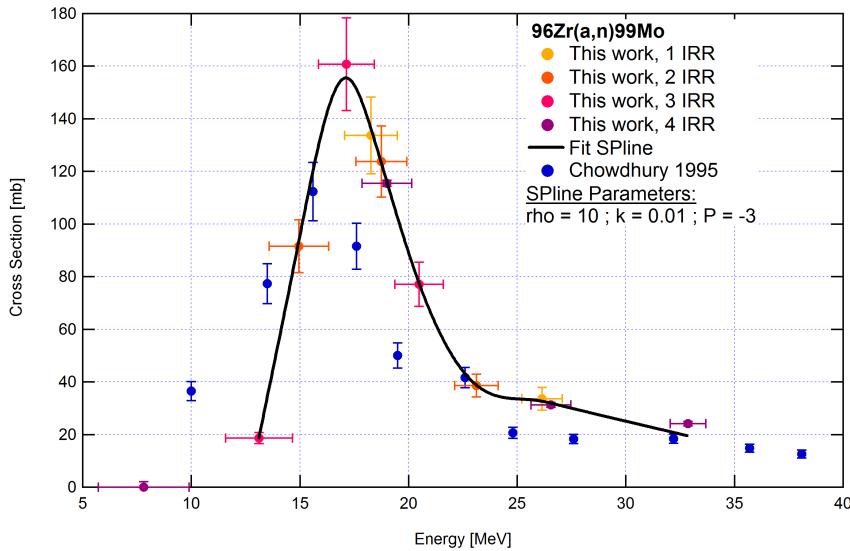
FIGURE 4.6: Evaluation of the $^{96}Zr(\alpha,n)^{99}Mo$ reaction and comparison with [21]. The interpolation of our data set has been done with $\rho = 10$.

The cross section values obtained in different irradiations show excellent agreement and indicate that the ideal energy range for ^{99}Mo production is 12-25 MeV. Figure 4.6 also shows the comparison of our results with the previous measurement [2]: there is good agreement in the trend of the cross section but our results presents a higher peak value and a shift of about 2 MeV towards higher energies. Figure 4.6 also reports the spline interpolation curve (i.e. a continuous function composed by pieces of cubic polynomials) of values obtained in this work, calculated by using a code developed in 2009 at ARRONAX by F. Haddad, S. David and E. Garrido. In the spline curve used at each i-*th* cross section value is associated a weight w_i, related to its experimental uncertainty δ_i (Equation 4.2):
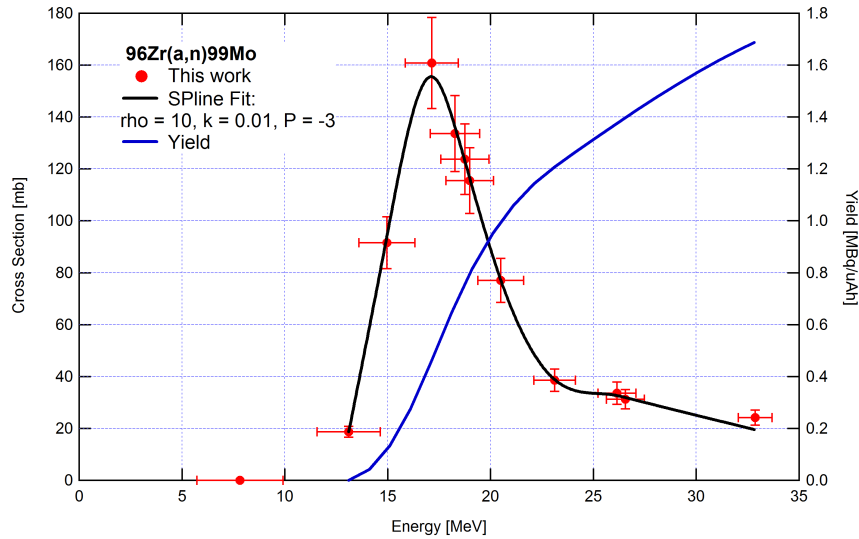
FIGURE 4.7: ^{99}Mo yield and ^{96}Zr(α,n)^{99}Mo interpolated cross section vs alpha energy.

$$w_i(\delta) = \rho(1 + k \cdot \delta_i)^P \qquad (4.2)$$

Where ρ, k and P are constants: $k = 0.01$, $P = $ -3 (in order to impose polynomial cubic functions), ρ is optimized for each reaction and for the ^{96}Zr(α,n)^{99}Mo cross section the value $\rho = 10$ was used.

4.2   Estimation of the ^{99}Mo production yields for the ^{96}Zr(α,n) reaction: comparison with the p-based routes

By using the same code and considering the spline curve for the ^{96}Zr(α,n)^{99}Mo reaction, the production yields of ^{99}Mo vs beam energy (Figure 4.7) and vs target thickness (Figure 4.8) have been estimated for the optimized α-beam energy ranging from 25 to 12 MeV.

Figure 4.8 shows that the target thickness required to produce 1.3 MBq/μAh is about 120 μm, providing about 16.7 (MBq/μAh)/(g/cm^2).

Some thermal estimations have also been done by using the heat equation in one dimension and considering the target (120 μm thick) perpendicular to the α-beam ($I = $ 100 μA), an energy lost in the target from 25 to 12 MeV and a thermal conductivity of Zirconium of 22.7 W/mK. Two estimations have been done, respectively for 5000
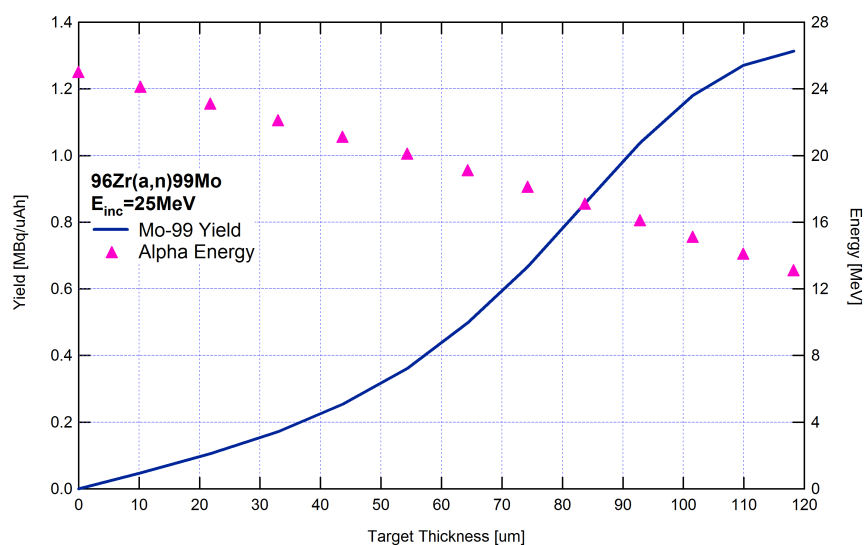
FIGURE 4.8: ^{99}Mo yield and alpha energy vs target thickness (^{96}Zr), considering E_P = 25 MeV.

TABLE 4.5: Results of the thermal estimations done considering a vertical target (^{96}Zr, 120 μm thick) irradiated with 100μA of α-beam, an energy loss ranging from 25 to 12 MeV in the target and a thermal conductivity of Zirconium of 22.7 W/mK.

Thermal Transfer Coefficient [W/m²K]	Temperature in the front of the target [K]	Temperature in the back of the target [K]
5000	1130	1120
10000	718	707

and 10000 W/m²K as thermal transfer coefficients, referred to different efficiencies of a forced cooling system with water at 293 K. Table 4.5 reports the results obtained; considering that the melting point of Zirconium is at 2128 K, in both cases (5000 and 10000 W/m²K) the temperatures achieved in the front and in the back of targets are lower than this maximum limit, showing the feasibility of this route also from a thermal point of view.

The ^{96}Zr(α,n)^{99}Mo reaction, assuming an efficient chemical extraction of ^{99}Mo from target, gives a final product characterized by high Specific Activity (SA), i.e. the ratio between the produced activity and target mass [Bq/g], as required in the manufacture of standard ^{99}Mo/^{99m}Tc generator systems.

Moreover, considering an efficient recovery process, the same target could be used for many irradiations, both reducing the final activity cost and without affecting the quality of resulting ^{99}Mo, since (α,n) is the only open channel for such production. A detail analysis of such aspects goes beyond the aim of this study; however, some considerations regarding the quality of resulting ^{99}Mo can be provided in case of α- and p-based routes. First of all considering ^{100}Mo(p,x)^{99}Mo and ^{96}Zr(α,n)^{99}Mo reactions the RadioNuclidic

Purity (RNP), i.e. the ratio between the ^{99}Mo activity and the total Mo-isotopes activity, is very high in both cases, since other Mo isotopes are stable. In fact, the only radioactive Mo-isotopes that could be produced are ^{93m}Mo and ^{93g}Mo (half-life 6.85 h and $4.0 \cdot 10^3$ y respectively) and the threshold energies of ^{100}Mo(p,p7n) and ^{96}Zr(α,7n) reactions are respectively 56.4 MeV and 54.9 MeV [69]. However, in case of the proton-induced on ^{100}Mo targets the extraction of ^{99}Mo is not possible and the resulting low SA product forces the use of alternative generator systems [7] or the direct production of ^{99m}Tc via the ^{100}Mo(p,2n) reaction. Both options have already been studied (and discussed in Chapter 1 and Chapter 3): in particular, many alternative generator systems have been proposed, such as gel generators [39, 40, 41, 44], nanocrystalline column matrix generators [45] and large centralized generator facilities [38]; also a ^{99m}Tc concentration technique has been analysed for large elution volume from low-SA generators [37]. On the other hand, the direct production of ^{99m}Tc is an interesting solution that however raises many issues due to the co-production of other Tc-isotopes, that could affect the final image quality [15, 16, 117] and increase the radiation dose to patients [110]; for these reasons, a careful analysis of irradiation conditions is mandatory, as discussed in Chapter 3 and in different studies [7, 9, 118].

In conclusion it has to be stressed that in order to estimate and compare activity costs related to α- and p-based routes, the full production chain has to be considered, including target manufacturing, irradiation time and cost and chemical processes needed to eventually extract and purify ^{99}Mo from target (α-induced case) or produce ^{99}Mo/^{99m}Tc generator systems (both cases). Moreover, an efficient recovery process is mandatory for reducing production costs: it has to be underlined that in principle the same ^{96}Zr target can be used for many irradiations, without affecting the final ^{99}Mo quality, as (α,n) is the only open channel and ^{99}Mo can be chemically separated from Zirconium. On the other hand, with re-used ^{100}Mo targets the produced ^{99}Mo presents a lower SA at each step, due to the decreasing amount of ^{100}Mo atoms and the presence of different reaction channels opened on other in-target produced Mo-isotopes. Considering the direct ^{99m}Tc production, in a recent paper by Gagnon et al. (2012) [18], the single re-use of enriched ^{100}Mo metal samples is analysed, demonstrating the feasibility of molybdenum recovery from a chemical point of view. However, the issue about how many times the material recovered might be reused, before the impact on the accelerator produced ^{99m}Tc-quality becomes critical, still needs to be defined. A detail analysis of all these aspects has to be carefully performed in order to guarantee high quality ^{99m}Tc. At the end it is important to remind that actually the Official European Pharmacopoeia[1] uniquely consider ^{99m}Tc coming from generator systems (prepared with ^{99}Mo produced

---

[1]European Pharmacopoeia, 7th Ed., Sodium pertechnetate (^{99m}Tc) injection (fission) (0124).

in fission- e/o n-induced reactions), causing a lack in the requirements that have to be fulfilled in case of accelerator-produced technetium.

Chapter 5

New cross section measurement for ^{67}Cu production and yield estimation

5.1 Evaluation of the ^{68}Zn(p,2p)^{67}Cu reaction

The ^{68}Zn(p,2p)^{67}Cu reaction has been already measured in different experimental campaigns, as reported in Figures 1.12 and 1.11 (Section 1.2.2). A new evaluation of this cross section has been done at the ARRONAX facility and it is here presented. Enriched ^{68}Zn powder has been used for the target preparation *via* electrodeposition on silver foil (Ag) support (Section 5.1.1). As discussed in this chapter, the most efficient way to produce ^{67}Cu is *via* the (p,2p) reaction on ^{68}Zn targets (Figure 5.1).

FIGURE 5.1: Scheme of ^{67}Cu production *via* (p,2p) reaction on ^{68}Zn target and ^{67}Ga co-production *via* (p,2n) reaction [69].

TABLE 5.1: Nuclear data used in the $^{68}Zn(p,2p)^{67}Cu$ cross section calculation.

	Half-life $\tau_{1/2}$	γ-line Energy [keV]	γ-line Intensity [%]
Cu-67	61.83 h *12*	184.577	48.7 *3*
		208.951	0.115 *5*
		300.219	0.797 *11*
		393.529	0.220 *8*
Cu-61	3.333 h *5*	282.956	12.2 *22*
		656.008	10.8 *20*
Ga-67	3.2617 d *5*	184.576	21.410 *10*
		208.950	2.460 *10*
		300.217	16.64 *12*
		393.527	4.56 *24*
Ga-66	9.49 h *3*	1039.220	37.0 *20*
Ni-57	35.60 h *6*	127.167	16.7 *5*
		1377.63	81.7 *24*
Na-22	2.6027 y *10*	1274.537	99.941 *14*
Na-24	14.997 h *12*	1368.626	99.9936 *15*
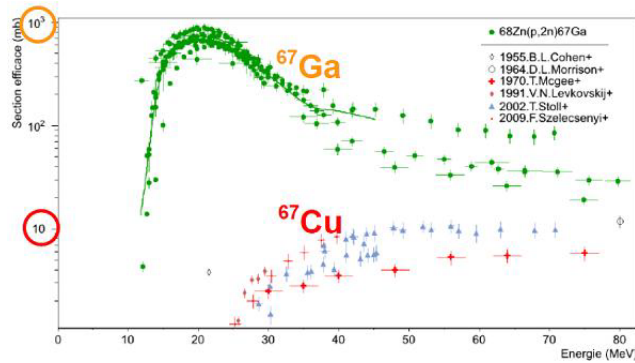
FIGURE 5.2: Evaluations of the $^{68}Zn(p,x)^{67}Cu,^{67}Ga$ cross sections up to 80 MeV [71].

During the irradiation other nuclides are co-produced in target, in particular some Cu- and Ga-isotopes, depending on the beam energy, respectively *via* (p,2pxn) and (p,xn) reactions. Among them the most important one is ^{67}Ga, that provides the same γ-lines of ^{67}Cu and similar half-life (about 78 hours), as shown in Table 5.1. In fact both nuclides turn into ^{67}Zn (and its nuclear excited levels) with different probabilities; this entails that the gammas emitted in the decay of ^{67}Cu and ^{67}Ga have the same energy and different abundance. Figure 5.2 reports the experimental evaluation of the $^{68}Zn(p,x)^{67}Cu,^{67}Ga$ cross sections [71] and shows the different orders of magnitude of such reactions. In fact, the nuclear cross section for the production of ^{67}Ga is about 10-100 times higher than the one for the ^{67}Cu production, depending on the energy.

The presence in irradiated samples of a nuclide with the same γ-lines of ^{67}Cu, similar

half-life and 10-100 times higher abundance (Table 5.1) does not permit the application of any easy technique aimed to the recognition of the activities and based on γ-spectrometry. As described in Section 5.1.3.1, an analytical method named *Branching Ratio* (BR) has been tested in order to recognize the ^{67}Cu and ^{67}Ga activities without a chemical process. The BR method is based on the different abundances of the gammas emitted and unfortunately it provides reasonable results with a very high uncertainty (about 50%), making this method useless in the cross section calculation.

For this reason, in order to separate ^{67}Cu from ^{67}Ga a chemical procedure has been applied after each irradiation, as described in Section 5.1.3. By using ^{61}Cu and ^{66}Ga as tracer nuclides for the Cu- and Ga-isotopes, the efficiency of the chemical process has been checked at each step of the procedure and for all irradiations. The hypothesis behind the use of tracers is that during a chemical process the isotopes of the same specie are not distinguishable and thus the efficiency of the treatment is the same for any Cu- and Ga-isotopes. By acquiring short spectra of the samples at the HPGe detector named *Research* (previously calibrated as described in Section 2.3), and using the γ-lines reported in Table 5.1, the activities at EOIB of ^{61}Cu and ^{66}Ga tracers have been calculated and used to know the efficiency ε of the chemical treatment. It is important to underline the use of tracer activities rescaled to EOIB, in order to correct for different decay rates. Equation 5.1 shows how the efficiency ε of the chemical treatment is estimated by calculating the ratio between the activity before (Act^I) and after (Act^F) the chemical procedure. Once known ε, the initial activities of ^{67}Cu and ^{67}Ga isotopes have been calculated by measuring the final ones and dividing them for the efficiency (Equation 5.2). Both Equation 5.1 and Equation 5.2 refer to Cu-isotopes but the same formulas have been applied for Ga-ones.

$$\varepsilon_{Cu} = \frac{Act^F_{Cu-61}}{Act^I_{Cu-61}} \tag{5.1}$$

$$Act^I_{Cu-67} = \frac{Act^F_{Cu-67}}{\varepsilon_{Cu}} = Act^F_{Cu-67} \cdot \frac{Act^I_{Cu-61}}{Act^F_{Cu-61}} \tag{5.2}$$

Once known the initial ^{67}Cu and ^{67}Ga activities at EOIB, it is possible to calculate the $^{68}Zn(p,x)^{67}Cu,^{67}Ga$ cross sections by using Equation 2.5. For energies lower than 50 MeV, the $^{nat}Ni(p,x)^{57}Ni$ reaction has been used as monitor (Figure 5.3), while for higher energy values the $^{27}Al(p,x)^{22}Na$ reaction has been taken as reference (Figure 5.4) [116].
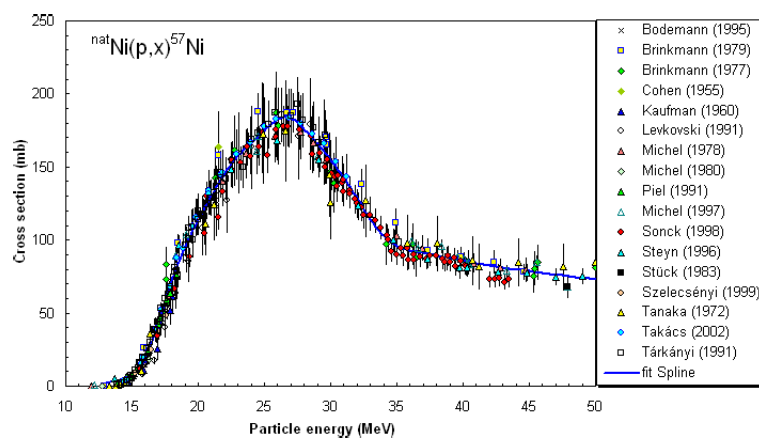
FIGURE 5.3: Recommended cross section of the ^{nat}Ni(p,x)^{57}Ni reaction [116].
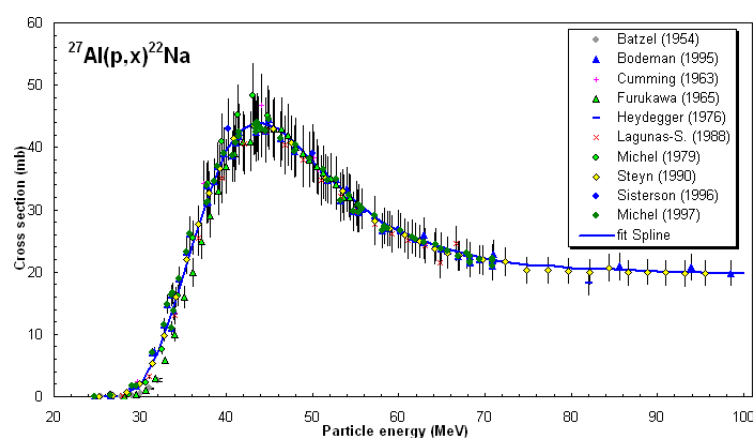
FIGURE 5.4: Recommended cross section of the ^{27}Al(p,x)^{22}Na reaction [116].

5.1.1 Target foil preparation: electrolytic deposition of enriched ^{68}Zn

In order to have thin homogeneous targets of enriched ^{68}Zn, a deposition of electrolytic solution containing ^{68}Zn metallic powder has been done on highly pure Ag foils (25 μm thick), used as support. All the foils (99% pure) were supplied by Goodfellow (London, England), while the enriched powder of ^{68}Zn (97% pure) was furnished by Chemgas (Boulogne, France). Table 5.2 reports the certified isotopic distribution of the enriched powder used as target and the comparison with natural zinc. It has to be noted that final results of the cross section are rescaled to 100% enriched Zn-68 and 100% pure materials.

The electrolytic deposition process is based on the oxydo-reduction principle between zinc ions (Zn^{2+}, oxidising agents) and water (H$_2$O molecules, reducing reagents), both contained in the electrolytic solution. This solution has been prepared by applying the following procedure:

TABLE 5.2: Isotopic distribution of the enriched ^{68}Zn used as target (Chemgas, Boulogne, France) and comparison with natural Zinc [69].

Isotope Content	Zn-64 [%]	Zn-66 [%]	Zn-67 [%]	Zn-68 [%]	Zn-70 [%]
Enriched ^{68}Zn	0.18	0.13	0.55	98.78	0.36
Natural ^{nat}Zn	49.17	23.73	4.04	18.45	0.61

- dissolving ^{68}Zn metal powder into nitric acid (HNO_3), obtaining a solution with Zn^{2+} and NO_3^- ions (few minutes);

- adding sulphuric acid (H_2SO_4), obtaining a solution with Zn^{2+}, NO_3^- and SO_4^{2-} ions

- heating the solution for 2 days, making the NO_3^- ions evaporate (68% of HNO_3 solution evaporates at 121°C) but not the SO_4^{2-} ones (the boiling point of H_2SO_4 is at 337°C)

- adding again some sulphuric acid and heat again for 2 days, in order to completely evaporate NO_3^- ions

- letting the electrolyte solution containing ^{68}ZnSO$_4$ cool down to room-temperature

Once prepared the electrolyte solution it is possible to proceed with the electrolytic deposition of enriched ^{68}Zn powder on Ag support. Figure 5.5 shows that inside the electrolytic cell of teflon (no. 1) the solution (no. 2) is kept and a platinum anode (no. 3) and a silver cathode (no. 4) are dunked in it. The cable for the electric connection of the cathode is also shown in Figure 5.5 (no. 5), as well as the reference electrode (no. 6), used for the measurement of the electric potential V applied to the system. During the electrolytic deposition, the heating plate (no. 7) keeps the system at the correct temperature [119]. Figure 5.5 shows the Ag foil that is the cathodic electrode (where the deposition of zinc took place); on the contrary, the device used for melting the solution is hidden: this precaution is taken in order to assure an homogeneous solution and thus an homogeneous deposition, avoiding a higher Zn^{2+} ions concentration on the bottom due to gravity.

In fact, many parameters influence the electrolytic deposition process, for example the potential V applied, the Zn^{2+} ions concentration, the temperature and the pH of the electrolyte solution. In order to obtain an homogeneous deposit, Thomas Sounalet (PhD student at ARRONAX) has studied the optimal conditions, founding the best values of different parameters involved in the electrolytic process.

The deposition of metallic zinc on the cathode is possible when the potential V applied to the solution is lower than the oxide/reducing couple potential. In case of Zn^{2+} ions
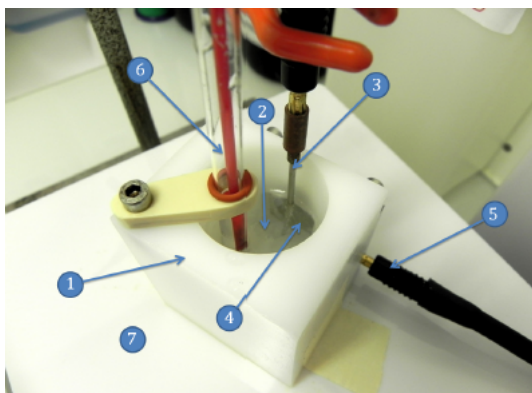
FIGURE 5.5: Picture of the electrolytic deposition apparatus [119].

and H_2O this limiting value V_L is $V_L = -0.76$ V. Thus applying smaller potential values it is possible to induce a zinc reduction of the cathode, as shown in Equation 5.3:

$$Zn^{2+} + 2e^- --> Zn \tag{5.3}$$

At the same time on the anode an oxidant process occurs, as described in Equation 5.4:

$$2H_2O --> 4H^+ + 4e^- + O_2 \tag{5.4}$$
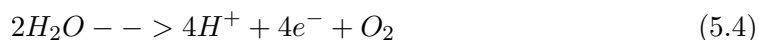
At the end of the electrolytic process an homogeneous target of metallic ^{68}Zn is obtained on the Ag support, as shown in Figure 5.6 (left). In order to test the homogeneity of the deposition surface, some images at the optical microscope have been taken and are also shown in Figure 5.6 (centre and right), respectively at 12 times and at 200 times magnification. Small holes on the target surface can be noted and are due to H_2 bubbles coming from H_2O reduction on cathode, a process that occurs simultaneously on cathode surface. The bubbles are smaller than 5 μm and can be neglected in the calculation of the target thickness.

Once confirmed the surface uniformity by profilometry, the deposition thickness can be deduced by weight, using a digital caliper and a calibrated balance (the calibration procedure is weekly applied). In fact, before starting the electrolytic deposition process the Ag support is weighted and its dimensions are measured. The same process is applied to the ^{68}Zn deposition and the calculation of the weight difference allows to get the mass of the ^{68}Zn deposition. Knowing zinc density ($\rho = 7.14$ g/cm^3) it is possible to precisely estimate the thickness of ^{68}Zn deposited.
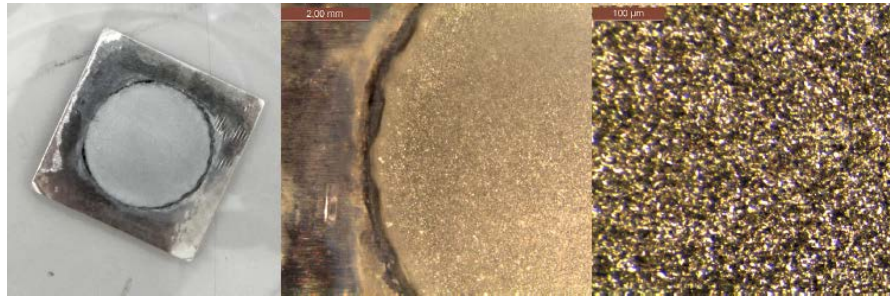
FIGURE 5.6: Photographs of a ^{68}Zn deposition on Ag support [119]: normal scale picture (left), 12 times magnification picture (centre) and 200 times magnification picture (right), the lasts taken with an optical microscope.
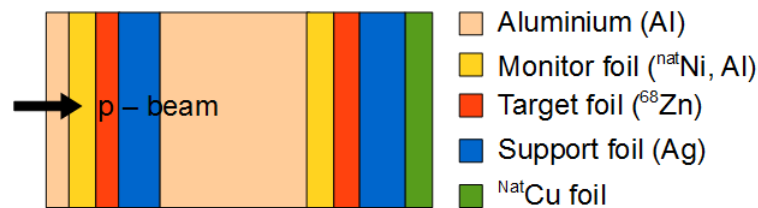
FIGURE 5.7: Scheme of a typical stacked target; as monitor has been used the ^{nat}Ni(p,x)^{57}Ni reaction for E < 50 MeV, while for E > 50 MeV the ^{27}Al(p,x)^{22}Na reaction.

5.1.2 Staked foil target preparation and irradiations

Due to the need of a chemical process and the short half-life of ^{61}Cu (about 3.3 hours, Table 5.1), only 2 target foils have been irradiated each time, as shown in a typical stacked target structure (Figure 5.7) and reported in Table 5.3.

In front of each target foil (^{68}Zn on Ag support) there was a circular monitor foil, with the same dimensions of the deposited zinc, as shown in Figure 5.8. In this way it can be assumed that the particle flux hitting the monitor foil is the same that irradiate the deposited ^{68}Zn, allowing the use of monitor reactions.

In order to fix the whole stacked target structure inside the target holder, a thin Al foil has been always insert in front of the stacked foils. Moreover, in order to produce an adequate activity of the Cu-tracer nuclide, for almost all irradiations a ^{nat}Cu foil has been added at the end of the stacked target (Figure 5.7), since *via* the (p,p+xn) reactions on ^{63}Cu (69.15%) and ^{65}Cu (30.85%) it is possible to produce an adequate amount of ^{61}Cu (Figure 5.9). Only in case of high energy beam (7th irradiation, E$_P$ = 70.4 MeV, Table 5.3) it is possible to produce a sufficient activity of ^{61}Cu directly in the target *via* the (p,2p+6n) reaction on ^{68}Zn, as reported in Figure 5.10.

Table 5.3 reports more details about the 9 irradiations performed at the ARRONAX facility, with some energy overlap between different stacks. All stacked foil targets used
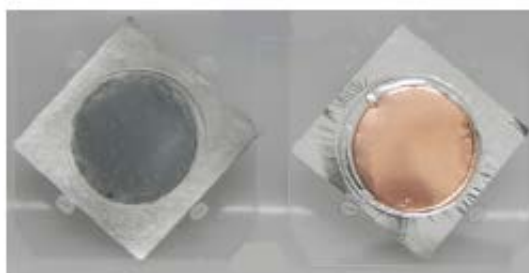
FIGURE 5.8: Photograph of a target foil (left) with a circular monitor foil exactly positioned on the ^{68}Zn deposition (right) [119].
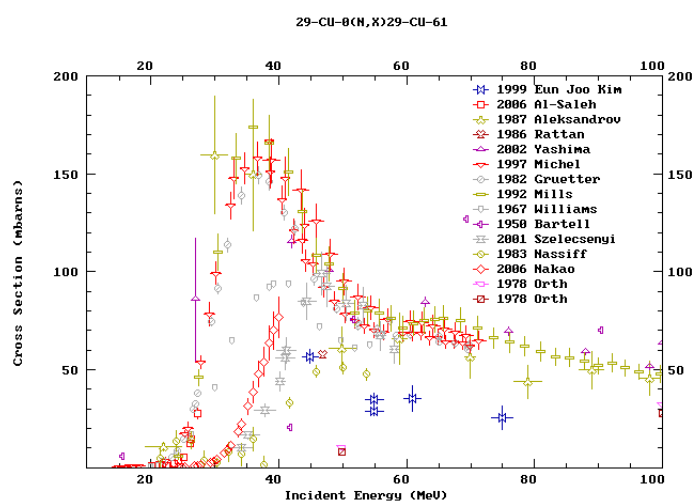
FIGURE 5.9: The $^{nat}Cu(p,p+xn)^{61}Cu$ reaction vs p-beam energy up to 100 MeV [71].
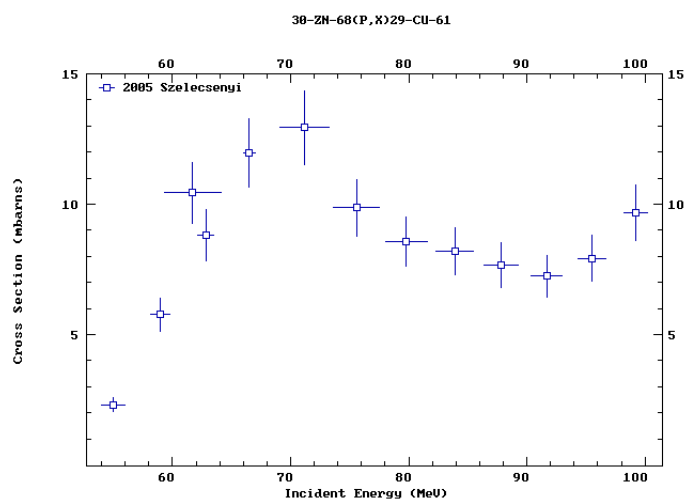
FIGURE 5.10: The $^{68}Zn(p,2p+6n)^{61}Cu$ reaction vs p-beam energy up to 100 MeV [71].

TABLE 5.3: Resume of the irradiations performed at the facility ARRONAX.

Irradiation No.	Irradiation Date	^{68}Zn foils No.	Energy p-beam [MeV]	Irradiation time [s]	Mean value current [nA]
1	10/07/2012	2	54.5	1800	104.5
2	25/07/2012	2	46.3	3600	101.6
3	13/08/2012	2	54.5	3660	152.8
4	29/08/2012	2	59.6	3600	167.2
5	03/12/2012	2	59.6	5400	205.4
6	10/12/2012	2	43.3	5400	211.8
7	21/05/2013	2	70.4	4200	188.2
8	27/06/2013	2	46.3	4320	228.6
9	01/07/2013	2	54.0	3600	208.7
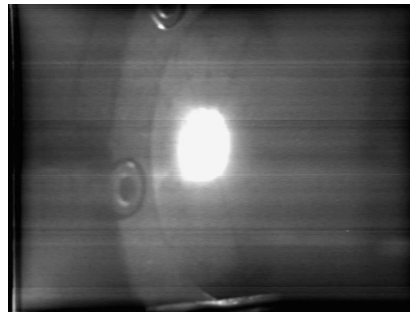
FIGURE 5.11: Picture of the p-beam at the end of the alignment process (8th irr.).

were containing 2 target foils[1] and were irradiated with the 70 MeV tunable p-beam for 30-90 minutes (depending on the case). The current used in the former irradiations was about 100 nA, while for later irradiations up to a mean value of 220 nA has been used.

Before positioned the stacked target on the beam line (Figure **??**), the proton-beam has been well centred on the target, as shown in Figure 5.11 for the case of the 8th irradiation ($E_P = 46.3$ MeV, I = 200 nA).

5.1.3 Separation Cu/Ga: the chemical procedure

About 14-15 hours after EOB[2] the following chemical procedure has been applied:

- the ^{68}Zn deposition has been dissolved into 4 mL of HNO_3 3M (Figure 5.12)

- the Ag foil has been taken and washed with 1 mL of HNO_3 3M and it is dissolved in a different becker by using 5 mL HNO_3 10M; the eventual ^{67}Cu activity lost in

---

[1]For the 6th irradiation an additional ^{nat}Zn foil has been added in front of the stacked target, preceded by its monitor ^{nat}Ni foil, in order to investigate the BR method.

[2]All irradiations have been performed in the late afternoon and the day after, early in the morning, the stacked target was taken from the beam line.

Ag has been evaluated by acquiring a spectra of the Ag dissolved foil (the activity lost in Ag support was always lower than 1 % and thus it was always considered negligible)

- the ^{nat}Cu foil was dissolved in 5 mL of HNO$_3$ 10M (Figure 5.13); its spectra was fast acquired and analysed, in order to know the total ^{61}Cu activity contained in the solution

- an aliquot of the solution with the dissolved ^{nat}Cu foil has been added to the ^{68}Zn solution, in order to get a solution with all tracers nuclide, named *mix* (in case of the 7th irradiation there was no need to add an aliquot of ^{nat}Cu solution, since a sufficient activity of ^{61}Cu was already in target produced)

- adding 1 mL of sodium chloride acid (NaCl) the precipitation of the Ag molecules in the *mix* solution has been induced and the solution has been filtered by using an appropriate paper (Figure 5.13), eliminating all the salts formed (in case of the 1st foil on the 3rd irradiation, a co-precipitation of Cu-salt in hydroxyde specie was noticed, as shown in Figure 5.13, probably due to a wrong pH of the solution)

- heating the filtered solution at about 150°C for 30-45 minutes only the salts (containing the active Cu- and Ga-nuclides) remained in the becker

- after cooling down the becker to room temperature, the remained salt are dissolved with 5 mL of HNO$_3$, in order to dissolve all the salts and to get a solution with pH = 2.25 (this was the optimal value found for the resin to separate Cu/Ga)

- the solution has been putted into the resin (Figure 5.13), in order to separate Cu- from Ga-nuclides

- the solution outcoming from the resin contained no Cu-isotopes and was named *xGa* (all elements other than Cu were present in this solution); an aliquot of 5 mL of xGa solution was taken in order to acquire its γ-spectra (obtaining Ga-isotopes activities)

- in order to release the Cu-elements from the resin about 20 mL of HNO$_3$ from 5M to 8M has been added; an aliquot of 5 mL of the outcoming solution, named *xCu*, was taken in order to acquire its γ-spectra (obtaining Cu-isotopes activities)

- in order to have the reference nuclide activities (^{57}Ni and ^{22}Na), also the monitor foils have been dissolved and 5 mL vials have been prepared for the γ-spectrometry acquisition

Table 5.4 and Table 5.5 resumes the results of the chemical procedure obtained for each irradiated foil, respectively for *xCu* and *xGa* solutions. When the activity of tracer
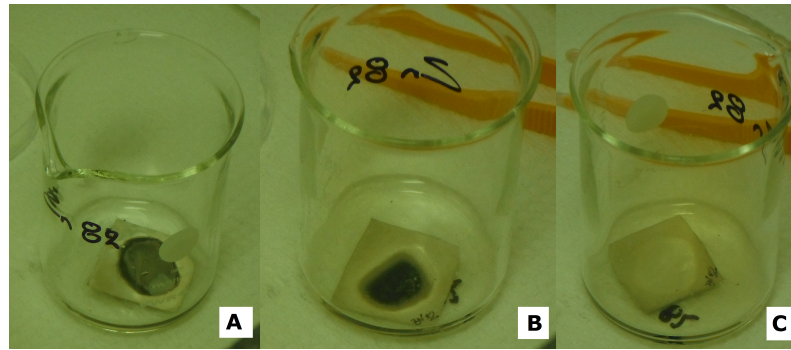
FIGURE 5.12: Photographs of the ^{68}Zn dissolution when nitric acid is added (8th irr. 2nd foil): A. Irradiated target foil placed in the becker; B. Dissoution process started; C. After few minutes all ^{68}Zn is dissolved and only the Ag foil is left.
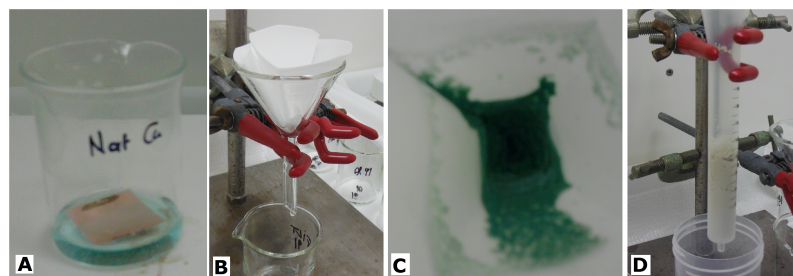
FIGURE 5.13: Photographs of some steps of the radiochemical procedure: A. ^{nat}Cu dissolution when nitric acid is added (light blue colour solution); B. Filtration procedure; C. Precipitation formed during the precipitation process for the 1st foil of the 3rd irr. (green colour due to Cu-oxidation) ; D. Resin used for the Cu/Ga separation (light ochre colour when Cu-isotopes are absorbed).

nuclides after the chemical procedure was below he detection limit (i.e. a number of counts N $\leq 2\sigma$, the variation of background in that energy range) or less than 1% of initial activity, the yield was considered negligible and thus it was not reported in Table 5.4 and 5.5.

Due to this complex chemical process, the Cu/Ga separation for the foils of the first irradiation failed, as well as for the 1st foil of the 3 irradiation (due to the co-precipitation of Cu-isotopes, shown in Figure 5.13, and a wrong pH in the solution poured in the resin). In fact, the value of Cu-yield into xGa solution was always negligible, except for the 1st foil of the 3rd irradiation, when $y_{Cu} = 0.895 \pm 7.6\%$. Table 5.4 and Table 5.5 show that even if the efficiency of the procedure was always lower than 85% (i.e. the percentage of Cu- and Ga-activities recovered at the end the chemical process), the separation was always satisfactory. In fact, the Ga-yield into xCu solution was always lower than 1.5% and *vice versa*, unless for the 5th irradiation case, when the ^{67}Ga activity in xCu was not negligible for both foils (Ga-yield about 5%, as reported in Table 5.4). Thus these results have been neglected in the estimation of the ^{68}Zn(p,2p)^{67}Cu cross section. On the contrary, for the 2nd foil of 4th irradiation the Ga-recovery in xGa solution was

TABLE 5.4: Results of the chemical yield obtained in xCu solution for all separation processes; when missing, the activities were below the detection limit or less than 1% of initial activity, given a negligible yield. The symbol (*) indicates that the separation was unsatisfactory and that the corresponding values have been neglected in the cross section calculation.

xCu solution	Cu Yield±Unc.	Cu Yield Unc [%]	Ga Yield±Unc.	Ga Yield Unc [%]
1 irr 1 f*	-	-	-	-
1 irr 2 f*	-	-	-	-
2 irr 1 f	0.561±0.048	8.6	-	-
2 irr 2 f	0.500±0.053	10.7	-	-
3 irr 1 f*	-	-	-	-
3 irr 2 f	0.757±0.050	6.6	0.002±0.000	11.6
4 irr 1 f	0.522±0.038	7.4	0.003±0.001	20.6
4 irr 2 f	0.646±0.053	8.1	0.002±0.001	34.3
5 irr 1 f*	0.349±0.028	8.1	0.048±0.006	11.6
5 irr 2 f*	0.201±0.019	9.6	0.044±0.006	14.8
6 irr 1 f	0.486±0.038	7.8	0.005±0.001	15.6
6 irr 2 f	0.415±0.033	7.9	0.003±0.000	14.1
7 irr 1 f	0.387±0.056	14.4	-	-
7 irr 2 f	0.538±0.068	12.7	0.001±0.000	36.9
8 irr 1 f	0.727±0.072	9.9	-	-
8 irr 2 f	0.734±0.101	13.8	0.001±0.000	28.8
9 irr 1 f	0.709±0.064	9.1	0.012±0.002	17.2
9 irr 2 f	0.729±0.078	10.7	-	-

about 2% and thus in this case the ^{66}Ga and ^{67}Ga cross sections were not estimated (Table 5.5).

5.1.3.1 The Branching Ratio (BR) method

As already mentioned, the presence in irradiated samples of ^{67}Ga, with the same γ-lines of ^{67}Cu, similar half-life and 10-100 times higher abundance (Table 5.1), does not permit the application of any easy technique based on γ-spectrometry and aimed to the recognition of those nuclide activities. However, an analytical method named *Branching Ratio* (BR) has been applied on acquired spectra, in order to recognize the ^{67}Cu and ^{67}Ga activities without a chemical process. The BR method is based on the different abundances of the γ-radiation emitted in the decay of ^{67}Cu and ^{67}Ga, and on the linear correlation between the activity Act of the nuclide of interest and the number of counts N revealed by the detector, as shown in Equation 5.5:

$$\begin{cases} N_{TOT}^{184} = k_1 \cdot Act_{Cu-67} + k_2 \cdot Act_{Ga-67} \\ N_{TOT}^{300} = k_3 \cdot Act_{Cu-67} + k_4 \cdot Act_{Ga-67} \end{cases} \tag{5.5}$$

TABLE 5.5: Results of the chemical yield obtained in xGa solution for all separation processes; when missing, the activities were below the detection limit or less than 1% of initial activity, given a negligible yield. The symbol (*) indicates that the separation was unsatisfactory and that the corresponding values have been neglected in the cross section calculation.

xGa solution	Cu Yield±Unc.	Cu Yield Unc [%]	Ga Yield±Unc.	Ga Yield Unc [%]
1 irr 1 f*	-	-	-	-
1 irr 2 f*	-	-	-	-
2 irr 1 f	-	-	0.755±0.079	10.5
2 irr 2 f	-	-	0.622±0.063	10.1
3 irr 1 f*	0.895±0.068	10.6	0.791±0.084	10.6
3 irr 2 f	-	-	0.694±0.068	9.8
4 irr 1 f*	-	-	0.021±0.003	13.5
4 irr 2 f	-	-	0.780±0.083	10.6
5 irr 1 f*	-	-	0.466±0.057	12.2
5 irr 2 f*	-	-	0.240± 0.036	15.0
6 irr 1 f	-	-	0.471±0.037	8.0
6 irr 2 f	-	-	0.388±0.046	11.8
7 irr 1 f	-	-	0.331±0.026	7.8
7 irr 2 f	-	-	0.538±0.040	7.4
8 irr 1 f	-	-	0.658±0.079	12.1
8 irr 2 f	-	-	0.838±0.099	11.8
9 irr 1 f	-	-	0.749±0.091	12.2
9 irr 2 f	-	-	0.608±0.073	11.9

where N_{TOT}^{184} and N_{TOT}^{300} are the number of counts respectively at the 184 and 300 keV peak; the four constants k_i^x [1/s] relate the activity Act of each nuclide to the number of counts N_{TOT}^x revealed by the detector at the energy x, as shown in Equation 5.6:

$$k_i^x = \frac{\varepsilon_i^x \cdot I_i^x (1 - e^{-\lambda_i t_L})}{\lambda_i} \tag{5.6}$$

where ε_i^x is the detector efficiency and I_i^x is the nuclide abundance at the energy x, λ_i is the nuclide decay constant and t_L is the Live time of the spectra analysed.

By solving the system shown in Equation 5.5, it is possible to obtain the ^{67}Cu and ^{67}Ga activities as a function of others parameters (all known), as reported in Equation 5.7 and Equation 5.8:

$$Act_{Cu-67} = \frac{N_{TOT}^{184}}{k_1} - \frac{k_2}{(k_1 k_4 - k_2 k_3)} \cdot \left(N_{TOT}^{300} - \frac{k_3}{k_1} \cdot N_{TOT}^{184} \right) \tag{5.7}$$

$$Act_{Ga-67} = \left(N_{TOT}^{300} - \frac{k_3}{k_1} \cdot N_{TOT}^{184} \right) \cdot \frac{k_1}{(k_1 k_4 - k_2 k_3)} \tag{5.8}$$

By applying the error propagation theory and considering that the covariance terms can be neglected since all elements are independent, the following Equation 5.9 has been used to estimate the uncertainty related to the activity (σ always refers to the total uncertainty of the corresponding parameter):

$$\sigma^2(Act_Y) = Act_Y^2 \cdot \left(\left(\frac{\partial Act_Y}{\partial N_{TOT}^{184}} \cdot \sigma(N_{TOT}^{184}) \right)^2 + \left(\frac{\partial Act_Y}{\partial N_{TOT}^{300}} \cdot \sigma(N_{TOT}^{300}) \right)^2 + \left(\frac{\partial Act_Y}{\partial k_i^x} \cdot \sigma(k_i^x) \right)^2 \right)$$
(5.9)

where $\sigma(k_i^x)$, neglecting the uncertainty related to each decay constant λ_i, is expressed by Equation 5.10:

$$\sigma^2(k_i^x) = \left(\frac{I_i^x(1 - e^{-\lambda_i t_L}))}{\lambda_i} \right)^2 \sigma^2(\varepsilon_i^x) + \left(\frac{\varepsilon_i^x(1 - e^{-\lambda_i t_L}))}{\lambda_i} \right)^2 \sigma^2(I_i^x) + \left(\varepsilon_i^x I_i^x e^{-\lambda_i t_L} \right)^2 \sigma^2(t_L)$$
(5.10)

Even if this method provides good estimations of the ^{67}Cu and ^{67}Ga activities (without applying a chemical procedure), the final huge uncertainties ($\sim 50\%$) related to these activities make the BR method completely useless for the cross section calculation (in which a final uncertainty of about 10-15% should be given).

For this reason, in order to get good estimations (with acceptable uncertainty values) of the ^{67}Cu and ^{67}Ga activities, a chemical procedure has been applied, as previously described.

5.1.4 γ-spectrometry and cross section calculation

About 14-15 hours after EOB, the chemical procedure and the γ-spectrometry have been started. The *Research* detector was previously calibrated with standard liquid sources, as described in Section 2.3. The counting time of the 5 mL aliquot of *xCu* and *xGa* solutions was about 30-120 minutes, while for ^{nat}Cu solution and other steps of the chemical procedure (such as *mix* and *filtered* solutions) the counting times were about 10-30 minutes. In order to always keep low values for the Dead Time (DT $< 10\%$) two geometries were used, named *g0* and *g1*, as described in Section 2.3.

The activities at EOIB have been calculated by using the software FitzPeaks [106], which requires for each sample some irradiation details (starting and stopping time), an efficiency calibration (Section 2.3) and an appropriated library, that was created by taking as reference nuclear data shown in Table 5.1 [69]. In order to calculate the monitor activities, in case of ^{57}Ni a weighted mean value of the activities corresponding to the

γ-lines at 127 and 1378 keV has been calculated, while ^{22}Na activity was calculated from the 1275 keV peak.

At this regard, particular attention has to be paid to the choice of the reference nuclide (specially to its recommended cross section), since in this work some problems have been found when the ^{27}Al(p,x)^{24}Na reaction was considered [116], as discussed in Appendix B. For this reason, at E > 50 MeV the ^{22}Na activity was always taken as reference.

The overall cross section uncertainty has been measured by taking the square root of the sum of the squares of the individual uncertainties: reference cross section (8 or 12%), detector efficiency (5%), activity uncertainty (< 10%), target thickness (1%), decay data errors ($\approx$ 1%) [69]. The uncertainty related to the monitor reaction and the nuclide activity are the biggest contribution to the overall uncertainty. As already mentioned, in this work it was always attributed to each reference value the uncertainty corresponding to the closest experimental value considered in the fit.

The energy uncertainty $\delta(E)$ for each cross section value has been evaluated considering an estimated value of 530 keV as initial beam energy uncertainty (value provided by IBA) and than calculating with the software SRIM the beam energy straggling in each foil. For example, considering an initial beam energy of 70.4 keV, the energy straggling in each foil of the stacked target was calculated also for the initial beam energies of 69.87 keV and 70.93 keV, obtaining respectively the lower and higher energy uncertainty limit.

Table 5.6 and Figure 5.14 report the cross section values of the ^{68}Zn(p,2p)^{67}Cu reaction obtained in this work in all runs.

The excellent agreement of the results obtained in different irradiations shows the repeatability of the method (Figure 5.14). In fact, only the lower energy values of the 8th irradiation (E = 40.8 MeV) seems to be higher than other results, but considering the error bars also this point is in agreement with others (especially with the higher energy values of the 6th irradiation, E = 42.5 MeV).

Figure 5.14 also shows the experimental points and the spline curve calculated by using $\rho = 0.001$, as well as the recommended cross section evaluated by [22, 97]. Our interpolation curve has been calculated considering the values of this work in the energy range 36-70 MeV, while for the lower (25-30 MeV) and higher (74-96 MeV) energy ranges have been taken into account the values of Stoll et al. [88] and Bonardi et al. [90], rescaled to 100% enriched Zn-68 targets. In the work of Bonardi et al. natural zinc targets have been used and thus also the reaction channel ^{70}Zn(p,x) contributes in the ^{67}Cu production, as discussed in Section 1.2.2.

In comparison with the recommended cross section, our evaluation of the ^{68}Zn(p,2p)^{67}Cu reaction is smaller (at E = 40 MeV the discrepancy is up to 35%), but a good agreement is achieved for the highest energy point (at E = 70 MeV both estimations provide a

TABLE 5.6: Results of the $^{68}Zn(p,2p)^{67}Cu$ cross section measurement.

	Energy and Unc. [MeV]	^{67}Cu Cross Section and Unc. [mb]	Cross Section Unc. [%]
6 irr. 2 f.	36.0 ± 0.7	5.3 ± 0.7	13.6
2 irr. 2 f.	39.9 ± 0.7	5.6 ± 0.8	14.7
8 irr. 2 f.	40.8 ± 0.7	7.8 ± 1.3	17.5
6 irr. 1 f.	42.5 ± 0.6	6.8 ± 1.0	14.2
2 irr. 1 f.	44.9 ± 0.4	6.9 ± 0.9	13.0
8 irr. 1 f.	45.7 ± 0.6	7.7 ± 1.1	14.2
9 irr. 2 f.	47.1 ± 0.7	8.0 ± 1.2	15.3
3 irr. 2 f.	49.1 ± 0.7	8.4 ± 1.2	14.6
9 irr. 1 f.	53.7 ± 0.6	9.1 ± 1.3	14.2
4 irr. 2 f.	54.6 ± 0.7	8.1 ± 1.3	16.2
4 irr. 1 f.	59.3 ± 0.6	9.0 ± 1.5	16.8
7 irr. 2 f.	66.1 ± 0.7	10.4 ± 1.8	17.0
7 irr. 1 f.	70.2 ± 0.6	11.6 ± 2.1	18.3
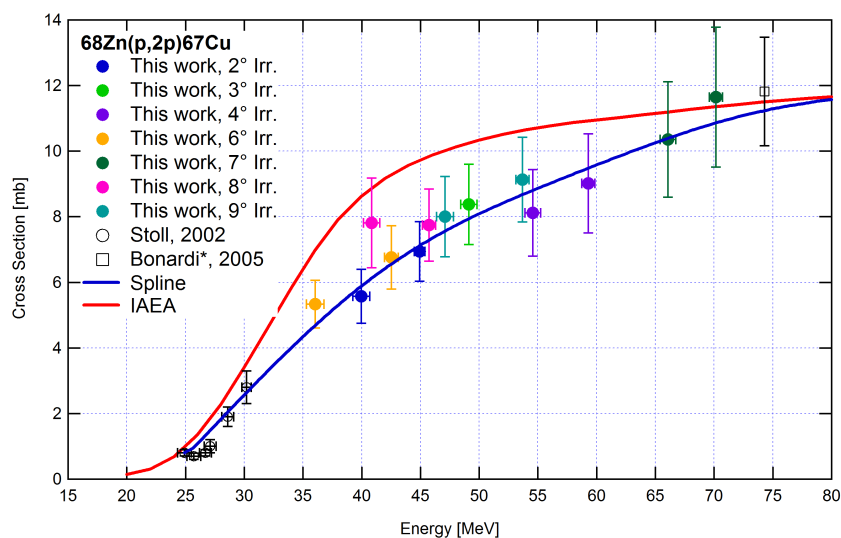
FIGURE 5.14: $^{68}Zn(p,2p)^{67}Cu$ reaction evaluated in this work in different irradiation runs. The reported spline curve takes into account our results and the values of Stoll et al. (25-30 MeV) and Bonardi et al. (74-96 MeV), rescaled to 100% enriched Zn-68 [88, 90]. The recommended cross section in the energy range 15-80 MeV is also given [97, 116].
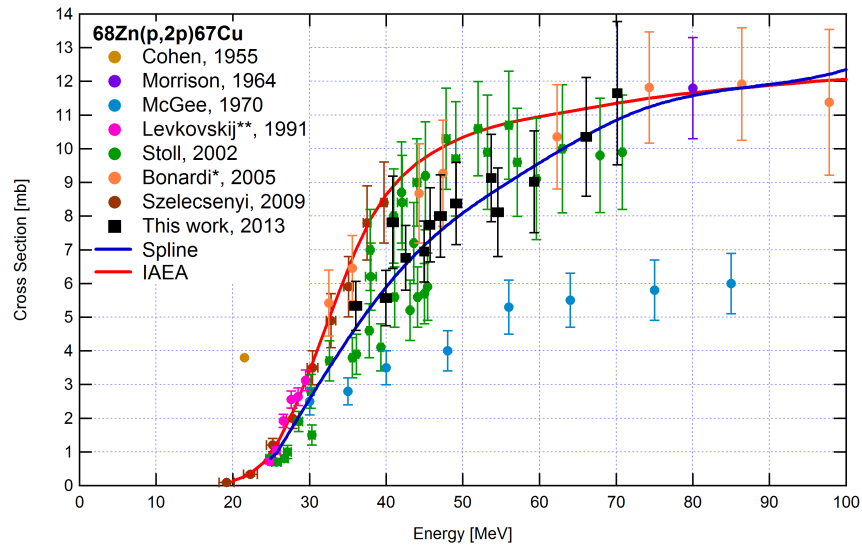
FIGURE 5.15: Evaluation of the ^{68}Zn(p,2p)^{67}Cu reaction and comparison with previous results [71], in the energy range 0-100 MeV.
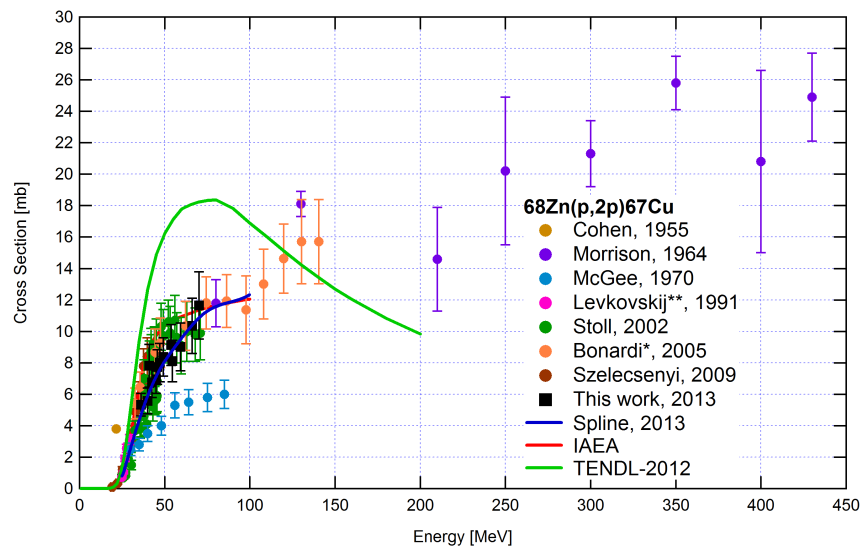
FIGURE 5.16: Evaluation of the ^{68}Zn(p,2p)^{67}Cu reaction and comparison with previous experimental results and theoretical cross section [23, 71], up to 450 MeV.

cross section of about 11.4 mb), as shown in Figure 5.14.

Figure 5.15 and Figure 5.16 show the results obtained in this work in comparison with all previous measurements, respectively up to 100 MeV and to 450 MeV.

As already mentioned in Section 1.2.2, the results of Cohen et al. [85] and McGee et al. [87] were not considered in the evaluation of the recommended cross section, and also in comparison with our values the discrepancy is evident (Figure 5.15). On the other hand our results agree with the evaluation of Stoll et al. [88] for the entire energy

range and for this reason such values have been taken into account in our spline curve at low energy (Figure 5.14). In the energy range 35-45 MeV (Figure 5.15), our results seem to perfectly describe an hypothetical mean value trend of the two series measured by Stoll et al., the lower around 5 mb and the higher around 10 mb (Figure 5.15). As already mentioned in Section 1.2.2, the lower series of values has not been taken into account in the evaluation of the recommended cross section. In particular on the IAEA website [22] it is reported: ≪*Data in the energy range 35-45 MeV were deleted due to systematic errors in that energy range (information from authors)*≫. However, in a private communication such comment has been not confirmed, since one of the authors rather says that no real explanation has been found in the interpretation of the lower series of values and that the comment on the IAEA website has been later added without authors' knowledge. Although the series of values around 5 mb was not affected by any systematic errors and no reason has been given for explaining such discrepancy, such points were neglected in the evaluation of the recommended cross section.

Regarding higher energy values (45-70 MeV), results obtained in this work show good agreement with the rescaled estimation of Bonardi et al. [90]. As already mentioned, those values have been taken into account in the recommended cross section estimation even if affected by the contribution of the $^{70}Zn(p,x)^{67}Cu$ reaction (as discussed in Section 1.2.2). For this reason in our calculation of the spline interpolation curve such values have been also considered for the high energy range (Figure 5.14).

In this work the $^{68}Zn(p,29)^{67}Cu$ reaction was not investigated in the lower (0-40 MeV) and higher (>70 MeV) energy range. However, from the trend of measured points, a discrepancy of about 20-30% can be noted at low energy in comparison with Szelecsenyi et al. [89], while a good agreement with the results of Bonardi et al. and Morrison et al. [86] can be surmised at high energy (Figure 5.16).

Appendix A reports the $^{68}Zn(p,x)^{66}Ga,^{67}Ga$ cross sections evaluated in this work, while B reports a brief discussion about the choice of the monitor reaction, since a discrepancy in the $^{27}Al(p,x)^{22}Na,^{24}Na$ reactions has been noted in this work.

5.2   Estimation of the ^{67}Cu production yield

In order to calculate the production yield of the reaction the code developed by F. Haddad, S. David and E. Garrido (2009) has been used, as previously described in Chapter 4. As already mentioned, the spline curve of our experimental evaluation has been done with the parameter $\rho = 0.001$, while in case of the IAEA recommended cross section the tabulated data available on the web site have been considered [22].

Once calculated the spline curve, the ^{67}Cu production yields vs beam energy have been
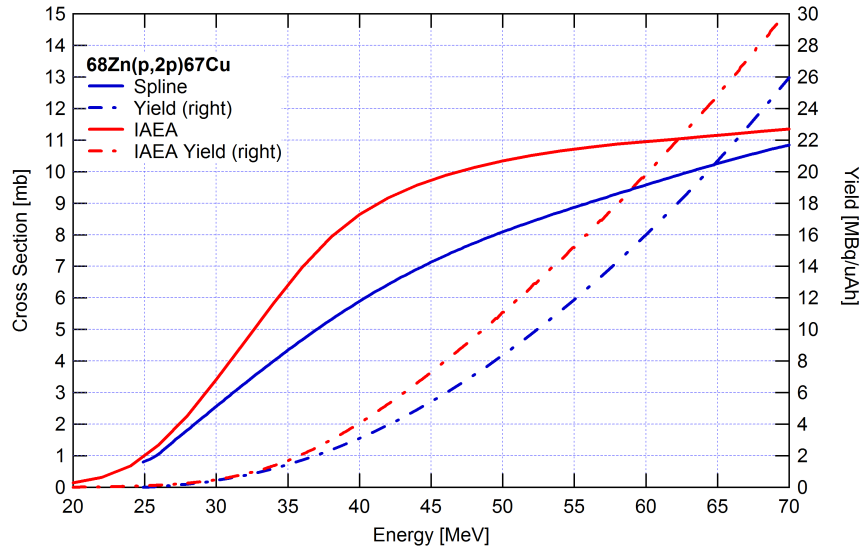
FIGURE 5.17: ^{67}Cu yield *via* the ^{68}Zn(p,2p) reaction calculated in this work and compared with the yield estimated by using recommended cross section [22, 97].

estimated for the ^{68}Zn(p,2p) reaction, as reported in Figure 5.17. As initial proton energy has been always considered E = 70 MeV, since actually it is the highest energy achievable with proton beams in cyclotrons used for producing nuclides with medical applications [2].

Figure 5.17 shows that the ^{67}Cu yield estimated from the recommended cross section is about 15% higher than the estimation made in this work: considering E = 70 MeV, it results respectively 30 and 26 MBq/μAh.

Figure 5.18 reports the ^{67}Cu yields and beam energy vs target thickness (^{68}Zn), based on our cross section evaluation, the recommended and theoretical ones [22, 23, 97], all in the optimized energy range of 70-30 MeV. These estimations show that considering the cross section measured in this work about 7 mm of ^{68}Zn are enough to produce 26 MBq/μAh, providing about 5.2 (MBq/μAh)/(g/cm^2). Considering the recommended cross section the yield is 13% higher than the one based on our estimation, providing about 30 MBq/μAh, while with the theoretical cross section the yield is 49 MBq/μAh, i.e. 47% higher than the one obtained with our values.

In order to compare the ^{67}Cu production *via* the ^{68}Zn(p,2p) reaction with the ^{70}Zn(p,x) reaction, the recommended and theoretical cross sections have been considered in case of 100% enriched ^{70}Zn targets [22, 23] and the corresponding spline curves have been calculated with $\rho = 1$. Once known the spline curves for the reactions on ^{70}Zn and ^{68}Zn targets, it was possible to estimate the ^{67}Cu production yield on natural zinc targets, by considering the ^{68}Zn(p,2p) and ^{70}Zn(p,x) contributions and rescaling them for the corresponding isotopic abundance (as reported in Table 5.2, ^{68}Zn is 18.45% and ^{70}Zn
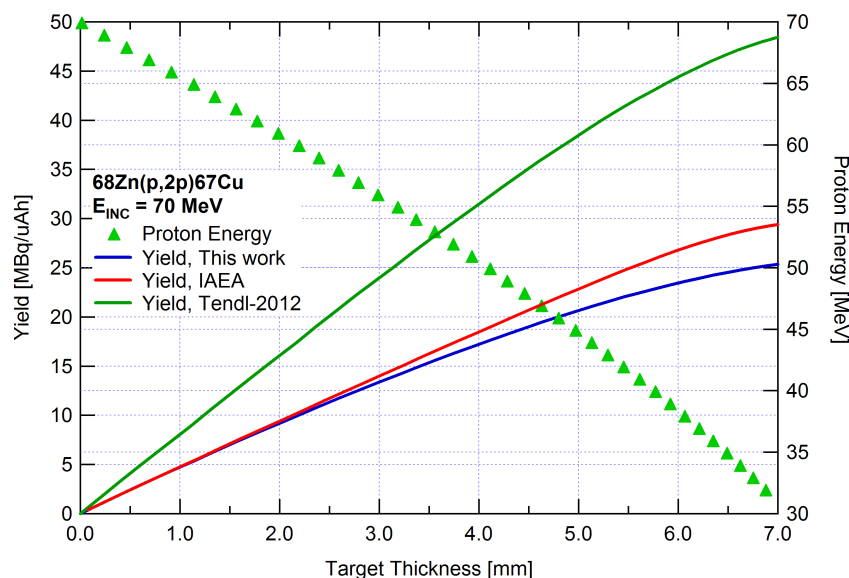
FIGURE 5.18: ^{67}Cu yield and *p*-energy vs target thickness (^{68}Zn) obtained considering the optimized energy window of 70-30 MeV and taking into account the cross section measured in this work, the recommended and the theoretical ones [22, 23, 97].
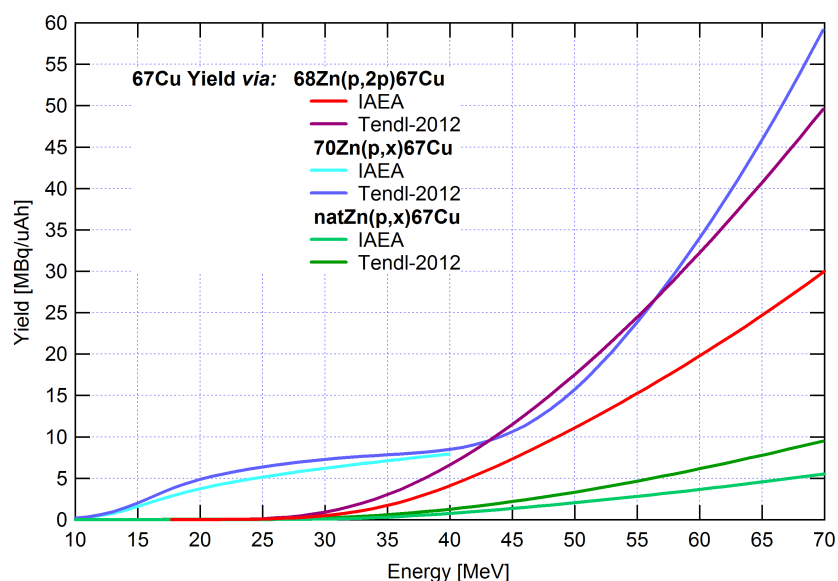
FIGURE 5.19: ^{67}Cu yield vs beam energy in case of the $^{68}Zn(p,2p)$, $^{70}Zn(p,x)$ and $^{nat}Zn(p,x)$ reactions, up to 70 MeV.

is 0.61% of natural zinc). In this way it was possible to estimate the ^{67}Cu production yield for the $^{nat}Zn(p,x)$ and the $^{70}Zn(p,x)$ reactions, as reported in Figure 5.19.

Figure 5.19 shows that the production yield on ^{nat}Zn targets is the lowest one, as expected. Moreover, it has to be noted that for ^{nat}Zn targets the ^{67}Cu yield presents the same trend of ^{68}Zn targets, since the contribution due to the $^{70}Zn(p,x)$ reaction is almost

TABLE 5.7: Resume of the estimated results for different ^{67}Cu production routes. All costs reported refer to single-use targets.

	Cross Section considered	Energy Range [MeV]	^{67}Cu Total Yield $[\frac{MBq}{\mu Ah}]$	Target Thickness [mm]	Target Mass [g]	Target Cost [kEuro]
^{68}Zn	This work	70-30	81.3	7.1	15.9	23.5
	IAEA	70-30	94.6	7.1	15.9	23.5
	TENDL	70-30	155.8	7.1	15.9	23.5
^{70}Zn	IAEA	40-5	25.1	3.5	7.9	86.7
	TENDL	70-5	185.7	9.4	21.1	232.9
^{nat}Zn	IAEA	70-5	17.3	8.8	19.7	0.10
	TENDL	70-5	29.8	8.7	19.5	0.10

negligible in the entire energy range.

It is also evident that in case of the ^{70}Zn(p,x) reaction the theoretical cross section from TENDL library provides a much higher yield than the one estimated from the recommended cross section. In fact in this case the recommended cross section, based on experimental evaluations, ends at 40 MeV and it never reaches 15 mb, while the theoretical one continues up to 200 MeV, showing in the energy range 50-200 MeV a cross section constantly higher than 20 mb (Figure 1.15). However, the trend of the ^{70}Zn(p,x) reaction has still to be confirmed by further experimental campaigns.

Figure 5.19 and the following Table 5.7 show that so far the ^{68}Zn(p,2p) reaction is the most efficient way to produce ^{67}Cu, when using proton-beams.

Once known target thicknesses, ^{67}Cu yields and target material prices, some estimations about the costs of ^{68}Zn, ^{70}Zn and ^{nat}Zn targets can be performed, as reported in Table 5.7. As already mentioned in Chapter 4, these rough estimations are based on an hypothetical beam diameter of 1 cm, refer to single-use targets and do not considered any target manufacturing costs. However, from these estimations is possible to sketch out the final activity costs related to each route, since the irradiation time (and thus its cost) and the chemical procedure are the same for all considered cases.

In case of ^{67}Cu production *via* the ^{68}Zn(p,2p) reaction, when comparing the evaluation based on our cross section measurement and on the recommended one from IAEA the same difference of about 14% is noticed on the total activity produced.

The ^{67}Cu production based on ^{nat}Zn targets seems to be a very convenient route, requiring a target 8.8 mm thick with an estimated cost of about 100 Euro only. However it is important to note that in this case many reaction channels for the production of different Cu-isotopes are opened and thus the final RNP of the resulting ^{67}Cu is lower than in case of enriched targets. In this work no estimations of precise contaminant activities are given, but a comment about this issue is remarked. Even when considering 100% enriched ^{68}Zn targets, the β^+-emitter ^{64}Cu is co-produced (half-life $\tau_{1/2} = 12.7$ h,

TABLE 5.8: Decay data of main Cu-isotopes [69].

	Half life $\tau_{1/2}$	Emitted Radiation	Decay Product
Cu-60	23.7 s	β^+, γ	Ni-60, stable
Cu-61	3.333 h	β^+, γ	Ni-61, stable
Cu-62	9.673 m	β^+, γ	Ni-62, stable
Cu-64	12.7 h	β^+, γ^4	Ni-64, stable
Cu-66	5.120 m	β^-, γ	Zn-66, stable
Cu-68	30.9 s	β^-, γ	Zn-68, stable
Cu-69	2.85 m	β^-, γ	Zn-69 ($\tau_{1/2} = 56.4$ m)

as reported in Table 5.8), together with the short half-life nuclide ^{66}Cu, that fast decays into ^{66}Zn (stable isotope).

Also in case of 100% enriched ^{70}Zn targets only short half-life contaminants are produced in addition to ^{64}Cu and ^{66}Cu, i.e. ^{68}Cu ($\tau_{1/2} = 30.9$ s) and ^{69}Cu, that both fast decay into ^{68}Zn (stable) and ^{69}Zn (radioactive, $\tau_{1/2} = 56.4$ m). On the other hand in case of ^{nat}Zn targets a larger amount of ^{64}Cu results at the EOB, since also the (p,p+d) and (p,2p+n) channels on ^{66}Zn are opened[3] (^{66}Zn is 27.73% of natural zinc). Moreover other Cu-nuclides are co-produced in ^{nat}Zn targets, such as ^{60}Cu, ^{61}Cu and ^{62}Cu, whose decay data are reported in Table 5.8.

At the end it has to be noted that in the IAEA report [97] it is emphasized that in practical production runs with thick targets a significant flux of energetic secondary neutrons is generated. In case of ^{68}Zn targets, this flux enhances the ^{67}Cu production *via* the (n,d) and (n,n+p) reactions, but it may also contribute to the production of other nuclides. Thus also this aspect has to be considered when planning a massive production of ^{67}Cu, paying particular attention to the co-production of Cu-isotopes.

---

[3]The ^{66}Zn(p,p+2n) reaction has a threshold energy $E_T = 19.1$ MeV, while the ^{66}Zn(p,d+n) reaction $E_T = 16.9$ MeV [69].

Conclusions

The activities described in this work, in the framework of LARAMED project, concern the study of accelerator-based routes aimed to the production of nuclides relevant to nuclear medicine: ^{99}Mo, ^{99m}Tc (two vital nuclides in diagnostics) and ^{67}Cu (a promising nuclide in Radio Immuno Therapy).

From the inception of LARAMED project, two scientific collaborations have started, one with the ARRONAX facility [5] and the other with different sections of INFN (Istituto Nazionale di Fisica Nucleare), establishing the APOTEMA project (funded by INFN for 2012-2014). The activities performed at ARRONAX have been focused on the measurement of ^{96}Zr(α,n)^{99}Mo and ^{68}Zn(p,2p)^{67}Cu nuclear cross sections, while APOTEMA project concerns alternative, accelerator-driven production of ^{99}Mo and ^{99m}Tc. In particular, two innovative production routes have been analysed: the p-induced reaction on enriched ^{100}Mo targets (basing on the performance of the incoming cyclotron at LNL) and the aforementioned α-induced reaction on enriched ^{96}Zr targets.

Considering the production of ^{99}Mo and ^{99m}Tc with proton beams, the already available evaluations of the ^{100}Mo(p,x)^{99}Mo,^{99m}Tc cross sections have been used to assess the best irradiation conditions aimed at a local production of these vital nuclides. In particular, the characteristics of the incoming cyclotron at LNL have been taken into account (p-beam with tunable energy ranging from 35 to 70 MeV, current of 500 μA), assuming 500 W/cm^2 as mean areal power density on target and commercially available enriched ^{100}Mo material [9].

Regarding ^{99}Mo production, the in-target activity with high energy p-beams is 3 times bigger than for 40 MeV-protons. However, even if these production levels seem to be enough to cover a regional demand, the resulting Specific Activities (SA) are a factor 10^2-10^4 lower than the ones commonly found in commercial generators. If the current industrial method for Mo/Tc generator manufacturing has to be maintained, the accelerator production of ^{99}Mo with protons seems to be not a favourable option, due to the high cost of enriched target material, the oversized alumina column needed, and the resulting large elution volumes.

A promising alternative is the direct production of ^{99m}Tc *via* the ^{100}Mo(p,2n) reaction,

as the resulting ^{99m}Tc SA are similar to the ones provided by standard Mo/Tc generators. In fact, the highest SA obtained with accelerators (considering 15 MeV beam and 1 hour irradiation) is about 20% lower than the SA resulting from an elution obtained with commercial generators, considering 24 hours elapsed from the previous elution.

However, the direct ^{99m}Tc production raises the issue of other Tc-isotopes co-production. For this reason, the Isotopic and RadioNuclidic Purities (IP and RNP) have been estimated for all irradiation conditions analysed; moreover, a preliminary evaluation of the influence of long-lived Tc-isotopes on radio-labelling procedures has been also carried out.

Results show that in case of 20 MeV protons and 3 hours irradiation, the RNP increases to values as high as 99% in about 1 hour after the End Of Bombardment (EOB), due to the fast decay of short-lived Tc-isotopes. Considering that the reference RNP value referred the generator-produced Tc is about 99.99%, this limit is basically approached if irradiations at proton energies as low as 15 MeV are performed, whatever the irradiation time chosen (RNP$_{15MeV}$ > 99.58%). It also results that the direct production of ^{99m}Tc with E $\geq$ 25 MeV has to be avoided, due to unsatisfactory RNP and IP values.

Even if the influence of long-lived nuclides ^{99g}Tc, ^{98}Tc, and ^{97g}Tc on dosimetry can be neglected, their possible impact on the radiochemical quality of accelerator-Tc labelled pharmaceuticals has to be considered [112]. In order to estimate this possible effect, a detailed study has been carried out by using eluates containing different amounts of ^{99g}Tc, miming the presence of all long-lived Tc-isotopes produced with ^{100}Mo(p,x)^{xn}Tc reactions [109]. A set of measurements has been performed with ^{99m}Tc eluted from standard ^{99}Mo/^{99m}Tc generator systems at different time from previous elution, in order to obtain various ratio R = ^{99g}Tc/^{99m}Tc, ranging from 4.34 to 11.84. By using these eluates, ten widely used radio-pharmaceutical kits have been reconstituted, in order to check their Radio-Chemical Purity (RCP) soon after the radio-labelling procedure and at the end of the stability period. In all cases the measured values resulted to be superior to standards required by the manufacturer: this result shows that the total amount of technetium ($^{99m+g}$Tc) does not affect either the RNP or the stability of final product, up to a ratio R = 11.84 (corresponding to an eluate obtained 72 hours after from previous elution).

It is important to remind that actually the Official European Pharmacopoeia[5] uniquely consider ^{99m}Tc coming from generator systems (prepared with ^{99}Mo produced in fission-e/o n-induced reactions), causing a lack in the requirements that have to be fulfilled in case of technetium directly produced with accelerators.

A different route aimed to the production of highly pure, high SA ^{99}Mo is based on the ^{96}Zr(α,n) reaction, measured only once in 1995 by Chowdhury et al. [21].

---

[5]European Pharmacopoeia, 7th Ed., Sodium pertechnetate (^{99m}Tc) injection (fission) (0124).

A new evaluation of this cross section has been performed at ARRONAX facility in the energy range 8-34 MeV, by using stacked-foil targets containing highly pure foils of natural Zirconium (purity > 99%). Since ^{96}Zr(α,n) is the only open channel for ^{99}Mo production, values obtained with ^{nat}Zr foils can be rescaled to 100% enriched ^{96}Zr targets.

Results obtained in different irradiation runs are in excellent agreement, showing the repeatability of the method and indicating as ideal energy window 25-12 MeV. In comparison with values obtained by Chowdhury et al. [21], the general trend of the cross section is similar, but our results show a higher peak value and a shift of about 2 MeV towards higher energies.

Taking into account a spline interpolation curve of our results, the ^{99}Mo yield has been estimated as a function of both particle energy and target thickness, considering the optimized energy range of 25-12 MeV. Due to the strong interaction of α-particles with matter, only 120 μm of ^{96}Zr are needed to produce about 1.3 MBq/μAh of ^{99}Mo, providing about 16.7 MBqcm^2/μAhg. Thermal calculations confirmed the feasibility of this route, proving that the temperatures achieved in the front and in the back of targets are lower than the Zirconium melting point (2128 K).

The ^{96}Zr(α,n)^{99}Mo reaction, assuming an efficient chemical extraction of ^{99}Mo from target, provides a final product characterized by high SA, as required in the manufacture of standard ^{99}Mo/^{99m}Tc generator systems. Moreover, considering an efficient recovery process, the same target could be used for many irradiations, reducing the final activity cost without affecting the quality of resulting ^{99}Mo, since (α,n) is the only open channel for its production. A detailed analysis of such aspects goes beyond the aim of this study; however, some considerations regarding the quality of resulting ^{99}Mo can be provided in case of α- and p-based routes.

First of all, considering ^{100}Mo(p,x)^{99}Mo and ^{96}Zr(α,n)^{99}Mo reactions, the RNP is very high in both cases, since other Mo isotopes are stable. In fact, the only radioactive Mo-isotopes that could be produced are ^{93m}Mo and ^{93g}Mo (half-life 6.85 h and 4.0·10^3 y respectively) with a threshold energy of 56.4 MeV and 54.9 MeV, respectively for the ^{100}Mo(p,p7n) and ^{96}Zr(α,7n) reaction [69]. However, in case of ^{100}Mo targets, the extraction of ^{99}Mo is not possible and the resulting low SA product forces to use alternative generator systems [7] or to direct produce ^{99m}Tc *via* the ^{100}Mo(p,2n) reaction. As previously mentioned, this is an interesting solution to meet local needs of ^{99m}Tc, that however raises many issues regarding the co-production of other short- and long-lived Tc-isotopes, that could affect the final image quality [15, 16, 117] and increase the radiation dose to patients [110]. For these reasons, further work is needed, especially to quantify the amount of Tc-isotopes for different irradiation conditions and to verify the quality of final products when recovered targets are used [9, 18, 118]; moreover, the

^{100}Mo(p,2n)^{99g}Tc cross section still needs to be investigated in the entire energy range, since it was measured only once up to 18 MeV [17].

In conclusion it has to be stressed that in order to estimate and compare activity costs related to α- and p-based routes, the full production chain has to be considered, including target manufacturing, irradiation time and cost and chemical processes needed to eventually extract and purify ^{99}Mo from target or produce ^{99}Mo/^{99m}Tc generator systems.

As reported in a recent paper by Qaim [79], today the major effort of the nuclear data research is towards developing therapeutic nuclides. In particular both LARAMED and ARRONAX facilities show interest in the production of ^{67}Cu, the most promising emerging nuclides in RAIT, whose limiting factor for a more widespread application in clinical trials is its availability [8].

In this work a new evaluation of the ^{68}Zn(p,2p)^{67}Cu cross section has been performed, by using the 70 MeV proton-beam provided by ARRONAX cyclotron and stacked-foil targets containing enriched ^{68}Zn powder electro-deposited on Silver support. Also in this case, results obtained in different irradiation runs are in excellent agreement, showing the repeatability of the method. A spline curve has been calculated considering the experimental values obtained in the energy range 36-70 MeV, while for the lower (25-30 MeV) and higher (74-96 MeV) energy ranges have been taken into account the values of Stoll et al. [88] and Bonardi et al. (rescaled to 100% enriched Zn-68 targets) [90]. In comparison with the recommended cross section [22, 97], our evaluation is smaller (at E = 40 MeV the discrepancy is up to 35%), but a good agreement is achieved for the highest energy point (at E = 70 MeV both estimations provide a cross section of about 11.4 mb).

In comparison with previous measurements, our results agree with the evaluation of Stoll et al. [88] for the entire energy range; in particular, considering the energy range 35-45 MeV, our results seem to perfectly describe an hypothetical mean value trend of the two series measured by Stoll et al., the lower around 5 mb and the higher around 10 mb. As already mentioned, the lower series of values has not been taken into account in the evaluation of the recommended cross section, although no systematic errors have been declared by authors and no reason was found to explain such discrepancy.

As already mentioned, in this work the ^{68}Zn(p,29)^{67}Cu reaction was not investigated at low (0-40 MeV) and high (>70 MeV) energies; however, from the trend of measured points, it is possible to extrapolate a discrepancy of about 20-30% at low energy in comparison with Szelecsenyi et al. [89], and a good agreement with the results of Bonardi et al. and Morrison et al. [86] for E >70 MeV.

Considering the spline curve obtained in this work, the ^{67}Cu production yield has been estimated as a function of both particle energy and target thickness, considering the

optimized energy range of 70-30 MeV. These estimations show that about 26 MBq/μAh of ^{67}Cu are produced in 7 mm of ^{68}Zn, providing about 5.2 MBqcm^2/μAhg. Considering the recommended cross section the yield is 13% higher than the one based on our estimation, given about 30 MBq/μAh, while with the theoretical cross section [23] the yield is 49 MBq/μAh, i.e. 47% higher than the one obtained with our values.

A comparison with proton-induced reaction on ^{70}Zn and ^{nat}Zn targets has been also given, considering both recommended and theoretical cross sections [22, 23]. As expected, the ^{67}Cu yield resulting from ^{nat}Zn targets is the lowest one, while in case of ^{70}Zn targets a big discrepancy can be noted in the production yield when considering the recommended and theoretical cross sections; in fact, in the energy range 50-200 MeV the ^{70}Zn(p,x) reaction is theoretically estimated to be always higher than 20 mb, but this trend has still to be confirmed by further experimental campaigns. For this reason, so far the ^{68}Zn(p,2p) reaction is the most efficient way to produce ^{67}Cu with accelerators. In this work no estimations of precise contaminant activities are given; however, considering 100% enriched ^{68}Zn targets, only the β^+-emitter ^{64}Cu and the short half-life ^{66}Cu are also produced, while in case of ^{70}Zn and ^{nat}Zn targets, many other Cu-isotopes are co-produced, such as ^{61}Cu, ^{62}Cu, ^{68}Cu and ^{69}Cu.

In conclusion it has to be remarked the need of further studies and experimental campaigns, in order to carry on with radiochemical analysis and cross section measurements (for example investigating the ^{68}Zn(p,2p)^{67}Cu reaction at higher energies), both aimed to the assessment of best irradiation conditions and at the evaluation of actual production costs.

Appendix A

^{68}Zn(p,xn)^{66}Ga,^{67}Ga reactions

Figure A.1 shows the ^{68}Zn(p,3n)^{66}Ga cross section obtained and compared with all previous measurements in the energy range 20-100 MeV [71]. Figure A.2 and Figure A.3 report the ^{68}Zn(p,2n)^{67}Ga cross section obtained and compared with all previous measurements [22, 71], respectively in the entire energy range (0-100MeV) and at high energies (20-100 MeV).

In both cases the general excellent agreement of results from different irradiation runs confirm the repeatability of the method. Moreover, the estimation of the ^{68}Zn(p,3n)^{66}Ga cross section is in perfect agreement with previous measurements (Figure A.1), while the evaluation of the ^{68}Zn(p,2n)^{67}Ga reaction shows that the recommended cross section has to be improved at high energies (E > 35 MeV), since it takes into account the results of Stoll et al. (2002) [88], overestimating the real trend of this reaction (Figure A.3).
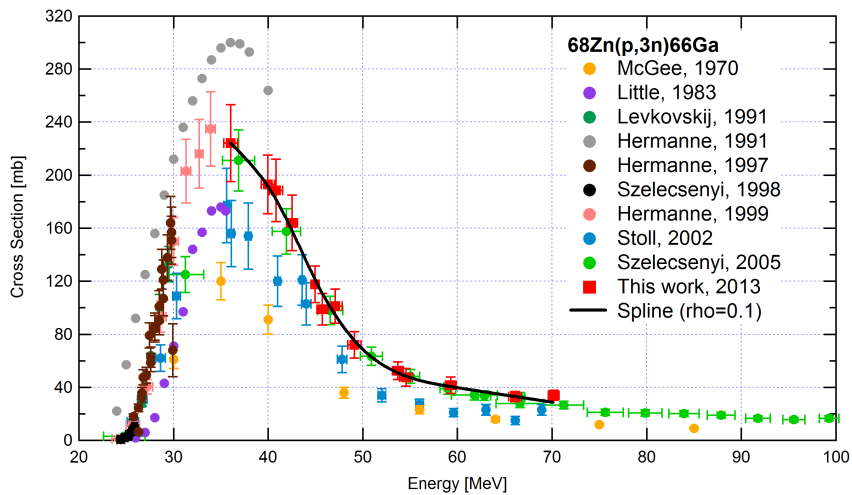
FIGURE A.1: ^{68}Zn(p,3n)^{66}Ga cross section obtained in this work and compared with all previous measurements [71], for the energy range 20-100 MeV.

97
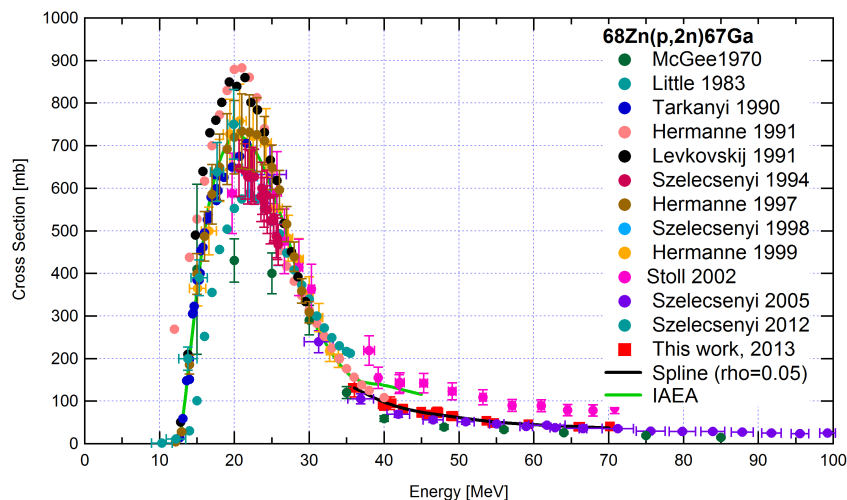
FIGURE A.2: ^{68}Zn(p,2n)^{67}Ga cross section obtained in this work and compared with all previous measurements and the recommended cross section [22, 71], for the energy range 0-100 MeV.
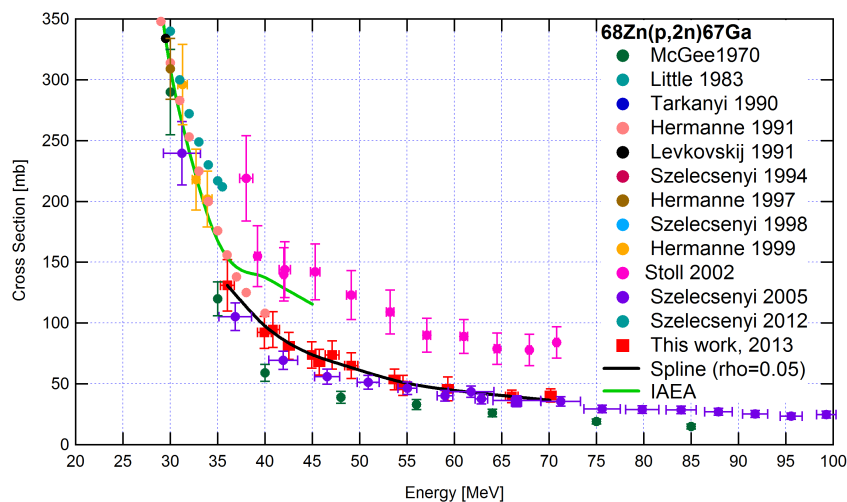
FIGURE A.3: ^{68}Zn(p,2n)^{67}Ga cross section obtained in this work and compared with all previous measurements and the recommended cross section [22, 71], for the energy range 20-100 MeV.

However, Figure A.2 confirms that the recommended cross section is correct up to about 35 MeV.

Appendix B

^{nat}Al(p,x)^{24}Na reaction

The choice of the monitor reaction plays a very important role in the cross section measurement. When choosing the monitor reaction for proton energies higher than 50 MeV, we decided to use highly pure Al foils on which is possible to produce both ^{22}Na and ^{24}Na, as respectively shown in Figure 5.4 and Figure B.1 [116]. In this case it is possible to estimate the cross section of one nuclide, for example ^{24}Na, by using as reference the activity and the reference cross section of the other nuclide, i.e. ^{22}Na. If the recommended cross sections are both correct, the estimated values of the ^{27}Al(p,x)^{24}Na reaction will lye on the reference curve.

However, we found a discrepancy between the estimated values of the cross section of the ^{27}Al(p,x)^{24}Na reaction and the recommended one.

In order to calculate the ^{27}Al(p,x)^{24}Na cross section we have used Equation 2.5, considering that in this case the target and monitor nuclides are both produced on the same foil; thus Equation 2.5 can be written as:

$$\sigma(E) = \sigma'(E) \frac{Act_{EOIB}(1 - e^{-\lambda' t_{IRR}})}{Act'_{EOIB}(1 - e^{-\lambda t_{IRR}})} \tag{B.1}$$

Figure B.2 shows the discrepancy found between the measured values of the ^{27}Al(p,x)^{24}Na cross section, performed by using ^{22}Na as reference nuclide, and the recommended one.
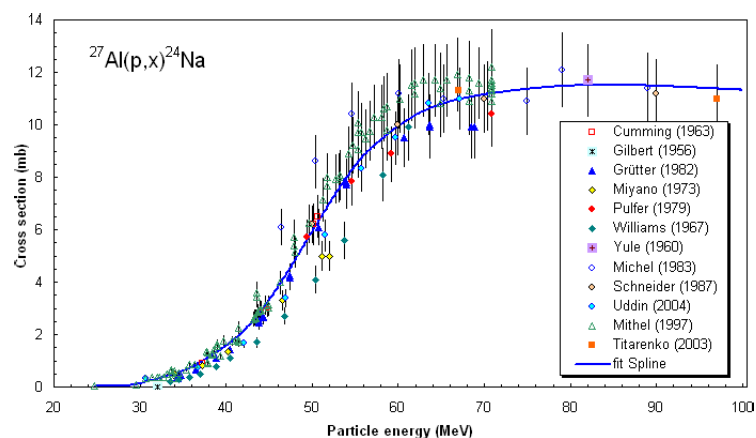
FIGURE B.1: Recommended cross section of the ^{27}Al(p,x)^{24}Na reaction [116].
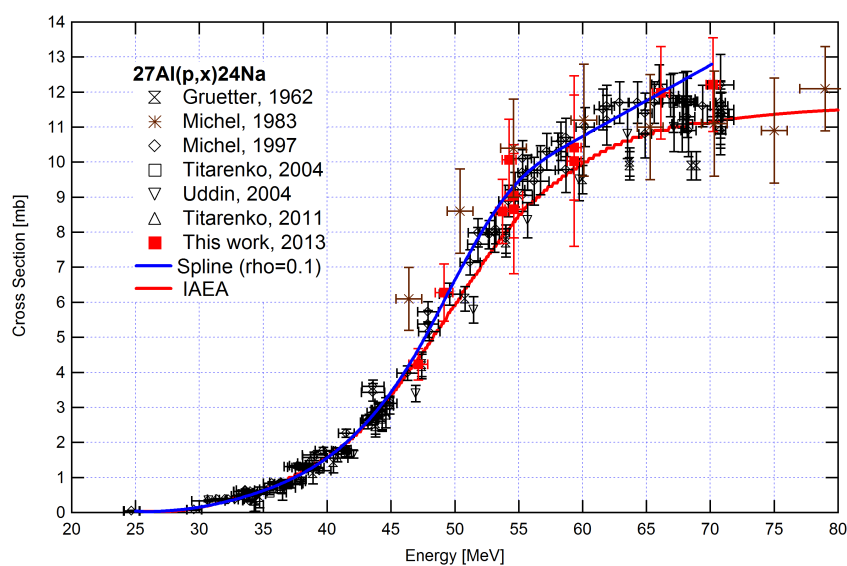
FIGURE B.2: ^{27}Al(p,x)^{24}Na cross section obtained in this work (considering ^{22}Na as reference nuclide) and compared with the recommended cross section and previous measurements considered in the evaluation of the recommended one [71].

List of Figures

List of Tables

Bibliography

[1] E Bradley, P Adelfang, and N Ramamoorthy. HoMogeneous acqueous solution nuclear reactors for the production of Mo-99 and other short lived radioisotopes. Technical report, International Agency Energy Atomic (IAEA), 2008.

[2] PW Schmor. Review of cyclotrons used in the production of radioisotopes for biomedical applications. *Proceedings of Cyclotrons 2010, Lanzhou (China)*, pages 419–424, 2010.

[3] SM Qaim. Nuclear data for medical applications: an overview. *Radiochimica Acta*, 89:189–196, 2001.

[4] Istituto Nazionale di Fisica Nucleare (INFN). Selective Production of Exotic Species (SPES). URL https://web.infn.it/spes/.

[5] F Haddad, L Ferrer, A Guertin, T Carlier, N Michel, J Barbet, and JF Chatal. ARRONAX, a high-energy and high-intensity cyclotron for nuclear medicine. *European Journal of Nuclear Medicine and Molecular Imaging*, 35:1377–1387, 2008.

[6] A Lokhov, R Cameron, C Westmacott, N Ramamoorthy, and E Bradley. The supply of medical radioisotopes. Review of potential Molybdenum-99/Technetium-99m production technologies. Technical report, Nuclear Energy Agency (NEA) and Organisation for Economic Co-operation and Development (OECD), 2010. IAEA-TECDOC-1601.

[7] MRA Pillai, A Dash, and FF Knapp. Sustained availability of ^{99m}Tc: Possible paths forward. *Journal of Nuclear Medicine*, 54:313–323, 2013.

[8] P Rowshanfarzad, M Sabet, AR Jalilian, and M Kamalidehghan. An overview of Copper radionuclides and production of ^{61}Cu by proton irradiation of ^{nat}Zn at a medical cyclotron. *Applied Radiation and Isotopes*, 64:1563–73, 2006.

[9] J Esposito, G Vecchi, G Pupillo, A Taibi, L Uccelli, A Boschi, and M Gambaccini. Evaluation of ^{99}Mo and ^{99m}Tc productions based on a high-performance cyclotron. *Hindawi Publishing Corporation; Special Issue - Molybdenum-99: Past and Present and Future*, 2013. URL http://dx.doi.org/10.1155/2013/972381.

[10] A Celler, X Hou, F Benard, and T Ruth. Theoretical modeling of yields for proton-induced reactions on natural and enriched Molybdenum targets. *Physics in Medicine and Biology*, 56:5469–5484, 2011.

[11] SM Qaim. The present and future of medical radionuclide production. *Radiochimica Acta*, 100:635–651, 2012.

[12] T Reuters. Analysis: A month on and Japan nuclear crisis still scarring. *International Business Times (Australia)*, 2011. URL http://www.ibtimes.co.in/articles/132391/20110409/japan-nuclear-crisis-radiation.htm.

[13] S Lahiri and M Maiti. Recent developments in nuclear data measurements and chemical separation methods in accelerator production of astatine and Technetium radionuclides. *Radiochimica Acta*, 100:85–94, 2012.

[14] E Bradley et al. Non-HEU production technologies for Molybdenum-99 and Technetium-99m. Technical report, International Agency Energy Atomic (IAEA), 2013. No. NF-T-5.4.

[15] B Guerin, S Tremblay, S Rodrigue, JA Rousseau, V Dumulon-Perreault, R Lecomte, JE van Lier, and A Zyuzin. Cyclotron production of ^{99m}Tc: an approach to the medical isotope crisis. *Journal of Nuclear Medicine*, 51(4):13N–16N, 2010.

[16] H Targholizadeh, G Raisali, AR Jalilian, N Rostampour, M Ensaf, and MK Dehghan. Cyclotron production of Technetium radionuclides using a natural metallic Molybdenum thick target and consequent preparation of [Tc]-BRIDA as a radio-labelled kit sample. *Nukleonika*, 55:113–118, 2010.

[17] K Gagnon, F Benard, M Kovacs, TJ Ruth, P Schaffer, JS Wilson, and SA McQuarrie. Cyclotron production of ^{99m}Tc: experimental measurement of the ^{100}Mo(p,x)^{99}Mo,^{99m}Tc and ^{99g}Tc excitation functions from 8 to 18 MeV. *Nuclear Medicine and Biology*, 38(38):907–916, 2011.

[18] K Gagnon, JS Wilson, CMB Holt, DN Abrams, AJB McEwan, D Mitlin, and SA McQuarrie. Cyclotron production of ^{99m}Tc: Recycling of enriched ^{100}Mo metal targets. *Applied Radiation and Isotopes*, 70:1685–1690, 2012.

[19] SM Qaim. Nuclear data relevant to the production and application of diagnostic radionuclides. *Radiochimica Acta*, 89:223–232, 2001.

[20] SM Qaim. Physics and chemistry and technology and quality assurance in radionuclide production for medical applications. In *Applications of radiotracers in chemical and enviromental and biological sciences*, volume 1, pages 1–22. 2006.

[21] DP Chowdhury, S Pal, SK Saha, and S Gangadharan. Determination of cross section. *NIMB*, 103:261–266, 1995.

[22] IAEA - Emerging Isotopes (Recommended Cross Sections), 2011. URL https://www-nds.iaea.org/radionuclides/emerging.html.

[23] Talys-based evaluated nuclear data library, 2013. URL ftp://ftp.nrg.eu/pub/www/talys/tendl2013/tendl2013.html.

[24] A Rys et al. Preliminary report on supply of radioisotopes for medical use and current developments in nuclear medicine. Technical report, European Commission, Health and consumers directorate-general, Public health and risk assessment, Health threats, 2009.

[25] R Alberto and H Braband. SPECT/PET imaging with Technetium, Gallium, Copper and other metallic radionuclides. In *Comprehensive Inorganic Chemistry II: From elements to applications*, volume 3, pages 785–817. 2013.

[26] A Duatti. Role of Tc-99m in diagnostic imaging. In *Technetium-99m Radiopharmaceuticals: Status and Trends*. 2009. IAEA Radioisotopes and Radiopharmaceuticals series No. 1.

[27] S Adak, R Bhalla, KK Vijaya Raj, S Mandal, R Pickett, and SK Luthra. Radiotracers for SPECT imaging: current scenario and future prospects. *Radiochimica Acta*, 100:95–107, 2012.

[28] A Andrighetto, G Prete, A Boschi, L Uccelli, and P Zanonato. An alternative method to produce isotopes for medical applications in the framework of the SPES Project: Mo-99 from UCx target. Technical report, Istituto Nazionale di Fisica Nucleare (INFN), Laboratori Nazionali di Legnaro (LNL), 2012.

[29] SM Qaim. Decay data and production yields of some non-standard positron emitters used in PET. *The Quarterly Journal of Nuclear Medicine*, 52(2):111–120, 2008.

[30] SM Qaim. Development of novel positron emitters for medical applications: nuclear and radiochemical aspects. *Radiochimica Acta*, 99:611–625, 2011.

[31] GK von Schulthess et al. Clinical Positron Emission Tomography/Magnetic Resonance Imaging Applications. *Semininars in Nuclear Medicine*, 43:3–10, 2013.

[32] Science Media Center of Canada (SMC), 2010. URL http://www.sciencemediacentre.ca/smc/index.php?option=com_content&view=article&id=94%3Aisotopes&catid=1%3Alatest-news&Itemid=49&lang=en.

[33] G Vecchi. Feasibility study for the production of Tc-99m with the legnaro cyclotron, Università degli Studi di Ferrara and Facoltà di Scienze Matematiche, Fisiche e Naturali, AA 2011/2012.

[34] E Browne and JK Tuli. Nuclear Data Sheets for A = 99. *Nuclear Data Sheets*, 112:275–446, 2011.

[35] GS Thomas and J Maddahi. The Technetium shortage. *Journal of Nuclear Cardiology*, 17:993–8, 2010.

[36] A Mushtaq. Can enriched Molybdenum-98 replace enriched Uranium? *Nonproliferation Review*, 16(2):285–292, 2009.

[37] S Chattopadhyay and MK Das. A novel technique for the effective concentration of ^{99m}Tc from a large alumina column loaded with low specific-activity (n,γ)-produced ^{99}Mo. *Applied Radiation and Isotopes*, 66:1295–1299, 2008.

[38] MP Zykov et al. Use of extraction generator for preparing a ^{99m}Tc radiopharmaceutical. *Radiochemistry*, 43(3):297–300, 2001.

[39] MT El-Kolaly. A ^{99}Mo/^{99m}Tc generator based on the use of Zirconium Molybdophosphate gel. *Journal of Radioanalytical and Nuclear Chemistry*, 170(2):293–298, 1993.

[40] P Saraswathy, SK Sarkar, RR Patel, SS Arora, and DVS Narasimhan. ^{99m}Tc gel generators based on Zirconium Molybdate-^{99}Mo: Process standardisation for production. *Radiochimica Acta*, 83(2):97–102, 1998.

[41] F Monroy-Guzman, LV Diaz-Archundia, and S Hernandez-Cortes. ^{99}Mo/^{99m}Tc generators performances prepared from Zirconium Molybate gels. *Journal of the Brazilian Chemical Society*, 19(3):380–388, 2008.

[42] P Saraswathy, A Dey, S Sarkar, C Kothalkar, P Naskar, G Arjun, S Arora, A Kohli, V Meera, V Venugopal, and N Ramamoorthy. Tc-99m generators for clinical use based on Zirconium Molybdate gel and (n,γ) produced Mo-99. In *29th International Meeting on Reduced Enrichment for Research and Test Reactors (RERTR)*, 2007.

[43] S Sarkar, C Kothalkar, P Naskar, P Saraswathy, A Dey, A Kohli, V Meera, and V Venugopal. Update on operational experience of Zirconium Molybdate – Mo-99 gel generator production in India. In *31th International Meeting on Reduced Enrichment for Research and Test Reactors (RERTR)*, 2009.

[44] F Monroy-Guzman, T Rivero Gutierrez, IZ Lopez Malpica, S Hernandez Cortes, P Rojas Nava, JC Vazquez Maldonado, and A Vazquez. Production optimization of ^{99}Mo/^{99m}Tc Zirconium Molybate gel generators at semi-automatic device: DISIGEG. *Applied Radiation and Isotopes*, 70:103–111, 2012.

[45] R Chakravarty, R Ram, A Dash, and MRA Pillai. Preparation of clinical-scale ^{99}Mo/^{99m}Tc column generator using neutron activated low specific activity ^{99}Mo and nanocrystalline g-Al$_2$o$_3$ as column matrix. *NuclearMedicine and Biology*, 39: 916–922, 2012.

[46] Tc Wiencek, GF Vandegrift, A Bakel, AA Leyva, and AS Hebden. Status and progress of foil and target fabrication activities for the production of ^{99}Mo from leu. In *30th International Meeting on Reduced Enrichment for Research and Test Reactors (RERTR)*, 2008.

[47] A Mushtaq. Desorption of ^{99}Mo from spent ^{99}Mo/^{99m}Tc generator. *Radioanalitical Nuclear Chemistry and Letters*, 199(2):89–94, 1995.

[48] T Ruth. Accelerating production of medical isotopes. *Nature*, 457:536–537, 2009.

[49] H Naik, SV Suryanarayana, KC Jagadeesan, SV Thakare, PV Joshi, VT Nimje, KC Mittal, A Goswami, V Venugopal, and S Kailas. An alternative route for the preparation of the medical isotope ^{99}Mo from the ^{238}U$(\gamma,$f$)$ and ^{100}Mo$(\gamma,$n$)$ reactions. *Journal of Radioanaitical Nuclear Chemistry*, 295:807–816, 2013.

[50] P Reimer, V Avrigeanu, SV Chuvaev, AA Filatenkov, T Glodariu, A Koning, AJ M Plompen, SM Qaim, DL Smith, and H Weigmann. Reaction mechanisms of neutrons on stable Mo below 21 MeV. *Physical Review, Part C, Nuclear Physics*, 2005.

[51] R Chakravarty, A Dash, and M Venkatesh. A novel electrochemical technique for the production of clinical grade ^{99m}Tc using (n,γ)^{99}Mo. *NuclearMedicine and Biology*, 37:21–28, 2010.

[52] F Tarkanyi, A Hermanne, S Takacs, M Sonck, Z Szucs, B Kiralya, and AV Ignatyuk. Investigation of alternative production routes of ^{99m}Tc: Deuteron induced reactions on ^{100}Mo. *Applied Radiation and Isotopes*, 2011.

[53] K Abbas, U Holzwarth, F Simonelli, J Kozempel, I Cydzik, A Bulgheroni, G Cotogno, C Apostolidis, F Bruchertseifer, and A Morgenstern. Feasibility of ^{99}Mo production by proton-induced fission of ^{232}Th. *NIMB*, 278:20–25, 2012.

[54] JE Beaver and HB Hupf. Production of ^{99m}Tc on a medical cyclotron: A feasibility study. *Journal of Nuclear Medicine*, 12:739–741, 1971.

[55] N Levkovskij. *Middle mass nuclides (A=40+-100) Activation cross sections by medium energy (E=10+-50 MeV) protons and a-particles (experiment and systematics).* Inter-Vesti, Moscow, 1991.

[56] MC Lagunas-Solar, PM Kiefer, OF Carvacho, CA Lagunas, and YP Cha. Cyclotron production of NCA Tc-99m and Mo-99 – An alternative non-reactor supply source of instant Tc-99m and Mo-99/Tc-99m generators. *Applied Radiation and Isotopes*, 42:643–657, 1991.

[57] B Scholten, RM Lambrecht, M Cogneau, HV Ruiz, and SM Qaim. Excitation functions for the cyclotron production of ^{99m}Tc and ^{99}Mo. *Applied Radiation Isotopes*, 51:69–80, 1999.

[58] S Takacs, Z Szucs, F Tarkanyi, A Hermanne, and M Sonck. Evaluation of proton-induced reactions on ^{100}Mo: New cross sections for the production of ^{99m}Tc and ^{99}Mo. *Journal of Radioanalytical and Nuclear Chemistry*, 257:195–201, 2003.

[59] MS Uddin, M Hagiwara, F Tarkanyi, F Ditroi, and M Baba. Experimental studies on the proton-induced activation reactions of Molybdenum in the energy range 22-67 MeV. *Applied Radiation and Isotopes*, 2004.

[60] MU Khandaker, AKMMH Meaze, K Kim, D Son, and G Kim. Measurements of the Proton-Induced Reaction Cross-Sections of ^{nat}Mo by Using the MC50 Cyclotron at the Korea Institute of Radiological and Medical Sciences. *Journal of the Korean Physical Society*, 48:821–826, 2006.

[61] MU Khandaker, MS Uddin, KS Kim, YS Lee, and GN Kim. Measurement of the cross-sections for the (p,xn) reaction in natural Molybdenum. *NIMB*, 262:171–181, 2007.

[62] MB Challan, MNH Cosman, and MA Abou-Zeid. Thin targets yields andEMPIRE-II predictions on the accelerator production of Technetium-99m. *NIMB*, 264:1–12, 2007.

[63] GN Kim, MU Khandaker, K Kima, KS Kim, MS Uddin, MW Lee, and YS Lee. Measurement of excitation functions of proton induced reactions on ^{nat}Mo, ^{nat}W and ^{nat}Zn up to 40 MeV. 2008.

[64] O Lebeda and M Pruszynski. New measurement of excitation functions for (p,x) reactions on ^{nat}Mo with special regard to the formation of ^{95m}Tc, $^{96m+g}$Tc, 99mTcand99Mo. *Applied Radiation and Isotopes*, 68:2355–65, 2010.

[65] P Chodash, CT Angell, J Benitez, EB Norman, M Pedretti, and H Shugart. Measurement of excitation functions for the ^{nat}Mo(d,x)^{99}Mo and ^{nat}Mo(p,x)^{99}Mo reactions. *Applied Radiation and Isotopes*, 69:1447–52, 2011.

[66] AA Alharbi, A Azzam, M McCleskey, B Roeder, A Spiridon, E SimMons, VZ Goldberg, A Banu, L Trache, and RE Tribble. Medical radioisotopes production: a comprehensive cross-section study for the production of Mo and Tc radioisotopes via proton induced nuclear reactions on ^{nat}Mo. 2011.

[67] MC Lagunas-Solar. Accelerator production of ^{99m}Tc with proton beams and enriched ^{100}Mo targets. Technical report, International Agency Energy Atomic (IAEA), 1999. IAEA-TECDOC No. 1065.

[68] F Tarkanyi, F Ditroi, A Hermanne, S Takacs, and AV Ignatyuk. Investigation of activation cross-sections of proton induced nuclear reactions on ^{nat}Mo up to 40 MeV: New data and evaluation. *NIMB*, 280:45–73, 2012.

[69] National Nuclear Data Center (NNDC) and Brookhaven National Laboratory (BNL), 2013. URL http://www.nndc.bnl.gov.htm.

[70] EA Skakun, VG Batij, YN Rakivnenko, and OA Rastrepin. Excitation functions and isomer ratios for up-to-9 MeV proton interactions with Zr and Mo isotope nuclei. *Soviet Journal of Nuclear Physics*, 46(17), 1987.

[71] Experimental Nuclear Reaction Data (EXFOR), 2013. URL http://www.nndc.bnl.gov/exfor/exfor.htm.

[72] SM Qaim. Radiochemical determination of nuclear data for theory and applications. *Journal of Radioanalytical and Nuclear Chemistry*, 284:489–505, 2010.

[73] SM Qaim. Therapeutic radionuclides and nuclear data. *Radiochimica Acta*, 89:297–302, 2001.

[74] I Novak-Hofer and PA Schubiger. Copper-67 as a therapeutic nuclide for radioimmunotheraphy. *European Journal of Nuclear Medicine*, 29:821–830, 2002.

[75] S Mirzadeh, LF Mausner, and SC Srivastava. Production of No- Carrier Added ^{67}Cu. *Applied Radiation and Isotopes*, 37:29–36, 1986.

[76] GL DeNardo, SJ DeNardo, CF Meares, Q Salako, DL Kukis, LF Mausner, JP Lewis, LF O'Grady, and SC Srivastava. Pilot therapy of lymphoma with fractionated Cu-67-BAT Lym-1. *Journal of Nuclear Medicine*, 34:93, 1993.

[77] LF Mausner, KL Kolsky, and SC Srivastava. Radionuclide development at BNL for nuclear medicine therapy. *Applied Radiation and Isotopes*, 49(4):285–294, 1998.

[78] HA O'Brien. The preparation of ^{67}Cu from ^{67}Zn in a nuclear reactor. *International Journal of Applied Radiation and Isotopes*, 20:121–124, 1969.

[79] SM Qaim. Evaluation of excitation functions of ^{100}Mo(p,d+pn)^{99}Mo and ^{100}Mo(p,2n)^{99m}Tc reactions: Estimation of long-lived Tc-impurity and its implication on the specific activity of cyclotron-produced ^{99m}Tc. *Applied Radiation and Isotopes*, 85:101–113, 2014.

[80] Ye. Skakun and SM Qaim. Excitation functions of the ^{64}Ni(α,p)^{67}Cu reaction for the production of ^{67}Cu. *Applied Radiation and Isotopes*, 60(33-39), 2004.

[81] J Kozempel, K Abbas, F Simonelli, A Bulgheroni, U Holzwarth, and N Gibson. Preparation of ^{67}Cu via deuteron irradiation of ^{70}Zn. *Radiochimica Acta*, 100: 419–423, 2012.

[82] S Kastleiner, HH Coenen, and SM Qaim. Possibility of production of ^{67}Cu at a small-sized cyclotron via the (p,α)-reaction on enriched ^{70}Zn. *Radiochimica Acta*, 84:107–110, 1999.

[83] R Schwarzbach, K Zimmermann, I Novak-Hofer, and PA Schubiger. A comparison of ^{67}Cu production by proton (67 to 12 MeV) induced reactions on ^{nat}Zn and enrched ^{68}Zn/^{70}Zn. In *Journal of Labelled Compounds and Radiopharmaceuticals*, volume 44, 2001.

[84] K Hilgers, T Stoll, Ye. Skakun, HH Coenen, and SM Qaim. Cross section measurements of the nuclear reactions ^{nat}Zn(d,x)^{64}Cu, ^{66}Zn(d,α)^{64}Cu, ^{68}Zn(p,αn)^{64}Cu for production of ^{64}Cu and technical developments for small scale production of ^{67}Cu via the ^{70}Zn(p,α)^{67}Cu process. *Applied Radiation and Isotopes*, 59:343–351, 2003.

[85] BL Cohen, E Newman, and TH Handley. (P,PN) + (P,2N) and (P,2P) Cross Sections in Medium Weight Elements. *Physical Review*, 99:723–727, 1955.

[86] DLMorrison and AA Caretto Jr. Recoil study of the Zn-68(p,2p)Cu-67 reaction. *Physical Review*, 133:B1165, 1964.

[87] T McGee, CL Rao, GB Saha, and L Yaffe. Nuclear interactions of Sc-45 and Zn-68 with protons of medium energy. *Nuclear Physics, Section A*, 150:11–29, 1970.

[88] T Stoll, S Kastleiner, YuN Shubin, HH Coenen, and SM Qaim. Excitation functions of proton induced reactions on ^{68}Zn from threshold up to 71 MeV and with specific reference to the production of ^{67}Cu. *Radiochimica Acta*, 90:309–313, 2002.

[89] F Szelecsenyi, GF Steyn, SG Dolley, Z Kovacs, C Vermeulen, and TN van der Walt. Investigation of the ^{68}Zn(p,2p)^{67}Cu nuclear reaction: New measurements up to 40 MeV and compilation up to 100 MeV. *NIMB*, 267:1877–1881, 2009.

[90] ML Bonardi, F Groppi, HS Mainardi, VM Kokhanyuk, EV Lapshina, MV Mebel, and BL Zhuikov. Cross section studies on ^{64}Cu with Zinc target in the proton energy range from 141 down to 31 MeV. *Journal of Radioanalytical and Nuclear Chemistry*, 264(1):101–105, 2005.

[91] NI Ayzatsikiy et al. Comparison of Cu-67 production at cyclotron and electron accelerator. In *Cyclotrons and their applications - 18th International Conference*, 2007.

[92] AK Dasgupta, LF Mausner, and SC Srivastava. A new separation procedure for^{67}Cu from proton irradiated Zn. *Applied Radiation and Isotopes*, 42(4):371–376, 1991.

[93] KL Kolsky, V Joshi, GE Meinken, LF Mausner, and SC Srivastava. Improved production and evaluation of ^{67}Cu for tumour radioimmunotherapy. *Journal of Nuclear Medicine*, 35:259, 1994.

[94] R Schwarzbach, K Zimmermann, P Blauenstein, A Smith, and PA Schubiger. Development of a simple and selective separation of ^{67}Cu from irradiated Zinc for use in antibody labelling: A comparison of methods. *Applied Radiation and Isotopes*, 46(5):329–336, 1995.

[95] T Katabuchi, S Watanabe, NS Ishioka, Y Iida, H Hanaoka, K Endo, and S Matsuhashi. Production of ^{67}Cu via the ^{68}Zn(p,2p)^{67}Cu reaction and recovery of ^{68}Zn target. *Journal of Radioanalytical and Nuclear Chemistry*, 277:467–470, 2008.

[96] DG Medvedev, LF Mausner, GE Meinken, SO Kurczak, H Schnakenberg, CJ Dodge, EM Korach, and SC Srivastava. Development of a large scale production of ^{67}Cu from ^{68}Zn at the high energy proton accelerator: Closing the ^{68}Zn cycle. *Applied Radiation and Isotopes*, 70:423–429, 2012.

[97] SM Qaim, F Tarkanyi, and R Capote. Nuclear Data for the Production of Therapeutic Radionuclides. Technical report, International Agency Energy Atomic (IAEA), 2011. 473.

[98] S Takacs, F Tarkanyi, M Sonck, and A Hermanne. Investigation of the ^{nat}Mo(p,x)^{96mg}Tc nuclear reaction to Monitor proton beams: New measurements and consequences on the earlier reported data. *NIMB*, 2002.

[99] D Ragheb, C Koumeir, A Guertin, F Haddad, V Metivier, N Michel, and N Servagent. Development of the PIXE analysis technique at high energy with the ARRONAX cyclotron. In *Application of Radiotracers and Energetic Beams in Sciences (ARCEBS)*, 2014.

[100] Various Authors. Technetium-99m Radiopharmaceuticals: Status and Trends. Technical report, International Agency Energy ctomic (IAEA), 2009. Radioisotopes and Radiopharmaceuticals series No. 1.

[101] WR Leo. *Techniques for Nuclear and Particle Physics Experiments*. Springer-Verlag, 1987.

[102] M Bonardi. The contribution to nuclear data for biomedical radioisotope production from the Milan Cyclotron Laboratory. In K OkaMoto, editor, *Consultants meeting on data requirements for medical radioisotope production*, pages 98–115. 1988.

[103] FH Attix. *Introduction to radiological physics and radiation dosimetry*. John Wiley and Sons, 1986.

[104] U Amaldi. *Fisica delle radiazioni*. Boringhieri, 1971.

[105] GF Knoll. *Radiation Detection and Measurement*. John Wiley and Sons, 2000.

[106] Fitzpeaks Gamma Analysis and Calibration Software, 2009. URL http://www.jimfitz.de{M}on.co.uk/fitzpeak.htm.

[107] H Piel and SM Qaim andG Stoeklin. Excitation functions of (p,xn)-reactions on ^{nat}Ni and highly enriched ^{62}Ni: possibility of production of medically important radioisotope ^{62}Cu at a small cyclotron. *Radiochimica Acta*, 57:1, 1992.

[108] M Gloris, R Michel, F Sudbrock, U Herpers, P Malmborg, and B Holmqvist. Proton-induced production of residual radionuclides in lead at intermediate energies. *NIMA*, 463:593–633, 2001.

[109] L Uccelli, A Boschi, M Pasquali, A Duatti, G Di Domenico, G Pupillo, J Esposito, M Giganti, A Taibi, and M Gambaccini. Influence of the generator in-growth time on the final radiochemical purity and stability of ^{99m}Tc radiopharmaceuticals. *Hindawi Publishing Corporation; Special Issue - Molybdenum-99: Past and Present and Future*, 2013.

[110] X Hou, A Celle, J Grimes, F Benard, and T Ruth. Theoretical dosimetry estimations for radioisotopes produced by proton-induced reactions on natural and enriched Molybdenum targets. *Physics in Medicine and Biology*, 57:1499–1515, 2012.

[111] TJ Morley, L Penner, P Schaffer, TJ Ruth, F Benard, and E Asselin. The deposition of smooth metallic Molybdenum from aqueous electrolytes containing Molybdate ions. *Electrochemistry Communications*, 15:78–80, 2012.

[112] SM Qaim. New trends in nuclear data research for medical radionuclide production. *Radiochimica Acta*, 101:473–480, 2013.

[113] Health and consumers directorate general preliminary report on supply of radioisotopes for medical use and current developments in nuclear medicine. Technical report, European Commision, 2009. Technical Report SANCO/C/3/HW.

[114] A Del Guerra et al. Performance evaluation of the fully engineered YAP-(S)PET scanner for small animal imaging. *IEEE Transactions on Nuclear Science*, 53(3): 1078–1083, 2006.

[115] A Hermanne, M Sonck, S Takacs, F Szelecsenyi, and F Tarkanyi. Excitation functions of nuclear reactions induced by alpha particles up to 42 MeV on ^{nat}Ti for Monitoring purposes and TLA. *NIMB*, 152:187–201, 1999.

[116] IAEA - Recommended Monitor reactions, 2009. URL https://www-nds.iaea.org/medical/{M}onitor_reactions.html.

[117] AR Jalilian, H Targholizadeh, GR Raisali, H Zandi, and M Kamali Dehgan. Direct Technetium radiopharmaceuticals production using a 30 MeV Cyclotron. *DARU Journal of Pharmaceutical Sciences*, 19(3):187–192, 2011.

[118] A Celler, X Hou, F Benard, P Schaffer, T Morley, M Vuckovic, and T Ruth. Patient dosimetry for cyclotron produced ^{99m}Tc radiopharmaceuticals. In *Annual Meeting of the Society of Nuclear Medicine and Molecular Targeting Probes - Radioactive and Nonradioactive*, 2011. Journal of Nuclear Medicine 53 (Supplement 1):1507.

[119] E Garrido. Production de radio-isotopes: de la mesure de la section efficace à la production, Université de Nantes, UFR Sciences et Techniques, 2011.